



**ČESKÉ  
VYSOKÉ  
UČENÍ  
TECHNICKÉ  
V PRAZE**

**Department of Mechanics,  
Biomechanics and Mechatronics**

**Effect of musculoskeletal model choice on  
hip joint loading prediction**

**MASTER'S THESIS**

**2021/2022**

**Bc. Jan Pluhař**

**Study programme:** (NAVSI) Applied science in mechanical engineering  
**Specialization:** (N071TBIO) Biomechanics  
**Supervisor:** prof. RNDr. Matej Daniel, Ph.D.

## I. OSOBNÍ A STUDIJNÍ ÚDAJE

Příjmení: **Pluhař** Jméno: **Jan** Osobní číslo: **466582**  
Fakulta/ústav: **Fakulta strojní**  
Zadávající katedra/ústav: **Ústav mechaniky, biomechaniky a mechatroniky**  
Studijní program: **Aplikované vědy ve strojním inženýrství**  
Specializace: **Biomechanika**

## II. ÚDAJE K DIPLOMOVÉ PRÁCI

Název diplomové práce:

**Vliv volby svalově-kosterního modelu na predikci zatížení kyčelního kloubu**

Název diplomové práce anglicky:

**Effect of musculoskeletal model choice on hip joint loading prediction**

Pokyny pro vypracování:

1. Stav techniky - přehled současných modelů
2. Výběr modelů kyčelního kloubu
3. Škálování
4. Inverzní statická optimalizace
5. Porovnání výsledků s experimenty
6. Diskuse a doporučení pro budoucí studie

Seznam doporučené literatury:

Hornová J, Iglíč A, Kralj-Iglíč V, Pedersen DR, Daniel M. Effect of patient-specific model scaling on hip joint reaction force in one-legged stance - study of 356 hips. Acta Bioeng Biomech. 2017;19(4):103-108.  
Debevec H, Pedersen DR, Iglíč A, Daniel M. One-legged stance as a representative static body position for calculation of hip contact stress distribution in clinical studies. J Appl Biomech. 2010 Nov;26(4):522-5. doi: 10.1123/jab.26.4.522.  
Stankovský V, Iglíč A, Kralj-Iglíč V, Kersnic B. The hip-joint resultant force in healthy male and female population: a comparative study. Acta Chir Orthop Traumatol Cech. 1996;63(4):211-3.

Jméno a pracoviště vedoucí(ho) diplomové práce:

**prof. RNDr. Matej Daniel, Ph.D. České vysoké učení technické v Praze, Fakulta strojní**

Jméno a pracoviště druhé(ho) vedoucí(ho) nebo konzultanta(ky) diplomové práce:

Datum zadání diplomové práce: **20.04.2022**

Termín odevzdání diplomové práce: **14.08.2022**

Platnost zadání diplomové práce: \_\_\_\_\_

prof. RNDr. Matej Daniel, Ph.D.  
podpis vedoucí(ho) práce

prof. Ing. Michael Valášek, DrSc.  
podpis vedoucí(ho) ústavu/katedry

doc. Ing. Miroslav Španiel, CSc.  
podpis děkana(ky)

## III. PŘEVZETÍ ZADÁNÍ

Diplomant bere na vědomí, že je povinen vypracovat diplomovou práci samostatně, bez cizí pomoci, s výjimkou poskytnutých konzultací. Seznam použité literatury, jiných pramenů a jmen konzultantů je třeba uvést v diplomové práci.

\_\_\_\_\_  
Datum převzetí zadání

\_\_\_\_\_  
Podpis studenta

## DECLARATION

I hereby declare this thesis represents my own work and has not been included in a thesis or dissertation submitted to Czech Technical University in Prague or any other institution for a degree, diploma or other qualifications. Wherever contributions of others are involved, every effort is made to indicate this clearly, with due reference to the literature, and acknowledgement of collaborative research and discussions.

In Prague 12. 8. 2022

Jan Pluhař

## ACKNOWLEDGEMENT

At this point, I would like to thank my supervisor, prof. RNDr Matej Daniel, for the opportunity to work on this topic. I would like to thank him for the professional supervision, numerous consultations, guidance, time and effort he has given me and which have greatly helped me to develop this master's thesis. I would also like to thank Dr. Veronika Kralj-Iglič, Full Professor, for accepting me into her research group at the University of Ljubljana and for the opportunity to participate in the research of hip dysplasia.

## ANNOTATION LIST

Author name:	Jan Pluhař
Thesis name:	Effect of musculoskeletal model choice on hip joint loading prediction
Czech name:	Vliv volby svalově-kosterního modelu na predikci zatížení kyčelního kloubu
Year:	2022
Study programme:	(NAVSI) Applied science in mechanical engineering
Department:	Department of Mechanics, Biomechanics and Mechatronics
Supervisor:	prof. RNDr. Matej Daniel, Ph.D.
Bibliographic data:	Number of pages: 72 Number of figures: 26 Number of tables: 10 Number of attachments: 1
Keywords:	hip joint, mathematical models, resultant hip force, scaling, optimization, one-legged stance, hip dysplasia, contact hip stress
Klíčová slova:	kyčelní kloub, matematické modely, reakční síla v kyčli, škálování, optimalizace, stoj na jedné noze, dysplazie kyčle, kontaktní napětí v kyčli
Annotation:	The thesis describes different approaches to estimating the resultant hip force. Two types of mathematical models are described: models using optimization and reduction methods. The resultant hip force calculated using sixteen models is compared with in-vivo measurements. In the second part, HIPSTRESS model is used to analyze hip dysplasia.
Anotace:	Diplomová práce popisuje různé přístupy k odhadu reakční síly v kyčli. Dva typy modelů jsou popsány: modely využívající redukční a optimalizační metody. Reakční síla v kyčli počítaná pomocí šestnácti modelů je porovnána s in-vivo měřeními. Ve druhé části je analyzována dysplazie kyčle pomocí HIPSTRESS modelu.

**LIST OF SYMBOLS**

$\vec{R}$	[N]	Resultant hip force
$R$	[N]	Magnitude of the resultant hip force
$\vec{W}$	[N]	Weight force
$\vec{F}_i$	[N]	Muscle force of the $i$ -th muscle or muscle fibre
$F_i$	[N]	Magnitude of the muscle force of the $i$ -th muscle or muscle fibre
$\vec{r}_W$	[m]	Moment arm of the weight force
$\vec{r}_i$	[m]	Moment arm of the $i$ -th muscle force or muscle fibre
$x$		Vector of unknown variables
$f(x)$		Objective function
$h(x)$		Function of equality constraints
$g(x)$		Function of inequality constraints
$B_L$		Lower bound for the unknown variables
$B_U$		Upper bound for the unknown variables
$w$		Weighted factor of the unknown variables
$p$		Power of the objective function
$F_{Ui}$	[N]	Upper boundary of the force $F_i$
$\vec{M}_{net}$	[Nm]	Net joint moment
$PCSA_i$	[m <sup>2</sup> ]	Physiological cross-sectional area of the $i$ -th muscle or muscle fibre
$f_i$	[N/m]	Average tension in the $i$ -th muscle
$A_i$	[-]	Relative cross-sectional area of the $i$ -th muscle
$\vec{s}_i$	[-]	Unit vector in the direction of the $i$ -th muscle or muscle fibre
$x, y, z$	[m]	Coordinates
$\psi, \nu, \varphi$	[°]	Euler XYZ body-fixed angles
$\mathbf{T}$		Transformation matrix
$\vec{r}_{ch}$	[m]	Position of a point located in the coordinate system of the child body
$\vec{r}_p$	[m]	Position of a point located in the coordinate system of the parent body
$\vec{r}_{femur}$	[m]	Vector from the femur's coordinate system to the attachment
$\vec{r}_{pelvis}$	[m]	Vector from the pelvis' coordinate system to the attachment
$\vec{r}_w$	[m]	Vector from the right femur's coordinate system to the shifted centre of mass relative to the right femur's coordinate system
$\vec{r}_{wj}$	[m]	vector from the origin of the right femur's coordinate system to the centre of mass of the $j$ -th body segment expressed in the coordinate system of the right femur
$m_j$	[kg]	mass of $j$ -th body segment
$\vec{s}_{di}$	[m]	coordinates of distal attachment of the $i$ -th muscle fibre in the coordinate system of the right hip
$\vec{s}_{pi}$	[m]	coordinates of proximal attachment of the $i$ -th muscle fibre in the coordinate system of the right hip
$F_{i\ min}$	[N]	Minimum force acting in the $i$ -th muscle fibre
$F_{i\ max}$	[N]	Maximal isometric force of the $i$ -th muscle fibre
$\sigma_{max}$	[N/m <sup>2</sup> ]	Stress in muscles
$F_{i\ min}$	[N]	Minimum force acting in the $i$ -th muscle fibre

$a_{min}$	[-]	<i>Minimum muscle fibre activity</i>
$a_i$	[-]	<i>Muscle fibre activity</i>
$F_{Mk}$	[N]	<i>Resultant muscle force</i>
$a_{Mk}$	[-]	<i>Resultant muscle activity</i>
$\vartheta_{R\text{ FRONTAL}}$	[°]	<i>Angle of the resultant hip force in the frontal plane</i>
$\vartheta_{R\text{ SAGITTAL}}$	[°]	<i>Angle of the resultant hip force in the sagittal plane</i>
$\vec{r}_F$	[m]	<i>Moment arm of the effective muscle</i>
$W_B$	[N]	<i>Magnitude of the weight force of the whole body</i>
$W_L$	[N]	<i>Magnitude of the weight force of the loaded leg</i>
$\vartheta_R$	[°]	<i>Angle of the resultant hip force in the frontal plane</i>
$\vartheta_{CE}$	[°]	<i>Centre-edge angle</i>
$\vartheta_F$	[°]	<i>Inclination of the effective muscle</i>
$L$	[m]	<i>Interhip distance</i>
$C$	[m]	<i>Width from the hip centre to the most lateral point of pelvis</i>
$H$	[m]	<i>Height from the hip centre to the most superior point of pelvis</i>
$x_F$	[m]	<i>x coordinate of the origin of the effective muscle</i>
$z_F$	[m]	<i>z coordinate of the origin of the effective muscle</i>
$p$	[N/m <sup>2</sup> ]	<i>Stress</i>
$p_0$	[N/m <sup>2</sup> ]	<i>Stress in the stress pole</i>
$\theta$	[°]	<i>Stress pole angle</i>
$r$	[m]	<i>Radius of the articular sphere</i>
$\vartheta$	[°]	<i>Angle in the mediolateral direction of the hip</i>
$\varphi$	[°]	<i>Angle in the anteroposterior direction of the hip</i>
$\vartheta_{RCE}, \vartheta_H$	[°]	<i>Angles introduced for the solution of nonlinear equation (64)</i>
$p_{max}r^2/W_B$	[-]	<i>Peak contact hip stress normalized by the body weight and the radius of the articular sphere</i>
$G_p r^3/W_B$	[-]	<i>Hip stress gradient index normalized by the body weight and the radius of the articular sphere</i>
$\vartheta_f$	[°]	<i>Functional angle</i>
$P$	[]	<i>Parameter P representing any variable</i>
$P_{difference}$	[-]	<i>Percentage difference of a parameter P</i>
$P_{after}$	[]	<i>Value of a parameter P after the operation</i>
$P_{before}$	[]	<i>Value of a parameter P before the operation</i>

## LIST OF FIGURES

Figure 1: Phases of a gait cycle [13].....	3
Figure 2: Hip's movement during a normal gait cycle [8] .....	4
Figure 3: Resultant hip force and its component during a normal gait cycle in "KWR" patient [2].....	5
Figure 4: Resultant hip force and its components during one-legged stance with the swing leg in the position of hip flexion in "KWR" patient [2], [16] .....	7
Figure 5: Difference between measured and estimated EMG signals using machine learning model in [32].....	12
Figure 6: Average resultant hip force and its components during a gait cycle in the control group [36].....	15
Figure 7: Three seconds of filtered EMG signal during one-legged stance [38] .....	18
Figure 8: Flow diagram of the choice of models .....	24
Figure 9: Comparison of gluteus medius muscle fibers in Arnold et al 2010 and Modenese et al 2011.....	26
Figure 10: Raabe et al 2016 model in the default position .....	28
Figure 11: Example of a joint (right knee) definition in the Rajagopal et al 2016 model ...	29
Figure 12: Topology view of the Rajagopal et al 2016 model .....	30
Figure 13: Difference between anatomical and effective attachments [54], [55].....	32
Figure 14: Comparison of the reaction force per body weight in different models. Minimum muscle activity for OpenSim models was set to zero .....	45
Figure 15: Comparison of the angle of the resultant hip force in the frontal plane in different models. Minimum muscle activity for OpenSim models was set to zero .....	46
Figure 16: Resultant hip force per body weight as a function of minimum muscle fibre activity.....	47
Figure 17: Resultant hip force angle $\vartheta_R$ in the frontal plane in the medial direction as a function of minimum muscle fibre activity.....	48
Figure 18: Resultant hip force angle $\vartheta_R$ in the sagittal plane in the anterior direction as a function of minimum muscle fibre activity.....	48
Figure 19: Resultant hip force $R/WB$ as a function of number of muscle fibres in models .....	49
Figure 20: Resultant hip force $R/WB$ as a function of number of muscles in models.....	50
Figure 21: Comparison of resultant muscle forces $FM$ between models for minimum muscle fibre activity set to 0% and 10% .....	52
Figure 22: Comparison of resultant muscle activity $aM$ between models for minimum muscle fibre activity set to 0% and 10%Discussion .....	53
Figure 23: Geometrical evaluation of X-Ray scan according to the HIPSTRESS model.....	38
Figure 24: Forces acting in the hip joint according to HIPSTRESS model.....	39
Figure 25: Visualisation of geometrical and biomechanical parameters used in HIPSTRESS model .....	44



Figure 26: X-Ray scans of two cases of the operation from centre C1 in which the stress on the contralateral side improved most (before and after the operation (A, B)) and in which worsened most (before and after the operation (C, D))..... 64

## LIST OF TABLES

Table 1: Muscle activity normalized by MVIC during the Y-Balance test. Adapted from Kaur et al., 2022 [42] .....	17
Table 2: Values of EMG signal measured during upright standing in the one-legged stance. Adapted from Prior et al., 2014 [19] .....	17
Table 3: List of models downloaded from OpenSim and used for the analysis .....	25
Table 4: Comparison of gluteus medius muscle segments in Arnold et al., 2010 and Modenese et al., 2011 models (*Total max ISO Force is calculated as a vector sum, viz section 4.3.9) .....	26
Table 5: Evaluation of hips before the first operation (initial parameters of the patients) on the operated side .....	54
Table 6: Evaluation of hips before the first operation (initial parameters of the patients) on the contralateral side .....	54
Table 7: Evaluation of hips on the operated side.....	55
Table 8: Evaluation of hips on the contralateral side.....	56
Table 9: Evaluation of hips on the contralateral side, which improved by more than 20% in stress.....	57
Table 10: Evaluation of hips on the contralateral side which got worse by more than 20% in stress.....	58

## CONTENTS

<b>1. Introduction .....</b>	<b>1</b>
<b>2. State of the art .....</b>	<b>2</b>
2.1. Hip joint.....	2
2.2. Gait.....	3
2.3. One-legged stance .....	5
2.4. Determination of the resultant hip force .....	8
2.5. Models using optimization methods .....	8
2.6. Models using reduction methods.....	12
2.7. Scaling of musculoskeletal models .....	13
2.8. EMG measurements of muscle activity during the one-legged stance.....	16
2.9. Hip dysplasia .....	18
<b>3. Aim of the work.....</b>	<b>20</b>
<b>4. Methods.....</b>	<b>23</b>
4.1. Source of models .....	23
4.2. Determination of the resultant hip force .....	24
4.3. Resultant hip force according to models using optimization methods .....	24
4.3.1. Calculation of the resultant hip force - process overview .....	26
4.3.2. One-legged stance position and scaling of models .....	27
4.3.3. Transformation of coordinates .....	29
4.3.4. Transformation of muscle attachments .....	31
4.3.5. Transformation of the centre of mass .....	33
4.3.6. Calculation of torques.....	33
4.3.7. Calculation of muscle forces .....	34
4.3.8. Calculation of resultant hip force and muscle activity .....	35
4.4. Resultant hip force according to models using reduction methods .....	36
4.4.1. Reasons for choosing HIPSTRESS model.....	37
4.4.2. Geometrical evaluation of X-Ray scans.....	37
4.4.1. Equilibrium in the hip joint .....	39
4.4.1. Stress distribution in the hip joint .....	40
4.5. Resultant hip force according to in vivo measurements.....	44
<b>5. Results.....</b>	<b>45</b>
<b>6. Discussion.....</b>	<b>59</b>
<b>7. Conclusion .....</b>	<b>66</b>
<b>Bibliography .....</b>	<b>69</b>

## 1. Introduction

Knowledge of resultant hip force is essential for understanding the function of normal and diseased joints, designing better treatments (implants, rehabilitation regimens), evaluating the effects of treatment, optimizing performance and obtaining clues to the pathogenesis of a disease. [1] Furthermore, the resultant hip joint must be known for tests on strength, fixation, wear and friction of implants, for optimizing their design and materials by computer simulation and for giving guidelines to patients and physiotherapists as to which activities should be avoided after a replacement. [2]

The first option how to estimate the resultant hip force is by *in vivo* measurements. Well-known measurements are the ones performed by Bergman using instrumented implants [2], [3]. A problem with these measurements is that they are done postoperatively and therefore cannot be used to estimate the resultant hip force in healthy people or in patients before surgery. The second option is using mathematical models that can be rescaled to match patient-specific anatomy or adapted to a visualization technique, e.g., computer tomography or X-Ray scans [4]. Mathematical models can be either two-dimensional or three-dimensional. They can be either simplified so that the resulting hip force can be calculated using reduction methods, or they can match the anatomy more precisely, which leads to the usage of optimization methods.

This work composes of two main parts. In the first part are described two types of mathematical models, which are based on a one-legged stance. That is considered a representative body position for the long-term effect of hip contact stress [5]. This part mainly focused on the models using optimization techniques. Twelve unique models were downloaded from OpenSim database [6], and data from these models were used to calculate the resultant hip force. The results were compared with results of the models using the reduction methods and with the *in vivo* measurements.

In the second part of the work, HIPSTRESS model was used for an analysis of periacetabular osteotomy, which is a surgical treatment of hip dysplasia. The research was focused on changes in the contralateral hip during the operation, as it had already been shown that a predecessor of the current model can evaluate hip dysplasia on the operated hip very well [7].

## 2. State of the art

### 2.1. Hip joint

The hip joint is a synovial joint of a ball and socket type that connects the lower limb with the axial skeleton. More precisely, it connects the femoral head and the acetabulum of the pelvis. It is the most stable joint in the human body. [8], [9]

The joint transmits the load from the upper body to the lower extremity. The stability of the hip joint is secured by the depth of the acetabulum, which can encompass almost entire femoral head, the fibrocartilaginous acetabular labrum, which is a collar surrounding the acetabulum and enlarging the surface area of the joint, the ligaments and joint capsule, which prevent excessive movement of the joint, and the muscles that allow, but also restrict movement. [8], [9]

Due to enlarging the surface area, the acetabular labrum helps to lower and distribute the transmitted loads. The acetabular labrum acts as a sensitive shock absorber, which helps to keep the synovial fluid in contact with the articular cartilage. [8], [9]

The hip joint allows a wide range of motion in all three planes: sagittal, frontal and transverse. These motions are following: flexion, extension, abduction, adduction and external and internal rotation. The greatest range of motion is in the sagittal plane, where the flexion can reach from  $100^{\circ}$  to  $140^{\circ}$ . In the frontal plane, the range of abduction is from  $10^{\circ}$  to  $45^{\circ}$  and the range of adduction is from  $10^{\circ}$  to  $30^{\circ}$ . The internal rotation can reach up to  $30^{\circ}$ , while the external rotation can reach up to  $60^{\circ}$ . If the hip is flexed, the ranges of internal and external rotations can reach up to  $60^{\circ}$  and  $90^{\circ}$ , respectively. The ranges of motion can, however, be influenced by gender, age, individual anatomy, history of injuries or level of physical activity of a specific person. [8], [9]

One of the most common diseases of the hip joint is arthritis, which causes a breakdown of hip tissue, leads to pain and eventually to an artificial hip joint replacement. Among other problems belong bursitis, when a bursa (sac with a fluid) becomes inflamed, avascular necrosis, which is a death of bone tissue caused by a lack of blood supply, or shape disorders, such as Perthes disease or hip dysplasia, which can eventually lead to arthritis. [10], [11] Most common types of hip fractures are femoral neck fractures and

intertrochanteric fractures. The fractures can be related to osteoporosis. They can be treated with either internal repair screws or hip replacement. [12]

## 2.2. Gait

Gait is a characteristic of the human species, a pattern of walking. It is characterized by periods of loading and unloading of the limbs and is defined as a period from one heel strike to another. For each leg, it consists of two phases, the stance phase and the swing phase, where the foot is and is not in contact with the ground, respectively. The stance phase is longer, taking about 60% of the gait cycle. The swing phase takes the remaining 40%, during which it is not touching the ground and all load is carried by the other leg. During a gait cycle, both feet are in contact with the ground for approximately 20% of the time. Additionally, the gait cycle can be divided into eight phases, as shown in Figure 1. The stance phase occurs between the heel strike and toe-off phase of the cycle.

While walking, the femur and the pelvis articulate against each other. Figure 2 shows hip angles during a normal gait cycle. The red vertical line represents heel-strike and the green vertical line is toe-off. Region A represents a stance phase and region B represents a swing phase of the gait. The angles represent a relative movement of the femur against the pelvis. During a gait cycle, the centre of gravity moves rhythmically up and down and side-to-side, both with a sinusoidal path. [8]

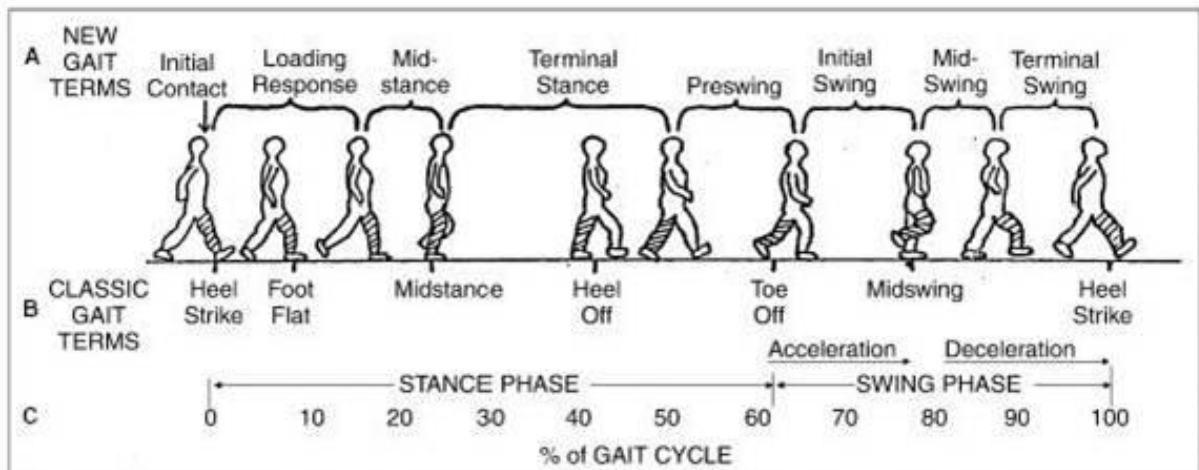


Figure 1: Phases of a gait cycle. After "Gait - Physiopedia" [13]

The gait is studied and analysed in order to support clinical decision-making in case of gait dysfunction. The gait analysis consists of several measurements. The core ones are the ones that measure kinematics (angles) and kinetics (forces and torques). The movement of

individual body segments during walking can be obtained by various motion analysis methods (video analysis, inertial units, direct exoskeleton sensors, etc.). Additional information can be obtained by an EMG measurement, which measures muscle activity by detecting electrical signals. Oxygen intake or distribution of foot contact pressure can be measured as well. One of the most important measurements is the measurement of the ground reaction force, usually obtained from force plates. The ground reaction force is a force between the ground and the foot. The ground reaction force can be used to further investigate human movement and gait patterns. It is also an important input into musculoskeletal mathematical models. [14], [15]

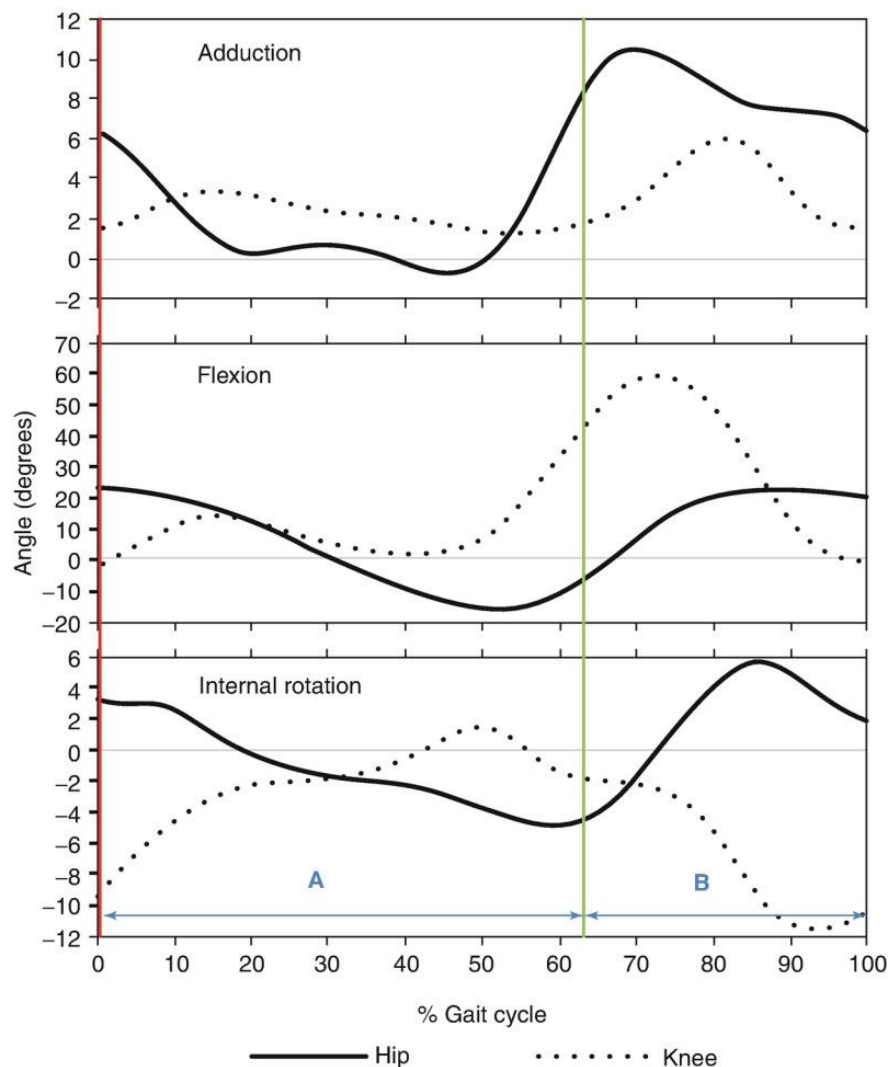


Figure 2: Hip movement during a normal gait cycle. After Galmiche et al., 2020 [8]

Measurements of the resultant hip joint during a gait cycle were performed by Bergman et al., 2001 [2], where the force was measured using an instrumented implant during routine daily activities. The resultant hip force and its components during a gait cycle are

shown in Figure 3 for a selected patient. Four patients were measured, and the peak value averaged over them was  $F_p = 238\% BW$ .

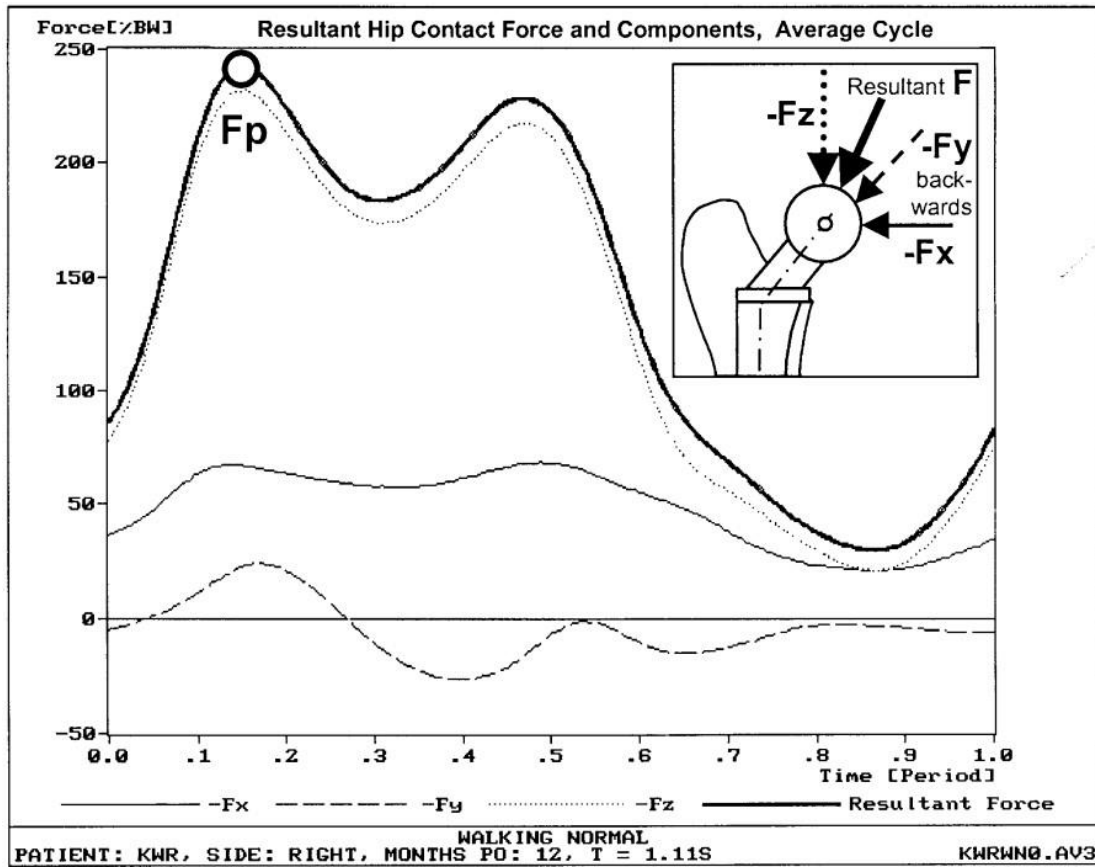


Figure 3: Resultant hip force and its component during a normal gait cycle in “KWR” patient.  
Adapted from Bergmann et al., 2001 [2]

### 2.3. One-legged stance

Activities in which a person touches the ground with only one foot occur in everyday life. While walking, a person stands on either left or right leg for about eighty per cent of the time. The single leg support is also essential when stepping into a bath or climbing stairs. The person must be able to keep balance on one leg during these tasks.

Unlike the gait cycle, there is no definition describing a one-legged stance. In Orthoload database [16] can be found many measurements of the resultant hip force during the one-legged stance with different positions of the unloaded leg and also with different positions of the arms. No direct instructions on how to perform the one-legged stance were also found for one-legged stance tests. Only the length of the test differs in different studies [17]. Johnsson et al., 2004 [17] suggest the position of arms to be kept along the body if possible. According to Shirley Ryan AbilityLab [18], the unloaded leg is supposed to be flexed. Several positions of the body during the one-legged stance were described by Prior

et al., 2014 [19]. The upright standing was described as a position in which the subject stands on the loaded leg with the right acromion, right greater trochanter, and right lateral malleolus vertically aligned ( $\pm 10^\circ$ ), with the loaded leg slightly flexed in the knee joint ( $\pm 10^\circ$ ), arms folded, head stable and eyes looking forward at a fixed point. The position of the unloaded leg was not described. However, from the pictures, it can be seen that the leg was flexed in the hip and knee, and the foot of the unloaded leg was kept behind the loaded leg with toes only a few centimetres above the ground.

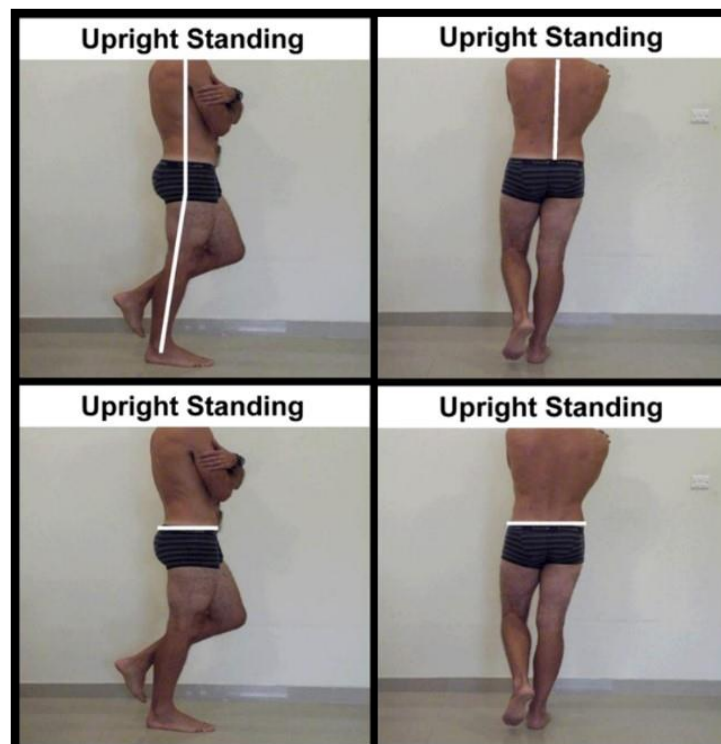


Figure 4: Upright standing position according to Prior et al., 2014. Adapted from Prior et al., 2014 [19]

The One-legged stance can be used as a test of balance or as a test for people with disabilities. A poor performance in the one-legged stance is connected with an increased chance of falls and injuries. One-legged stance balance was investigated by Johnsson et al., 2004. The stance was performed for 30 seconds after the lift-off of the swing leg. Balance was evaluated according to the ground reaction force. It was shown that the stance can be divided into a dynamic phase, lasting the first five minutes, and a static phase following the dynamic one. The dynamic phase is characterised by a larger and rapidly decreasing variability of the ground reaction force. In the static phase, the variability of the ground reaction force levels off as the standing person gains a steady position. The measured value of the variability during the static phase significantly differed between the young and the



elderly group, with a median of approximately 0,5% and 0,8% of body weight, respectively. It was suggested that the first five seconds are crucial when assessing balance during the one-legged stance. [17]

The one-legged stance was suggested to be a representative body position for the long-term effect of hip contact stress. It was shown that the contact stress distribution during the one-legged stance is very similar to the averaged stress distribution during a gait cycle. [5]

A measurement of resultant hip force and its components during the one-legged stance can be seen in Figure 5. The measurement was performed in the same patient as the measurement of a gait cycle shown in Figure 3. It can be seen that the resultant hip force during the one-legged stance reaches higher values than the peak value of the resultant hip force during the gait cycle.

Thigh muscle injuries commonly occur during single leg loading tasks and patterns of muscle activation are thought to contribute to these injuries. [19]

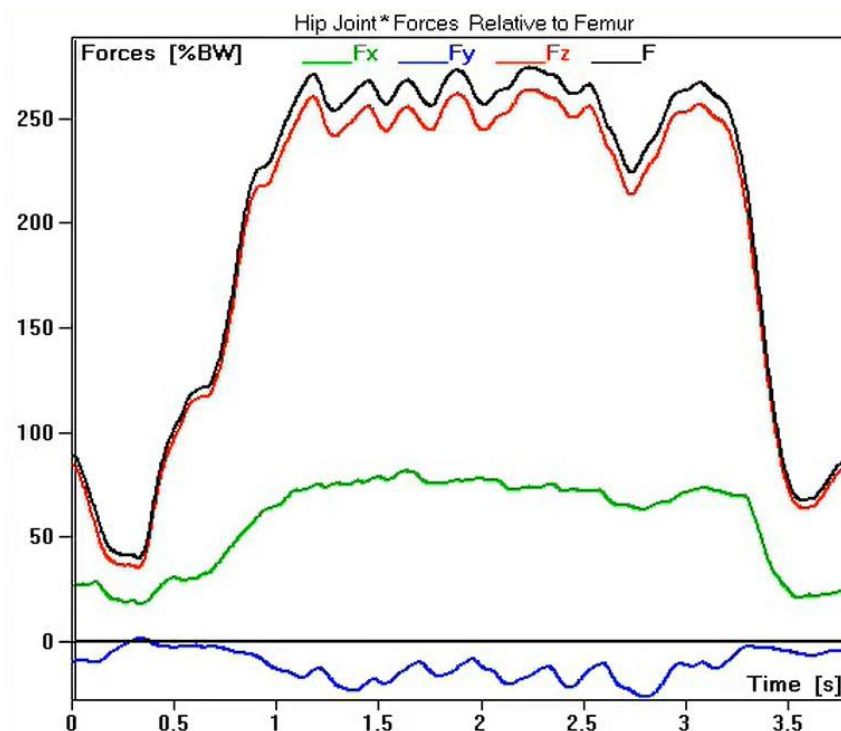


Figure 5: Resultant hip force and its components during one-legged stance with the swing leg in the hip flexion position in "KWR" patient. Adapted from "Database « OrthoLoad" [16]

## 2.4. Determination of the resultant hip force

The resultant hip force can be estimated either by direct in vivo measurements, as shown in previous chapters, or by mathematical modelling. In general, to determine the resultant hip force in a static position, the equilibrium must be solved:

$$\vec{R} + \vec{W} + \sum \vec{F}_i = \vec{0} \quad (1)$$

$$\vec{r}_W \times \vec{W} + \sum \vec{r}_i \times \vec{F}_i = \vec{0} \quad (2)$$

where the resultant hip force  $\vec{R}$  and magnitudes of the  $i$ -th muscle forces  $\vec{F}_i$  are unknown variables,  $\vec{r}_W$  is a moment arm of a weight force  $\vec{W}$  and  $\vec{r}_i$  is a moment arm of the  $i$ -th muscle force  $\vec{F}_i$ . In more complex models, forces of passive structures like tendons and ligaments could also be considered.

General problem denoted as the muscle redundancy is that the number of unknown muscle and joint forces exceeds the number of equilibrium equations. It means that the system of equations (1) and (2) is mathematically indeterminate. Such a mechanical system may be said to be underspecified, i.e. there is an infinite number of solutions. To tackle this limitation, two strategies are used. The first type of models solves the system of linear equations using reduction methods. The models are simplified, containing fewer muscles to achieve the same number of unknown variables as equations. The second type of models postulates the existence of further constraints, e.g. provides a cost function that values individual solutions. The cost functions in biomechanics are denoted as performance criteria, and then it is assumed that the body activates muscles for a given activity to maximize performance. The system of linear equations is then solved by optimization methods.

After the forces of individual muscles contained in the model are obtained by solving the equation (1) using either reduction or optimization methods, the resultant hip force can be obtained from the force equilibrium (2).

## 2.5. Models using optimization methods

If the number of unknown variables exceeds the number of equations of equilibrium, the solution becomes mathematically indeterminate, and it is necessary to use an optimization method. The larger number of variables allows to incorporate a larger number

of muscles into a model, which allows the model to be more complex and closer to the real anatomy. These models aim to get as close to reality as possible, not only in the human body's anatomy but also in physiology.

OpenSim [20], [21] and AnyBody [22] are softwares that can be used for many types of musculoskeletal modelling and simulations, including computations of resultant hip force in the static one-legged stance position. This work was focused on the models available for OpenSim software. OpenSim is a freely available, user-extensible software system that lets users develop models of musculoskeletal structures and create dynamic simulations of movement [23]. The musculoskeletal models are written in XML code with .osim extension. The musculoskeletal models consist of bones and muscles, both with many given attributes. OpenSim was not used directly in this work, but the models served as source files. The way the models are built is described in section 4. along with the implementation in this work. A visualization of an OpenSim model can be seen in Figure 12.

In general, any optimization problem can be solved in three steps. Firstly, an optimization function containing the unknown variables is established. Afterwards, equality and inequality constraints related to the unknown variables are introduced. Also, boundaries of the unknown variables can be set. And finally, the solution of the problem is found by maximizing or minimizing the objective function. Mathematically, the optimization problem can be formulated as follows: [24]

$$\text{minimize/maximize } f(x) \quad (3)$$

$$\text{subject to: } h_i(x) = 0 \quad (4)$$

$$g_i(x) \leq 0 \quad (5)$$

$$B_L \leq x_k \leq B_U \quad (6)$$

$$\text{where: } i = 1, 2, 3, \dots I \quad (7)$$

$$j = 1, 2, 3, \dots J \quad (8)$$

$$k = 1, 2, 3, \dots K < I \quad (9)$$

where  $f(x)$  is an objective function, also called a cost function or performance criterion, which can be either maximized or minimized,  $h(x)$  is a function of equality constraints associated with the objective function that corresponds to torque equilibrium equations,

$g(x)$  is a function of inequality constraints associated with the objective function,  $x$  is a vector of unknown variables, i. e. muscle forces,  $B_L$  and  $B_U$  are lower and upper bounds for the unknown variables and  $E, I, K$  are numbers of equality and inequality constraints and unknown variables, respectively. [24]

The unknown variables represent anatomical structures, mostly only muscles for simplicity, but they can also represent other structures, such as ligaments or tendons. These structures are bounded by bounds based on physiology in order not to exceed limits of the human body. Bounds can be, for example, minimal or maximal muscle forces. The objective function can have a form of linear or nonlinear criteria and represents a physiological or biomechanical quantity, for example, muscle stress or energy consumption. The equality and inequality constraints can also have linear or nonlinear forms and are connected to kinematics or statics, for example, they can represent the beginning and end of a movement or a resulting torque in joints. [24]

An objective function, constraints and bounds can be formulated as follows, respectively:

$$\text{minimize } \sum_{i=1}^N w_i (\bar{F}_i)^p \quad (10)$$

$$\text{subject to } \overrightarrow{M}_{net} = \sum_{i=1}^N \vec{r}_i \times F_i \quad (11)$$

$$0 \leq F_i \leq F_{Ui} \quad (12)$$

where  $\vec{F}_i$  is a force of the  $i$ -th muscle,  $\vec{r}_i$  is a moment arm of the  $i$ -th muscle,  $\overrightarrow{M}_{net}$  is a net joint moment,  $F_{Ui}$  is an upper boundary of the force  $\vec{F}_i$  and  $w_i$  is a weighted factor of the unknown variables in the objective function. According to power  $p$ , the objective function is either linear or nonlinear. The nonlinear functions show better results if compared to EMG measurements and show better ability for physiologically realistic prediction of co-activation of muscles. [24]

In the appendix of Tsirakos et al., 1997 [24] is a comprehensive list of linear and nonlinear criteria of the objective function. Among the most cited ones belong:

$$\min \sum_{i=1}^N (F_i)^p \quad (13)$$

$$\min \sum_{i=1}^N \left( \frac{F_i}{PCSA_i} \right)^p \quad (14)$$

$$\min \sum_{i=1}^N \left( \frac{F_i}{F_{Ui}} \right)^p \quad (15)$$

where  $PCSA_i$  is a physiological cross-sectional area of the  $i$ -th muscle. The results of using these objective functions are also described in Tsirakos et al., 1997. Using the objective function from the equation (14) with  $p = 3$  was shown to be a suitable objective function for both static and dynamic tasks in Crowninshield and Brand, 1981 [25], [26]. The objective function represents the stress of muscles. It was also shown that it can predict the co-activation of muscles in a physiologically realistic manner.

Recent research by Nasr et al., 2021 [27] shows a possibility of replacing static optimization with an inverse muscle model using machine learning. In this research, a recurrent neural network (RNN) was developed to estimate the pattern of muscle activation signals from kinematic and dynamic data. The input parameters of the model are joint angle, joint velocity, joint acceleration, joint torque and activation torque. The output is a predicted EMG signal of muscles. The model yields a normalized regression between experimental data and estimated muscle activation in the range of 88–91%. The model was suggested to be used for real-time rehabilitation or sports evaluation devices. In Figure 6 can be seen the predicted EMG signals of muscle performance of upper extremity muscles during flexion and extension movement of shoulder compared with the measured signals.

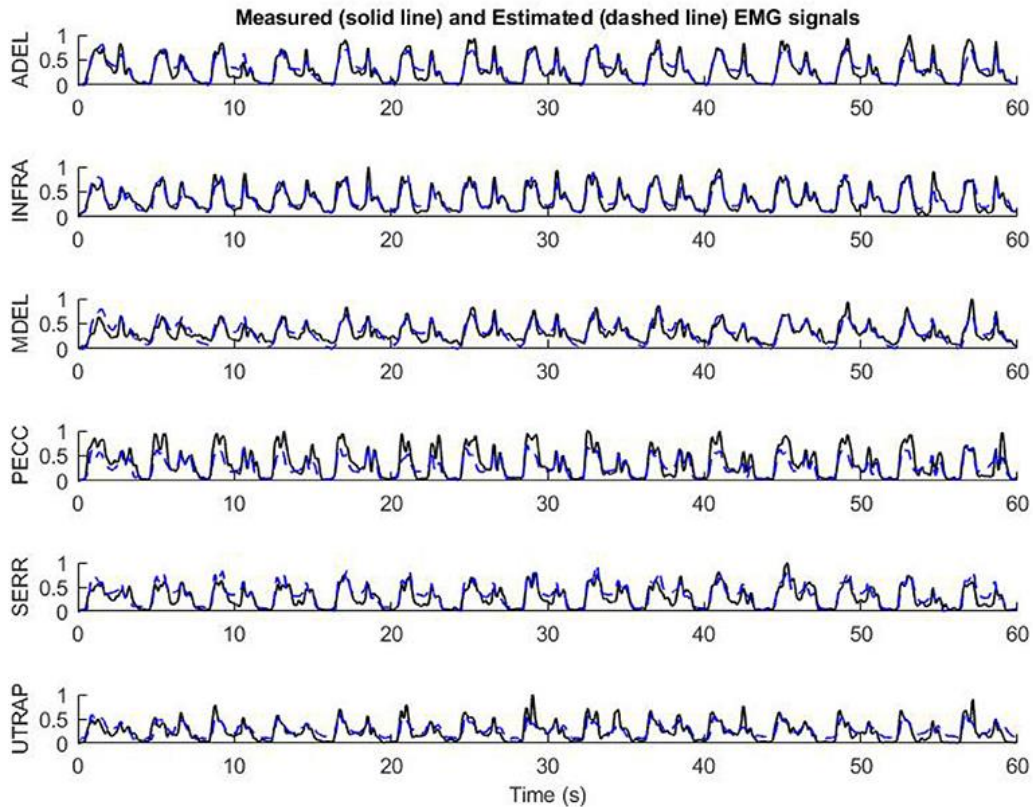


Figure 6: Difference between measured and estimated EMG signals using machine learning model. After Nasr et al., 2021 [27]

## 2.6. Models using reduction methods

The most simplified models of the hip joint are two-dimensional models of Pauwels [28], Debrunner [29] and Uršič [7]. In two dimensions, the system of equations (1) and (2) reduces to three equations, two for components of joint forces and one for torques. It implies that only one muscle representing the function of abductors exists in the model. The muscle originates from the pelvis and inserts on the greater trochanter, but the position of the origin differs for each model. These models are based on the one-legged stance. There are acting three forces in the hip joint: a force of the abductor muscle  $\vec{F}$  acting in the direction of the muscle, resultant hip force  $\vec{R}$  acting directly through the hip joint rotation centre and reduced body weight force  $\vec{W}_{red}$  (body weight force excluding the weight of loaded leg) acting vertically in the centre of mass. It is shifted in the direction of unloaded leg in the models of Pauwels [28] and Debrunner [29]. In Uršič's model [7], the shift of the centre of mass is neglected. [30]

The model according to Blumentritt [31] is also two-dimensional, however, it is based on a two-legged stance, contains two muscle groups (a pelvi-trochanteric group similar to

the abductor force of the previous models and a spino-crural group, which is the force of rectus femoris) and an additional dynamic (acceleration) force, which should be equal to zero for the static position. The model also contains reduced body weight force and resultant reaction force in the hip joint. [30]

Unlike the previous models, the model of Iglíč [32] is three-dimensional. The model is based on the one-legged stance and consists of reduced body weight, resultant hip force and nine muscle forces divided into three groups. The force of the  $i$ -th muscle  $\vec{F}_i$  can be calculated as follows:

$$\vec{F}_i = f_i A_i \vec{s}_i \quad (16)$$

where  $A_i$  is a relative cross-sectional area of the  $i$ -th muscle,  $\vec{s}_i$  is a unit vector in the direction of the  $i$ -th muscle and  $f_i$  is an average tension in the  $i$ -th muscle. It is assumed that the average tension is equal for each muscle in individual muscle groups. Therefore, there are three unknown variables of average tensions and three unknown variables of the reaction force vector. [32]

These models are adapted for each patient according to individual musculoskeletal geometry obtained from anteroposterior radiographs. The models of Pauwels [28], Debrunner [29], Blumentritt [31] and Iglíč [32] were compared by Eschweiler et al., 2012 [30], Eschweiler et al., 2017 [33] or by Asseln et al., 2013 [34]. Eschweiler et al., 2012 compared three digitally reconstructed radiographs in anteroposterior direction generated based on computed tomography datasets from three patients, while Eschweiler et al., 2017 evaluated X-Rays of patients undergoing a primary total hip arthroplasty before and after the operation. Asseln et al., 2013 compared X-Rays of three patients from the Orthoload database.

Uršič created the model to predict hips with increased risk for early coxarthrosis [7]. There were analysed 172 X-Ray images of hips that were subjected to Perthes disease in the childhood.

## 2.7. Scaling of musculoskeletal models

Scaling of musculoskeletal models is performed in order to match patient-specific anatomy. Bones in a model can be rescaled either by a single general or multiple rescaling factors specific to individual bones. [35] Another option is to create a musculoskeletal

model which can be adapted directly to computer tomography (CT), magnetic resonance or X-Ray scans. The scaling of a model influences the sizes of the bones as well as muscle attachments. It was shown that muscle lengths [35], muscle moment arms [35], [36] and muscle forces [37] could be predicted considerably differently by models based on magnetic resonance scans and by models based on generic scaling. [4]

Scaling of models based on generic scaling can be done either uniformly (isotropic scaling) or non-uniformly (anisotropic scaling). The isometric scaling assumes that the shapes of the bones and the proportional dimensions between the bones are very similar in every human. In that case, all bones are scaled by one characteristic parameter, for example, by width of the pelvis or by the interhip distance (the distance between centres of femoral heads). As opposed to that, in anisometric scaling, each bone can be scaled by its own parameter. [4]

In Hornová et al. [4], three different approaches to scaling were compared for a two-dimensional musculoskeletal model of the hip according to patient-specific data from anteroposterior radiograms. Two of them were isotropic and one of them was anisotropic. It was shown that when the hips were scaled anisotropically, the resultant hip force normalized by the body weight during the one-legged stance was statistically significantly lower and its variance was considerably higher. The isotropic scaling gave almost the same results of the resultant hip force generalized by the body weight for each patient regardless of the patient-specific input geometrical parameters. It indicates that the resultant hip force depends primarily on a reference musculoskeletal model. The reason is that muscle attachments were scaled in the same proportion in which the lever arm of the body weight force was scaled. The difference between the values of resultant hip force when scaled isotropically and anisotropically was up to a patient's body weight.

Isotropic and anisotropic scaling approaches can also be found in computer modelling. In Song et al., 2019 [38], three approaches to scaling a three-dimensional OpenSim model were suggested and compared. The first one was the least patient-specific, while the third one was the most. In the first one, called "generic", each bone segment was uniformly scaled according to its own scaling factor. This factor was derived from distance ratios between experimental and corresponding virtual markers using a Scale Tool in OpenSim. Virtual markers of an OpenSim model can be seen in Figure 12. In the second approach,



called “nonuniform”, the pelvis was scaled based on three scaling factors derived from the difference between CT scans in three dimensions (height, width and depth) and the baseline model. Other bone segments were scaled uniformly in the same way as previously. In the third approach, called “CT-Geometry”, the pelvis in the OpenSim model was entirely removed and replaced by a new one based on CT reconstructions. Other segments were scaled uniformly as previously. Hip joint centres were moved to patient-specific locations and muscle attachments were updated using patient-specific pelvis geometry and anatomical descriptions. This approach is rather a definition of a new model than a scaling method. The resultant hip force using these approaches was calculated using an OpenSim model during a gait cycle. It was not found in the article which model was used, but it can be assumed that it was Harris et al. 2017 [39], since Michael D. Harris is one of the co-authors of the research paper and since the model citation [39] several times occurs in the paper. A comparison of the resultant hip force for the three approaches can be seen in Figure 7 for patients belonging to a control group. The Grey shaded area represents  $\pm 1$  standard deviation, and highlighted vertical bands indicate the time of the peak force during early stance and mid-to-late stance, respectively.

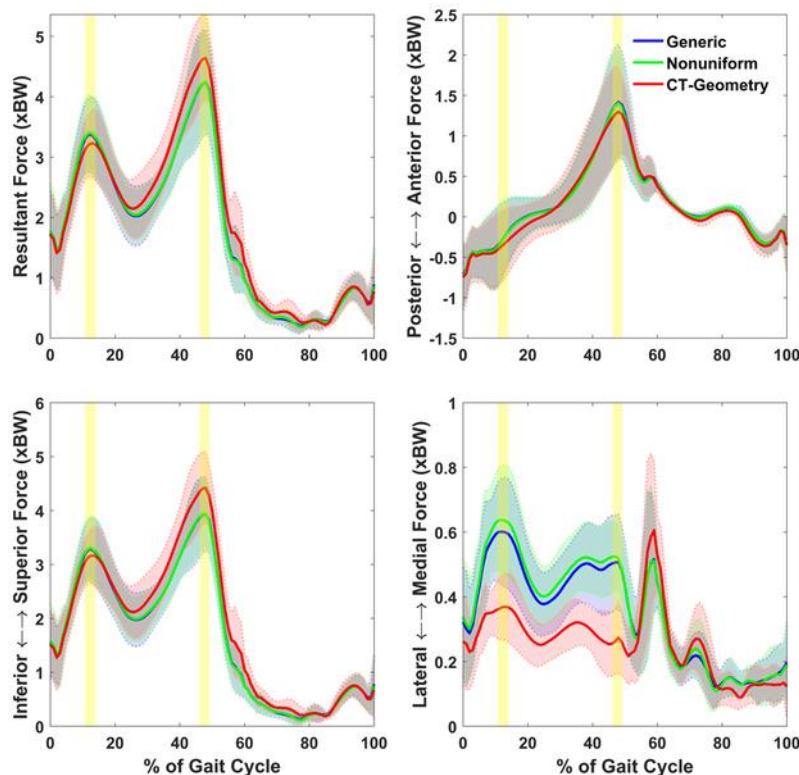


Figure 7: Average resultant hip force and its components during a gait cycle in the control group.  
After Song et al., 2019 [38]

## 2.8. EMG measurements of muscle activity during the one-legged stance

Electromyography (EMG) is a technique which can be used to measure muscle activity. It is performed by two electrodes either on the surface of the skin in case of superficial muscles or by inserting them into the muscle through the skin in the case of deep muscles.

The EMG signal needs to be normalized to obtain results that can be compared. Between normalization techniques belong, for example, one-legged stance or maximal voluntary isometric contraction (MVIC), which is probably the most common normalization technique. Its advantage is that it compares how active a muscle is relative to its maximal capacity. However, that is also a disadvantage because the measured person must be able and willing to use maximum strength. Other methods can also be found, for example, the submaximal voluntary contraction method used in Prior et al., 2014 [19]. [40]

The literature provides limited information regarding EMG measurements of muscles in the hip area (originating from the pelvis and inserting into the femur, tibia or patella) during the one-legged stance.

In Bolgla et al., 2011 [41], the activity of some muscles was measured in women with patellofemoral syndrome. The activity of gluteus medius in women belonging to the control group was around 9% of MVIC.

The activity of the lower extremity and trunk muscles during a performance of a Y-Balance test was measured by Kaur et al., 2022 [42]. This test is performed while standing on one leg, however, the measured person moves with the other leg, and the test is used to measure dynamic balance, functional symmetry and stability of the lower extremity. The standing and measured leg was the one on which the participant would stand to kick a ball. The participant moved the other leg in anterior, posterolateral, and posteromedial directions. Table 1 shows the results of measurements of muscles in the hip area when the participant was standing on a stable surface. The muscle activity is given as the percentage of MVIC.

<b>Directions</b>	<b>Anterior</b>	<b>Posterolateral</b>	<b>Posteromedial</b>
<b>Muscles</b>	<b>Mean ± SD</b>	<b>Mean ± SD</b>	<b>Mean ± SD</b>
Gluteus maximus	10.5 ± 6.4	12.9 ± 7.6	11.8 ± 6,0
Gluteus medius	35.5 ± 25.7	23.4 ± 15.1	36.5 ± 19.2
Medial hamstrings	30.8 ± 17.5	18.1 ± 10,4	19.3 ± 10,3
Biceps femoris	19.3 ± 10.9	23.6 ± 12.9	15.3 ± 8.8
Rectus femoris	32.0 ± 22.8	33.2 ± 27,1	42.4 ± 32.8

*Table 1: Muscle activity normalized by MVIC during the Y-Balance test. Adapted from Kaur et al., 2022 [42]*

Muscle activity during the one-legged stance was also measured by Prior et al., 2014 [19]. They measured how the position of the pelvis and trunk influences the activity of several muscles. A drawback of that measurement for this work is how the EMG signal was normalized. It was not normalized by MVIC, but signals from different postures were normalized to an “upright standing” reference posture (shown in Figure 4), which is a submaximal voluntary contraction normalization method. Therefore, it is not possible to compare the results of muscle activity with any other measurements. However, from the results of EMG measurement in the “upright standing” position, it is still possible to compare values of the measured EMG signal (root mean square over a stable four-second period) between the muscles during this particular measurement. The results are shown in Table 2.

<b>Muscle</b>	<b>Mean ± SD (SEM)</b>
Adductor longus	4.87 ± 1.80 (2.46)
Biceps femoris	18.76 ± 22.77 (7.93)
Gluteus maximus	9.25 ± 7.12 (2.65)
Gluteus medius	25.08 ± 18.34 (3.15)
Rectus femoris	26.28 ± 27.93 (10.03)
Semitendinosus	17.71 ± 12.68 (9.41)
Tensor fasciae latae	47.96 ± 31.09 (11.78)

*Table 2: Values of EMG signal measured during upright standing in the one-legged stance. Adapted from Prior et al., 2014 [19]*

In the work of Norcross et al., 2010 [40], the focus was aimed at EMG normalization techniques. EMG signal of some muscles during the one-legged stance was measured. In Figure 8 can be seen filtered EMG signal from five muscles in the hip area.

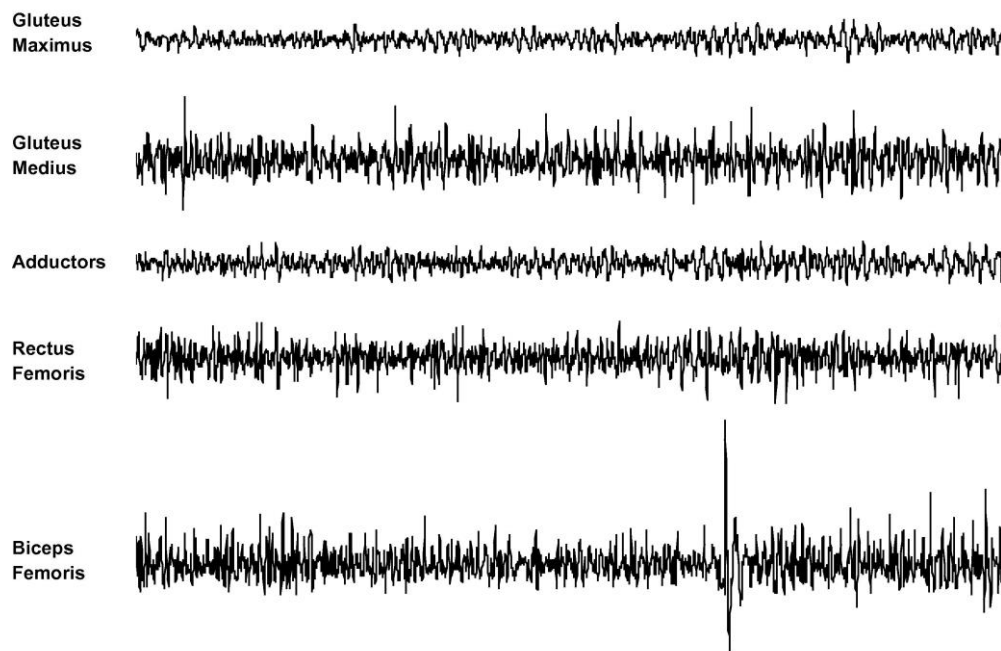


*Figure 8: Three seconds of filtered EMG signal during the one-legged stance. After Norcross et al., 2010 [40]*

## 2.9. Hip dysplasia

Hip dysplasia is a hip disorder caused by not fully or wrongly developed acetabulum, which cannot adequately contain and support the femoral head. If left untreated, hip dysplasia can result in arthritis of the hip joint. It can be present from birth but can also be developed during adulthood. The surgical treatment for hip dysplasia is called a periacetabular osteotomy. [43]

Several approaches to how to perform the periacetabular osteotomy exist. In general, the pelvis is cut in several places around the acetabulum, turned and placed in a more convenient position. Afterwards, the pelvis is secured with screws. [44]

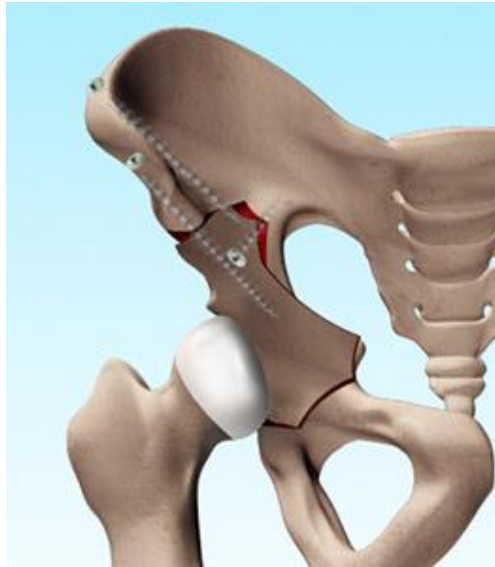


Figure 9: Periacetabular osteotomy. After [45]

From the biomechanical point of view, hip dysplasia can be estimated based on several criteria. Historically, a hip was considered dysplastic if the lateral centre-edge angle (also known as Wiberg angle) decreased below twenty degrees. This angle can be easily estimated from X-Ray scans. [46]

A newer approach is based on mathematical modelling. HIPSTRESS model for force and stress is a two-dimensional model using reduction methods was used to analyse dysplastic hips by Mavčič et al., 2002 [47] and Pompe et al., 2003 [48]. The model is based on the one-legged stance (which is considered a representative body position for the long-term effect of hip contact stress [5]) and is evaluated according to anteroposterior radiographs. Parameters introduced for the assessment of hip dysplasia were peak contact hip stress normalized by the body weight  $p_{max}/W_B$  and hip stress gradient index normalised by the body weight  $G_p/W_B$ . Drawback of these parameters was that they were dependant on the radius of the femoral head. Its size isn't always known because of the unknown magnification of an X-Ray image. Therefore, the parameters were further normalized by the radius by Uršič et al., 2021 [7], resulting in dimensionless peak contact hip stress  $p_{max}r^2/W_B$  and dimensionless hip stress gradient index  $G_p r^3/W_B$ . It was suggested that dysplastic hips are those, for which  $p_{max}r^2/W_B > 2$  [7] or  $G_p r^3/W_B > 0$  [48].

### 3. Aim of the work

The previous studies indicate that the individual geometry of the hip or the scaling method might considerably influence the resultant hip joint. Although several models of the hip region have been introduced, there is little information on how the results of these models could be compared. Therefore the primary aim of the thesis was to quantify to which extent the choice of the musculoskeletal model influences the resultant hip force.

As this work focused on calculating the resultant hip force using models using optimization methods, for which the anatomy is based on OpenSim models, another goal was to compare forces in muscles acting in the hip joint area and compare calculated forces with the measurements from the literature. For the purpose of the study, the following hypotheses were established:

**Hypothesis 1: The resultant hip force is determined mainly by equilibrium equations and does not differ considerably if all models are scaled for one patient.** It was shown that there is a considerable difference in the resultant hip force between patients. However, if the models were scaled uniformly for all patients, the difference in hip joint loading was negligible. [4] As the models have similar muscle groups and should oblige the same equilibrium equations, it was assumed that by scaling the models to the same patient, the difference in the hip joint loading determined by individual models would be slight.

**Hypothesis 2: Anatomically more accurate models will provide a more realistic estimation of the hip joint loading than models with fewer muscles.** There are two types of models that can be used for the determination of the resultant hip force (described in sections 2.5 and 2.5). It was hypothesised that since the anatomy of models in the OpenSim database is based on real measurements and since they contain more muscles than the models using reduction methods, the resultant hip force calculated in the models using optimization methods would be more accurate to the actual measurements.

**Hypothesis 3: Incorporating passive muscle tension will increase the hip joint loading.** Human resting muscle (myofascial) tone is the passive tension of skeletal muscle that derives from its intrinsic (EMG-silent) molecular viscoelastic properties. [49] The passive tension is usually neglected in biomechanical models. Therefore, a minimum muscle activity was set for the muscles to represent the passive tension. It was expected

that with higher muscle passive tension, the muscle forces and the resultant hip force would also increase.

**Hypothesis 4: The resultant hip force will be lower in models with a higher number of muscles.** The expectation was based on a hypothesis that if a model has a greater number of muscles, it is possible to better distribute forces to the muscles, resulting in a lower resultant hip force.

**Hypothesis 5: Individual muscle forces will differ considerably between models.** OpenSim models consist of several muscles, which may subsequently be composed of many segments (fibres). The aim was to find a way how to calculate a resultant force in a muscle and compare the muscle forces between models. Considering many drawbacks of the EMG measurements found in the literature (described in section 2.8), it was expected that according to the results from Norcross et al., 2010 [40], Kaur et al., 2022 [42] and Prior et al., 2014 [19], the most active muscles with the highest forces would be gluteus medius and rectus femoris. The lowest forces and muscle activity were expected in the gluteus maximus and adductor muscles. According to Prior et al., 2014, it was expected that high forces would also be found in tensor fasciae latae. However, the individual muscle involvement depends on the torque generating capacity of the individual muscle, which might differ between the models. In addition, each model contains a different number of muscles and muscle fibres, which may include variations in geometry. Therefore, it was assumed that the muscle forces would vary between the models as well.

The thesis composes of two main parts. While the first part focuses on a comprehensive analysis of different types of musculoskeletal models, the aim of the second part was to select a model for clinical study based on the previous analysis and suitability for the purpose. The clinical study was a part of ongoing research on hip dysplasia at the University of Ljubljana. The aim was to evaluate the hips of patients who underwent a periacetabular osteotomy according to a mathematical model. The model chosen for the study was a two-dimensional HIPSTRESS model using reduction methods. The reasons for this choice are described in section 4.4.1. As it had already been shown that such a model can predict hip dysplasia very well, the primary purpose of this study was to investigate whether the periacetabular osteotomy has an impact not only on the operated hip but also on the unoperated hip on the contralateral side. The aim was to determine whether changing the

geometry of the hip by performing a surgery improves, worsens or preserves the contralateral hip unchanged.



## 4. Methods

### 4.1. Source of models

The criteria differed depending on whether the model was based on optimization or reduction methods. The criteria for models based on the reduction methods was that the model had to be based on the one-legged stance.

The choice of models based on optimization methods was limited to the models available for the OpenSim software. The models were searched in OpenSim Documentation [6]. The documentation includes OpenSim core models maintained by the OpenSim team at Stanford University and models contributed by members of the OpenSim community. On the 24<sup>th</sup> of May 2022, a total of 37 models were available in the documentation. The models had to fulfil the following criteria:

- To be a human musculoskeletal model.
- To contain muscles in the hip area, i.e., originating from the pelvis and inserting into the femur, tibia or patella.
- To be still supported and to be downloadable

Some models were based on others, only developing them further but remaining unchanged in the hip joint area, containing the same muscles with the same parameters. These duplicate models were also excluded from the analysis. Two additional models were excluded during the analysis because they contained too few muscles that it was not possible to solve the optimization problem.

In total, four models based on reduction methods and twelve models based on optimization methods were used for the analysis.

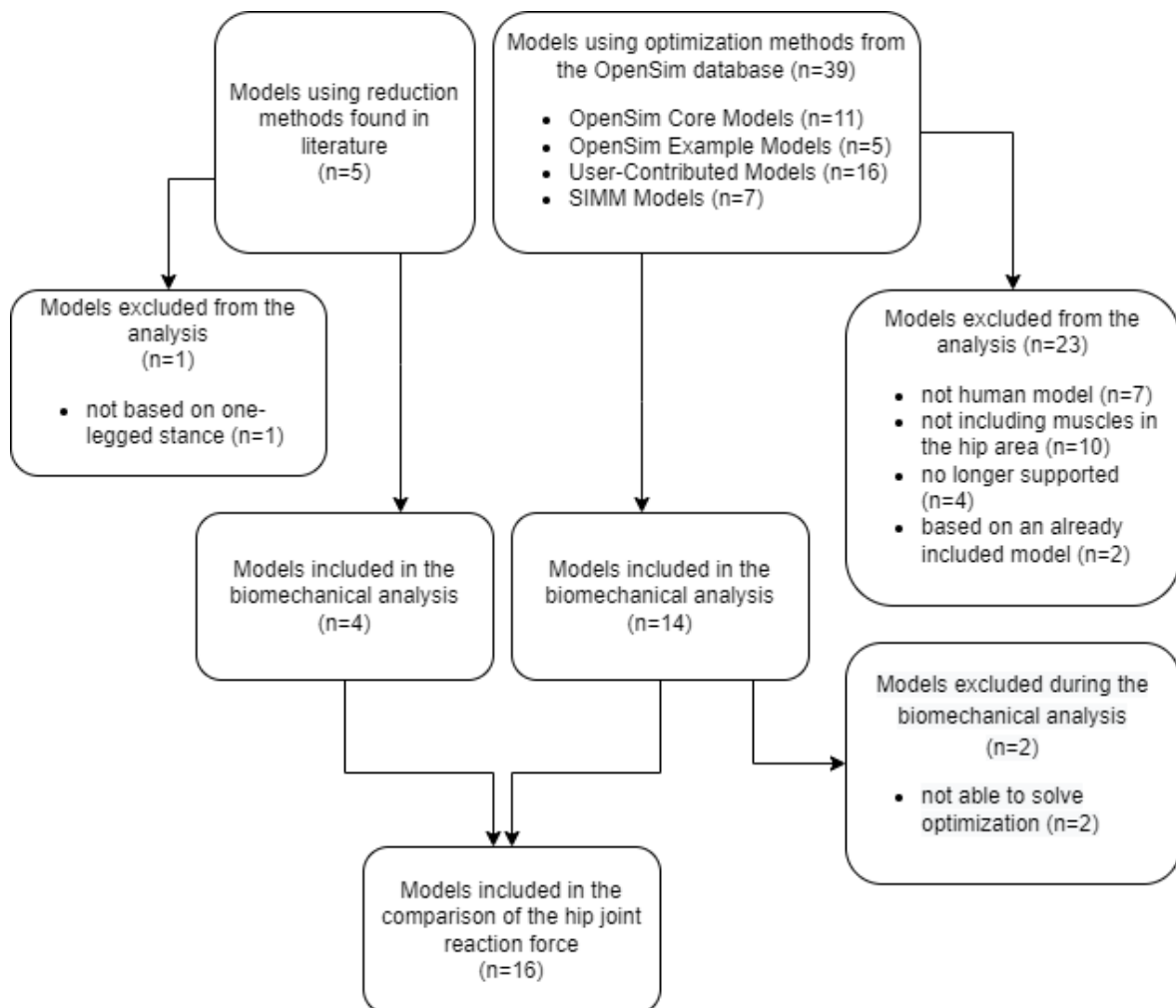


Figure 10: Flow diagram of the choice of models

## 4.2. Determination of the resultant hip force

The aim of this work was to compare muscle forces and the resultant hip force estimated from chosen musculoskeletal models. The models based on reduction methods and models based on optimization methods were included in the study. The predicted loading forces were further compared with the results of in vivo measurements. The following chapters describe the calculation processes and procedures for obtaining the data from measurements.

## 4.3. Resultant hip force according to models using optimization methods

According to the criteria, twelve models from the OpenSim database were used for the analysis. They are listed in Table 3. OpenSim core models were named by their names from the OpenSim documentation and user-contributed models were named after their authors

and related articles' publication dates. It is also stated where the model was downloaded from and how many muscles and muscle fibres it contains.

<b>Model number</b>	<b>Model name</b>	<b>Number of fibres</b>	<b>Number of muscles</b>	<b>Available from, cited papers</b>
1	Arnold et al., 2010	28	19	<a href="https://simtk.org/projects/lowlimbmodel09">https://simtk.org/projects/lowlimbmodel09</a> , [50]
2	Hamner et al., 2010	27	19	<a href="https://simtk.org/projects/runningsim">https://simtk.org/projects/runningsim</a> , [51]
3	Rajagopal et al., 2016	25	16	<a href="https://simtk.org/projects/full_body">https://simtk.org/projects/full_body</a> , [52]
4	Lai et al., 2017	25	16	<a href="https://simtk.org/projects/model-high-flex">https://simtk.org/projects/model-high-flex</a> , [53]
5	Modenese et al., 2011	95	23	<a href="https://simtk.org/projects/low_limb_london">https://simtk.org/projects/low_limb_london</a> , [54]
6a	Bruno et al., 2015 female	28	14	<a href="https://simtk.org/projects/spine_ribcage">https://simtk.org/projects/spine_ribcage</a> , [55]–[57]
6b	Bruno et al., 2015 male	28	14	<a href="https://simtk.org/projects/spine_ribcage">https://simtk.org/projects/spine_ribcage</a> , [55]–[57]
7	Harris et al., 2017	27	20	<a href="https://simtk.org/projects/hip_muscles">https://simtk.org/projects/hip_muscles</a> , [39]
8	Shelburne et al., 2010	27	20	<a href="https://simtk.org/projects/hip_muscles">https://simtk.org/projects/hip_muscles</a> , [39]
9	Raabe et al., 2016	37	19	<a href="https://simtk.org/projects/fullbodylumbar">https://simtk.org/projects/fullbodylumbar</a> , [58]
10	Gait2392	27	19	Included in the download package with OpenSim
11	Gait2354	18	14	Included in the download package with OpenSim

*Table 3: List of models downloaded from OpenSim and used for the analysis*

Each model was created for a different application. Therefore, there are considerable differences between them. The differences can be found in the number of muscles included, the number of muscle fibres representing a muscle, the maximal isometric forces of muscle fibres and the weight of body segments.

The difference in the way the muscles are modelled can be seen in the following example. There is a comparison of the number of muscle fibres and their maximal isometric forces for gluteus medius. The comparison is made between Arnold et al., 2010 model, which contains 28 muscle fibres, and Modenese et al., 2011 model, which is the model with the highest number of muscle fibres, 93 in total. Gluteus medius in Modenese et al., 2011 is created by more muscle fibres with lower maximal isometric force per each of them but similar on the whole muscle, if related to the weight force, as can be seen in Table 4.

Gluteus medius is illustrated in Figure 11 for both models to understand better how the muscles are modelled.

Muscle name	Arnold et al., 2010	max ISO Force [N]	Modenese et al., 2011	max ISO Force [N]
Gluteus medius	glmed1_r	881	GLUT_MED_ANT_1_R	234
	glmed2_r	617	GLUT_MED_ANT_2_R	234
	glmed3_r	702	GLUT_MED_ANT_3_R	234
			GLUT_MED_ANT_4_R	234
			GLUT_MED_ANT_5_R	234
			GLUT_MED_ANT_6_R	234
			GLUT_MED_POST_1_R	375
			GLUT_MED_POST_2_R	375
			GLUT_MED_POST_3_R	375
			GLUT_MED_POST_4_R	375
			GLUT_MED_POST_5_R	375
			GLUT_MED_POST_6_R	375
<b>Total max ISO force [N] *</b>		<b>2062</b>		<b>3446</b>
<b>(per body weight)</b>		<b>(27,5)</b>		<b>(27,8)</b>

Table 4: Comparison of gluteus medius muscle segments in Arnold et al., 2010 and Modenese et al., 2011 models (\*Total max ISO force is calculated as a vector sum, viz section 4.3.9)

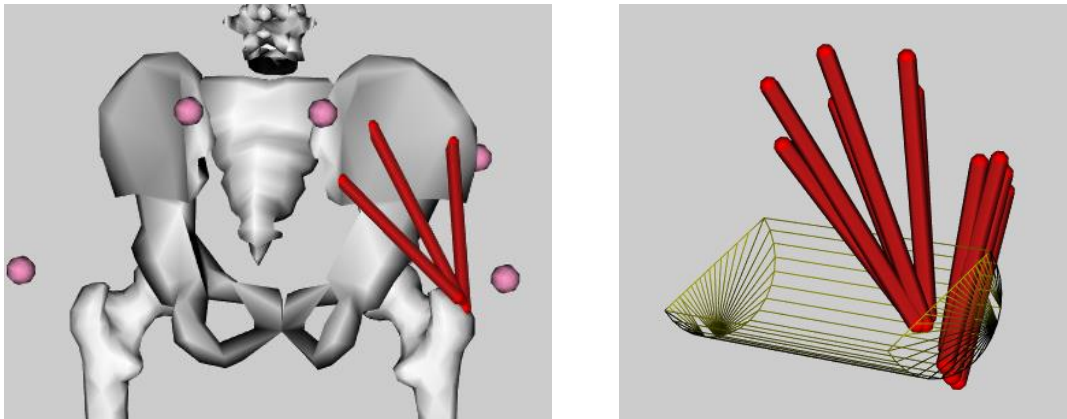


Figure 11: Comparison of gluteus medius muscle fibres in Arnold et al., 2010 and Modenese et al., 2011 models

#### 4.3.1. Calculation of the resultant hip force - process overview

One-legged stance is considered to be a representative static body position for the calculation of the hip contact stress distribution [5]. In this work, the posture of the models was standing upright on both legs with arms alongside the body. The one-legged stance was accomplished by removing one leg during the calculation steps. A slight pelvis rotation in the frontal plane during the one-legged stance was neglected.

While standing on one leg, several forces are acting in the hip joint. There is a body weight force excluding the weight of the loaded leg  $\vec{W}$ , forces of muscle fibres originating from the pelvis and inserting into the femur, tibia or patella  $\vec{F}_i$  and a resultant hip force  $\vec{R}$ . Equations for equilibrium in the hip are:

$$\vec{R} + \vec{W} + \sum \vec{F}_i = \vec{0} \quad (17)$$

$$\vec{r}_W \times \vec{W} + \sum \vec{r}_i \times \vec{F}_i = \vec{0} \quad (18)$$

where  $\vec{r}_W$  is a moment arm of the weight force and  $\vec{r}_i$  is a moment arm of the  $i$ -th muscle fibre force. All forces and moment arms need to be acting in the same coordinate system, which was decided to be the coordinate system of the right femur.

As there are more unknown variables (the resultant hip force and muscle fibre forces) than equations, the problem is statically indeterminate, and the equilibrium needs to be solved by an optimization method. The equation (18) was solved by Python's optimization tool `scipy.optimize.minimize` using SLSQP (Sequential Least Squares Programming) solver [59]. The optimization criterion used was:

$$\min \left( \sum \left( \frac{F_i}{F_{i \max}} \right)^3 \right) \quad (19)$$

where  $F_{i \max}$  is the maximal isometric force of the  $i$ -th muscle fibre. The optimized muscle fibre forces were inserted into (17) and the resultant hip force was calculated. All the forces were finally divided by the body weight to obtain relative forces, which can be compared between individual models.

OpenSim models are stored in files ending with `.osim` extension. They are written in XML language. For extracting data from the files, Python's `lxml` toolkit [60] was used.

#### **4.3.2. One-legged stance position and scaling of models**

As described in section 2.3, there is no detailed description of how the one-legged stance should be performed and measured. For this reason, and for simplicity, each model was kept in its anatomical position. That is an upright standing posture with both legs on the ground and arms alongside the body. The one-legged stance was accomplished by removing the left leg from calculation steps. Additionally, as suggested by Iglíč [32], the

pelvis should be slightly rotated by  $0,5^\circ$  in the frontal plane laterally above the loaded leg. That was neglected for simplicity.

The anatomical position of models can be seen in Figure 12 on an example of Raabe et al., 2016 model. Bones have white colour, muscles are coloured white, by blue colour are illustrated wrapping objects and pink dots represent a marker set, which is used for scaling the model based on experimentally obtained data.

The coordinate system of each model is the same, the x-axis representing the sagittal axis pointing anteriorly, the y-axis representing the longitudinal axis pointing superiorly and the z-axis pointing laterally to the right side of the body representing the horizontal axis.

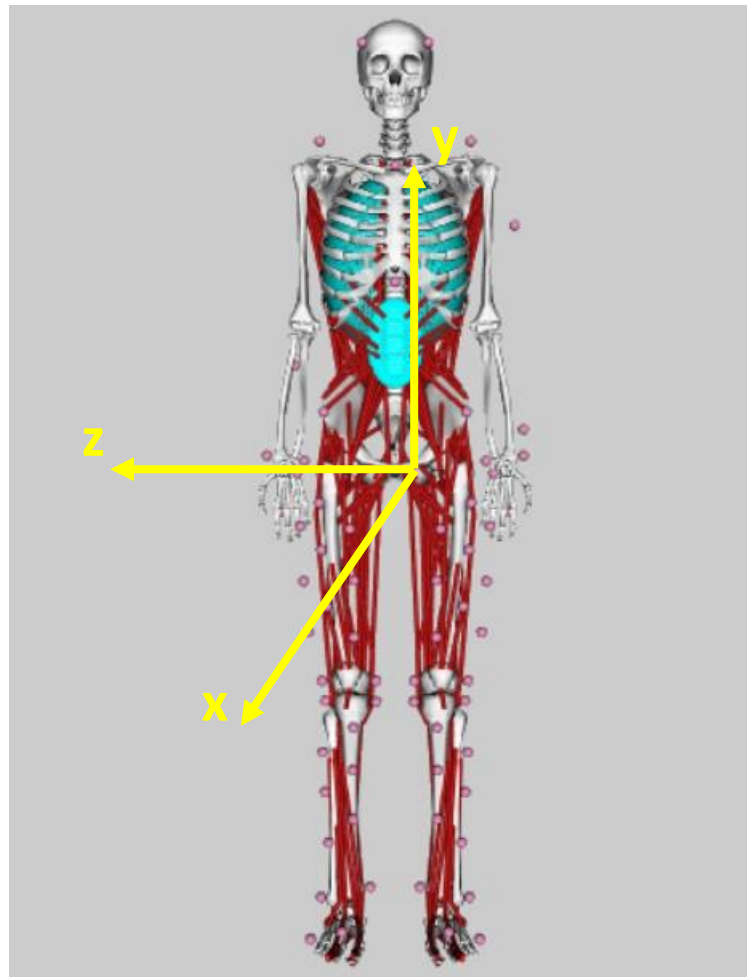


Figure 12: Raabe et al., 2016 model in the anatomical position

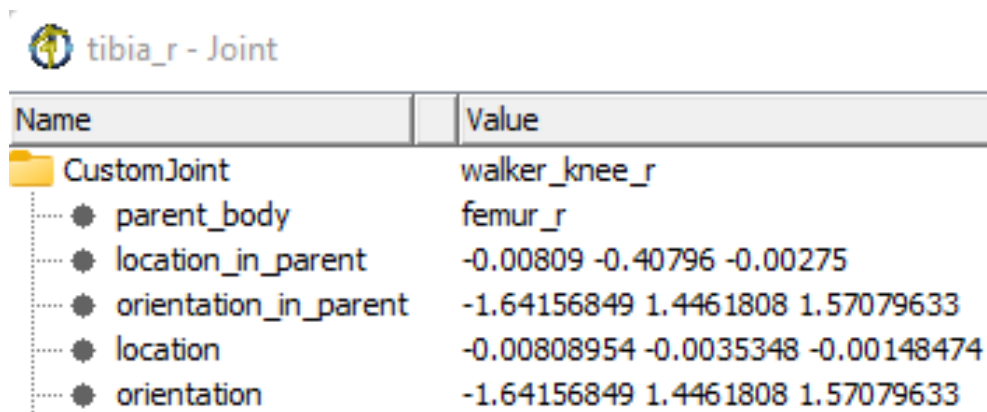
The scaling of a model is used to match the anatomy of a particular patient. An effect of scaling, which is patient-specific, was described in section 2.7. Since there was no measurement of patients, the scaling could not be performed patient-specific. Therefore,

an isometric scaling was adopted for all models, where the interhip distance was equalized between the models.

### 4.3.3. Transformation of coordinates

In order to be able to calculate the equations for equilibrium (17) and (18), it was necessary to transform all muscle attachments to the same coordinate system, the one of the right femur, which was considered the loaded leg. It was also necessary to recalculate the positions of bodies' mass centres relative to the right femur's coordinate system.

The OpenSim model of the human body is divided into individual body segments. Each body segment has its coordinate system and inertial properties: mass, mass centre and moments of inertia. The segments are connected by joints defined by their position and connection between their parent and child bodies. For example, the knee joint's parent body is the femur and the child body is the tibia. The joint contains information about its location and orientation in both bodies. The location is given as a translation vector in  $x$ ,  $y$  and  $z$  coordinates and the orientation is given as Euler XYZ body-fixed angles  $\psi$ ,  $\nu$  and  $\varphi$ . An example of how the joint is defined can be seen in Figure 13 for the knee joint of the right leg. In Figure 14 can be then seen the whole topology view of Rajagopal et al., 2016 model. Other models are built in a very similar way. The tree nodes with brackets are bodies, and the tree nodes without brackets are joints that connect bodies. It can be seen that the topmost body is the ground which is connected to the pelvis, the topmost body of the musculoskeletal model.



Name	Value
CustomJoint	walker_knee_r
parent_body	femur_r
location_in_parent	-0.00809 -0.40796 -0.00275
orientation_in_parent	-1.64156849 1.4461808 1.57079633
location	-0.00808954 -0.0035348 -0.00148474
orientation	-1.64156849 1.4461808 1.57079633

Figure 13: Example of a joint (right knee) definition in Rajagopal et al., 2016 model

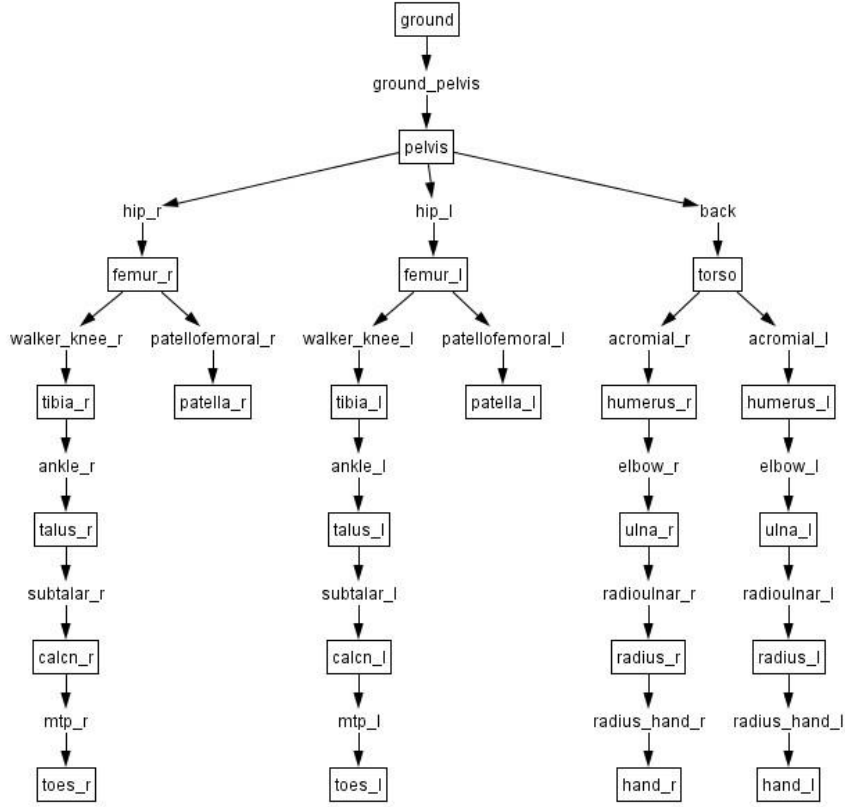


Figure 14: Topology view of the Rajagopal et al., 2016 model

The transformation from a child to a parent body can be performed according to the following equations:

$$T_{p-ch} = T_p T_{ch} \quad (20)$$

$$T_p = T_{xyz_p}(x_p, y_p, z_p) T_{xrot_p}(\psi_p) T_{yrot_p}(v_p) T_{zrot_p}(\varphi_p) \quad (21)$$

$$T_{ch} = (T_{xrot_{ch}}(\psi_{ch}) T_{yrot_{ch}}(v_{ch}) T_{zrot_{ch}}(\varphi_{ch}))^T T_{xyz_{ch}}(-x_{ch}, -y_{ch}, -z_{ch}) \quad (22)$$

where  $T_{p-ch}$  is a transformation matrix from a parent to a child coordinate system,  $T_p$  is a transformation matrix from a parent coordinate system to a joint and  $T_{ch}$  is a transformation matrix from a joint to a child coordinate system.  $T_{xyz}$  represents a translational transformation matrix in x, y and z coordinates and  $T_{xrot}$ ,  $T_{yrot}$ ,  $T_{zrot}$  are rotational transformation matrices about x, y and z axes, respectively. The resulting rotational transformation matrix for a child body is transposed because the angles represent the transformation from a child body to a joint, but the opposite way is required. For the same reason, the translations in x, y and z coordinates are negative.



A position of a point located in the coordinate system of a body can be expressed as a vector  $\vec{r}_{ch}$ . To recalculate this point to a parent's coordinate system as a vector  $\vec{r}_p$  can be done by using the calculated transformation matrix:

$$\vec{r}_p = \mathbf{T}_{p-ch} \vec{r}_{ch} \quad (23)$$

#### **4.3.4. Transformation of muscle attachments**

Muscles in OpenSim models are defined by attachment points of many types that create a muscle path. "Fixed points" are attachments which do not change their position in relation to their parent body. "Via points" are also not changing position relative to the parent body, but they are not directly connected to it. They are not always active, only when a specified joint angle reaches a certain range. "Moving muscle points" are attachments whose position relative to their parent body changes according to a function. "Wrap points" are attachments whose position changes relative to their parent body automatically by OpenSim to move on the surface of a wrapping object. Every muscle must be formed by at least two fixed points as the origin and insertion of the muscle. Other points serve for adjusting the muscle path. [61]

The attachment points could also be divided into anatomical and effective muscle attachments. The anatomical attachments are directly connected to the bone surface and therefore, they are the first and the last fixed points. However, the muscle path between anatomical attachments does not have to be representative for the mechanical effect of the muscle. The attachments that form the muscle path, which is representative for the mechanical effect of the muscle, are called effective attachments. The difference between anatomical and effective attachments can be seen in Figure 15. [62], [63]

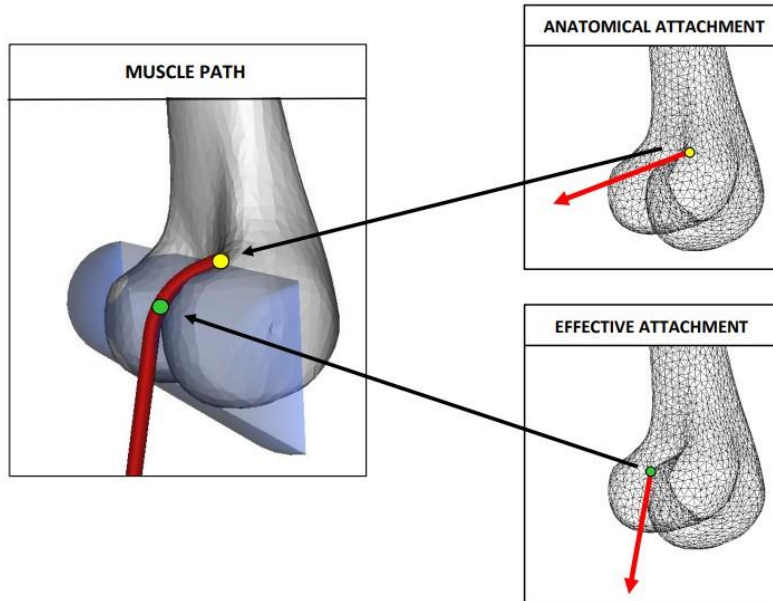


Figure 15: Difference between anatomical and effective attachments [62], [63]

For this work, effective attachments were used. They were obtained from OpenSim models files using MuscleForceDirection plugin [62], [63] available from [64].

In order to run the MuscleForceDirection plugin in OpenSim's Analyze Tool, it is required to insert a motion file with information on how individual joint angles change in time. A list of joint angles was extracted from models using Python and its lxml library. Their values were set to zero as the one-legged stance is a static pose in the anatomical position of the model. The muscles that do not originate from the pelvis and insert into the femur, tibia or patella were excluded from the analysis.

The attachments were obtained in the global coordinate system, i.e., in the coordinate system of the ground. The coordinate systems of the ground and pelvis merge. The transformation from the pelvis' to the femur's coordinate system was done by a simple translation because only the location in the parent is defined for the hip joint in every model. Since the transformation is done from the child body to the parent body, the translation is expressed in negative values. It means that the transformation of attachments from the global coordinate system to the femur's coordinate system was done by the following equation:

$$\overrightarrow{r_{femur}} = \mathbf{T}_{xyz_p}(-x_p, -y_p, -z_p)\overrightarrow{r_{pelvis}} \quad (24)$$

where  $\overrightarrow{r_{femur}}$  is a vector from the femur's coordinate system to the attachment and  $\overrightarrow{r_{pelvis}}$  is a vector from the coordinate system of the pelvis to the attachment.

#### 4.3.5. Transformation of the centre of mass

Each body segment contains information about its mass and its centre of mass with respect to its coordinate system. Therefore, calculating its position relative to the right femur's coordinate system is necessary. Since the right leg is the loaded leg, its mass does not contribute to the weight force acting in the hip joint. Therefore, the centre of mass is shifted laterally above the unloaded leg and slightly posteriorly.

Figure 14 shows that the pelvis is the topmost parent body for all segments contributing to the weight force. Positions of the centres of mass of the individual segments were recalculated relatively to the pelvis coordinate system according to the equations (20), (21), (22) and (23). The transformation from the pelvis to the right femur was performed the same way as it was done for the attachments originating on the pelvis: by translation according to the equation (24). The position of the shifted centre of mass is then calculated according to the equation (25), where  $\vec{r}_w$  is a vector from the right femur's coordinate system to the shifted centre of mass relative to the right femur's coordinate system,  $m_j$  is a mass of j-th body segment and  $\vec{r}_{wj}$  is a vector from the origin of the right femur's coordinate system to the centre of mass of the j-th body segment expressed in the coordinate system of the right femur.

$$\vec{r}_w = \frac{\sum m_j \vec{r}_{wj}}{\sum m_j} \quad (25)$$

#### 4.3.6. Calculation of torques

The torque of weight force is calculated as  $\vec{r}_w \times \vec{W}$ , where  $\vec{r}_w$  is a vector from the right femur's coordinate system to the shifted centre of mass relative to the right femur's coordinate system.  $\vec{W}$  is a weight force of the body without the loaded leg.

The torque of muscle forces is calculated as  $\sum \vec{r}_i \times \vec{F}_i$ , where  $\vec{r}_i$  is a vector from the right femur's coordinate system to the origin of the i-th muscle fibre relative to the right femur's coordinate system.  $\vec{F}_i$  is a muscle fibre force of the i-th muscle fibre. The equation for the torque of muscle forces can be rewritten as:

$$\sum \vec{r}_i \times \vec{F}_i = \sum (\vec{r}_i \times \vec{s}_i) F_i \quad (26)$$

where  $\vec{s}_i$  is a unit vector in the direction of the muscle fibre force  $\vec{F}_i$  and  $F_i$  is its magnitude, which is the subject of the optimization results. The unit vector  $\vec{s}_i$  has the direction of the  $i$ -th muscle fibre and was calculated as follows:

$$\vec{s}_i = \frac{\vec{s}_{di} - \vec{s}_{pi}}{|\vec{s}_{di} - \vec{s}_{pi}|} \quad (27)$$

where  $\vec{s}_{di}$  and  $\vec{s}_{pi}$  are coordinates of distal and proximal attachments of the  $i$ -th muscle fibre in the coordinate system of the right hip and  $|\vec{s}_{di} - \vec{s}_{pi}|$  is the length of the  $i$ -th muscle.

#### 4.3.7. Calculation of muscle forces

The equilibrium of the hip joint in the one-legged stance is defined by two vector equations, which means six equations in total. Since there are at least 17 muscle fibres in each analysed model influencing the equilibrium of the hip joint, the system is statically indeterminate. It means that there is an infinite number of solutions and an optimization criterion has to be used to solve the system. The equation for torque equilibrium (18) was solved in Python using the SLSQP solver of the `scipy.optimize.minimize` method. The minimum muscle fatigue criterion was used:

$$\min \left( \sum_i^N \left( \frac{F_i}{PCSA_i} \right)^3 \right) \quad (28)$$

Where  $PCSA_i$  is a physiological cross-sectional area of the  $i$ -th muscle fibre, and  $N$  is a number of muscle fibres in a given model. The cross-sectional area can be expressed as the product of the maximal isometric force of the  $i$ -th muscle fibre  $F_{i \max}$  and stress in muscles  $\sigma_{\max}$ :

$$PCSA_i = F_{i \max} \sigma_{\max} \quad (29)$$

Since  $\sigma_{\max}$  is considered to be the same for each muscle fibre, it does not influence the optimization results, and the minimum fatigue criterion can be rewritten to its final form as:

$$\min \left( \sum_i^N \left( \frac{F_i}{F_{i \max}} \right)^3 \right) \quad (30)$$

The muscle fibre force of the  $i$ -th muscle fibre cannot exceed its maximal isometric force and cannot be negative. Therefore, it was necessary to set boundaries for the optimized forces:

$$F_{i \min} \leq F_i \leq F_{i \max} \quad (31)$$

where  $F_{i \min}$  is a minimum force acting in the  $i$ -th muscle fibre and can be calculated as a product of the maximal isometric force of the  $i$ -th muscle fibre and a minimum muscle fibre activity  $a_{\min}$ , which cannot be lower than 0.

$$F_{i \min} = F_{i \max} a_{\min} \quad (32)$$

The equation (18) was set as the equality constraint. The result of the optimization process was the magnitude of each muscle fibre force  $F_i$  acting in the direction of the unit vector  $\vec{f}_i$ . The magnitudes were then divided by the weight force of the whole body to obtain a nondimensional value of the muscle fibre forces relative to the body weight.

#### 4.3.8. Calculation of resultant hip force and muscle activity

The muscle fibre forces  $\vec{F}_i$  obtained from the optimization were inserted into the equation (17) and the resultant hip force was calculated according to that as:

$$\vec{R} = -\vec{W} - \sum \vec{F}_i \quad (33)$$

The magnitude of the resultant hip force was then divided by the magnitude of the weight force of the whole body to obtain the relative resultant hip force.

The direction of the resultant hip force was described by angles  $\vartheta_{R \text{ FRONTAL}}$  in frontal plane and  $\vartheta_{R \text{ SAGITTAL}}$  in sagittal plane calculated as follows:

$$\vartheta_{R \text{ FRONTAL}} = \tan(-R_z / R_y) \quad (34)$$

$$\vartheta_{R \text{ SAGITTAL}} = \tan(R_x / R_y) \quad (35)$$

where  $R_x$ ,  $R_y$  and  $R_z$  are components of the resultant hip force. By  $\vartheta_{R \text{ FRONTAL}}$  is described how medially is the force acting in the frontal plane and by  $\vartheta_{R \text{ SAGITTAL}}$  is described how anteriorly the force is acting in the sagittal plane.

The muscle fibre activity of the  $i$ -th muscle fibre  $a_i$  means how much active the muscle fibre is during the one-legged stance. It can be calculated as the magnitude of calculated muscle force divided by the maximal isometric force of the  $i$ -th muscle fibre.

$$a_i = \frac{F_i}{F_{i \max}} \quad (36)$$

#### 4.3.9. Calculation of resultant muscle force and resultant muscle activity

Some muscles in the models are composed of several muscle fibres. The number of muscle fibres per muscle can differ for each model, which makes it difficult to compare these forces between the models. Therefore, the resultant muscle force of the  $k$ -th muscle  $F_{Mk}$  was introduced as a vector sum of  $N$  muscle fibre forces of the  $k$ -th muscle:

$$F_{Mk} = \left| \sum_{i=1}^N \vec{F}_{ki} \right| \quad (37)$$

The resultant muscle force was afterwards divided by the weight force of the whole body to obtain relative forces, which could be compared between models.

The resultant muscle activity of the  $k$ -th muscle  $a_{Mk}$  was calculated as an average muscle activity of  $N$  muscle fibre activities of the  $k$ -th muscle:

$$a_{Mk} = \frac{\sum_{i=1}^N a_{ki}}{N} \quad (38)$$

#### 4.4. Resultant hip force according to models using reduction methods

Four models of Pauwels [28], Debrunner [29], Iglíč [32] and Uršič [7] were chosen for the analysis and the comparison with the results obtained from the models using optimization criteria. Values of the resultant hip force calculated by the first three models were taken from the study of Eschweiler et al., 2012 [30]. The average value and standard deviation were calculated for each model. The value of the resultant hip force calculated by Uršič's model [7] was taken from the study of Uršič et al., 2021 [7] for hips evaluated as "Normal" according to hip stress gradient index classification.

The following chapters describe the model (called HIPSTRESS according to its predecessors) used for the clinical study. The model is based on Uršič's model [7] with two adjustments. The position where the body weight force acts was moved from the middle

of the interhip distance more laterally above the unloaded leg, and the method of how a nonlinear equation (64) is solved was improved to be computed numerically. A very similar approach could be used for other two-dimensional models using reduction methods.

#### 4.4.1. Reasons for choosing HIPSTRESS model

One of the goals of this thesis was to select a suitable model for the clinical study based on the analysis of available models using reduction and optimization methods and the type of application. The main reason for choosing a two-dimensional model using reduction methods was its simplicity and suitability. Hip dysplasia is evaluated based on two-dimensional X-Ray scans, and a two-dimensional model can be directly adapted to X-Ray scans, providing patient-specific scaling. Hip dysplasia is evaluated according to a specific pelvis and hip joint geometry, which can be anatomically distorted. Scaling a three-dimensional model with many muscles according to an X-Ray scan would be complicated. The simplicity also allows the surgeons to make easy calculations. HIPSTRESS model was chosen for the possibility of comparing the results with previous studies in which its predecessors were used.

#### 4.4.2. Geometrical evaluation of X-Ray scans

HIPSTRESS model is a two-dimensional model composed of two segments, the loaded leg, the lower segment, and the rest of the body, the upper segment. The two segments are connected by the hip joint. The one-muscle model is based on the one-legged stance, and it is evaluated according to patients' X-rays, as seen in Figure 16.

The X-Ray scan needs to be levelled the way that the pelvis is vertically positioned. The centre of the femoral head is found by creating a circle which fits the region of the femoral head where the highest load is expected. The centre of the circle is considered to be the origin of the coordinate system of the hip. The most lateral and superior points of the pelvis are found, and the distances from the hip origin to these points are considered as the width  $C$  and height  $H$ , respectively. The interhip distance  $L$  is measured as a horizontal distance between the centres of the femoral heads. The origin of the effective muscle is located by the coordinates  $x_F = 1/2C$  and  $z_F = 3/4H$ . The insertion of the effective muscle lies on the greater trochanter. This point is found by connecting the greater trochanter's most lateral and superior point in the femoral coordinate system, drawing a perpendicular line

in the middle of the connection and locating the point where the contour of the greater trochanter is crossed. The femoral coordinate system is obtained by drawing z-axis along the femoral bone canal. The inclination of the effective muscle with respect to the z-axis of the hip coordinate system defines  $\vartheta_F$  angle. Centre-edge angle  $\vartheta_{CE}$  is measured as the inclination of a line connecting the origin of the hip coordinate system with the most lateral point of acetabular bony contour with respect to the z-axis. The same procedure is made for both hips. Centres of the femoral heads in Figure 16 seem to lie on the same horizontal line. It does not apply in all cases. Generally, the centres do not lie at the same horizontal line and the circles that define them do not have the same radius. Such a case can be seen in Figure 28A. Each hip is evaluated separately, only the interhip distance  $L$  is common.

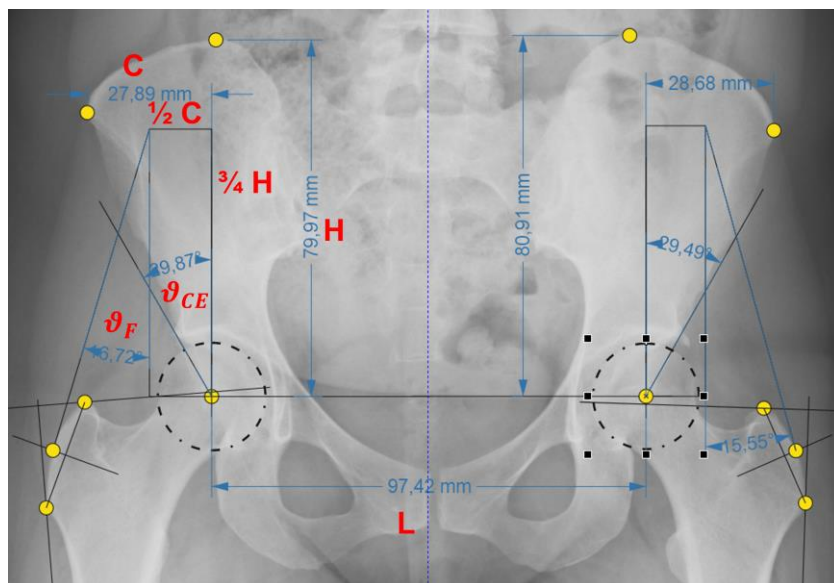


Figure 16: Geometrical evaluation of X-Ray scan according to HIPSTRESS model



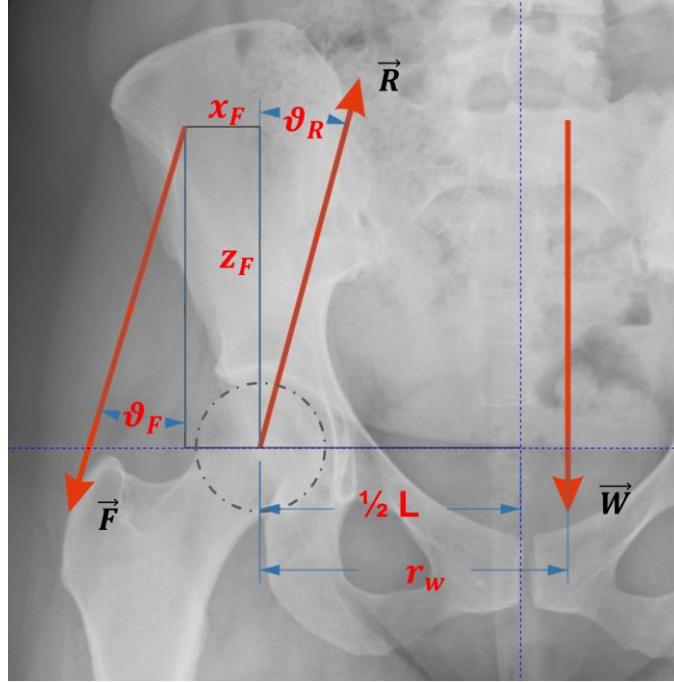


Figure 17: Forces acting in the hip joint according to HIPSTRESS model

#### 4.4.1. Equilibrium in the hip joint

The equilibrium in the hip joint is maintained by three forces: a weight force  $\vec{W}$  of the upper segment, a muscle force  $\vec{F}$  of the effective muscle originating on the pelvis and inserting on the greater trochanter and a resultant hip force  $\vec{R}$  acting in the centre of the hip joint. The system of forces can be seen in Figure 17. The equilibrium of forces and torques in the hip joint can then be expressed as:

$$\vec{W} + \vec{F} + \vec{R} = 0 \quad (39)$$

$$\vec{r}_W \times \vec{W} + \vec{r}_F \times \vec{F} = 0 \quad (40)$$

where  $\vec{r}_W$  and  $\vec{r}_F$  are moment arms of the weight and the effective muscle forces, respectively. Since the model is two-dimensional, y components of the forces and moment arms are neglected, and vectors of forces and moment arms can be expressed as: [7]

$$\vec{W} = (0, -(W_B - W_L)) \quad (41)$$

$$\vec{F} = (-F \sin \vartheta_F, -F \cos \vartheta_F) \quad (42)$$

$$\vec{R} = (R \sin \vartheta_R, R \cos \vartheta_R) \quad (43)$$

$$\vec{r}_W = (r_w, 0) \quad (44)$$

$$\vec{r}_F = (-x_F, z_F) \quad (45)$$

where  $W_B$  and  $W_L$  are weight forces of the whole body and the loaded leg, respectively. The weight of the loaded leg was considered to be  $W_L = 0,161W_B$  [65], from which the weight force  $W = 0,839W_B$ . The x component of the weight force moment arm represents the centre of mass of the upper segment:

$$r_W = \frac{W_B c - W_L b}{W_B - W_L} \quad (46)$$

where the meaning and determination of the parameters  $b$  and  $c$  is according to McLeish and Charnley, 1970 [66]  $b = 0,48L/2$  and  $a = 1,01L/2$ . The x component of the weight force moment arm is the first improvement of this model over the previous Uršič's model [7], where it was not moved above the unloaded leg and was equal to half of the interhip distance.

Using the equations (41)-(46), the equilibrium can be rewritten as:

$$R \sin \vartheta_R = F \sin \vartheta_F \quad (47)$$

$$R \cos \vartheta_R = F \cos \vartheta_F + 0,839W_B \quad (48)$$

$$F(x_F \cos \vartheta_F + z_F \sin \vartheta_F) = 0,839r_W W_B \quad (49)$$

from which the unknown parameters  $F, R, \vartheta_R$  can be derived as normalized parameters:

$$\frac{F}{W_B} = \frac{0,839r_W}{x_F \cos \vartheta_F + z_F \sin \vartheta_F} \quad (50)$$

$$\frac{R}{W_B} = \frac{F \sin \vartheta_F}{W_B \sin \vartheta_R} \quad (51)$$

$$\tan \vartheta_R = \frac{\sin \vartheta_F}{\cos \vartheta_F + 0,839 \frac{W_B}{F}} \quad (52)$$

#### 4.4.1. Stress distribution in the hip joint

The resultant hip force  $\vec{R}$  can be obtained as an integral of a stress  $p$ :

$$\vec{R} = \int p \vec{dA} \quad (53)$$

where  $\vec{dA}$  is an area element with a vector pointing in the normal direction to the area element. The integration is performed over the load-bearing surface. Only normal stress is

considered, shear stresses are neglected for a small value of the frictional coefficient corresponding to forces acting in the hip joint [67]–[70].

If unloaded, the femoral head and the acetabulum are represented by two concentric spheres. When the load is applied, the spheres become non-concentric. The point where these spheres are closest to each other is called the stress pole. At this point, the highest load is applied. For HIPSTRESS model, the stress pole lies in the frontal plane. The inclination between the line connecting the stress pole and the centre of the femoral head with respect to the vertical direction is called stress pole angle  $\theta$ . The stress  $p$  in the stress pole is marked  $p_0$ . If moving away from the stress pole on the articular surface, the stress decreases according to cosine law:

$$p = p_0 \cos \gamma \quad (54)$$

where the angle  $\gamma$  is an angle between the line connecting the origin of the coordinate system with the stress pole and the line connecting the origin with a chosen point on the articular surface. [70]

The equation for the stress distribution (54) can be inserted into the equation for the resultant hip force (53). This integration is solved in spherical coordinate system described by radius  $r$  and angles  $\vartheta$  in mediolateral direction and  $\varphi$  in anteroposterior direction. The system is oriented the way, that its z-axis points in the direction of the highest load. It means that it is inclined by the stress pole against the hip joint coordinate system, which can be seen in Figure 18. In this system,  $\cos \gamma$  is expressed as  $\cos \varphi \cos \vartheta$ . Components of the equation for the resultant hip force are then described by the following set of equations: [70]

$$R_x = p_0 r^2 \int \cos^3 \varphi d\varphi \int \cos \vartheta \sin \vartheta d\vartheta \quad (55)$$

$$R_y = p_0 r^2 \int \cos^2 \varphi \sin \varphi d\varphi \int \cos \vartheta d\vartheta \quad (56)$$

$$R_z = p_0 r^2 \int \cos^3 \varphi d\varphi \int \cos^2 \vartheta d\vartheta \quad (57)$$

Borders of the load bearing area are the rim of acetabular bony contour described by the centre edge angle on the lateral side and the place where the stress vanishes on the other sides, i.e., where the angle equals  $\pi/2$ , and therefore the cosine equals zero. That means that the angles are within intervals  $\vartheta = [\vartheta_{CE} - \theta, \pi/2]$  and  $\varphi = [-\pi/2, \pi/2]$ . By solving the equations within the boundaries, components of the resultant force are obtained: [70]

$$R_x = \frac{2}{3} p_0 r^2 \cos^2(\vartheta_{CE} - \theta) \quad (58)$$

$$R_y = 0 \quad (59)$$

$$R_z = \frac{2}{3} p_0 r^2 \left( \frac{\pi}{2} + \vartheta_{CE} - \theta + \frac{1}{2} \sin 2(\vartheta_{CE} - \theta) \right) \quad (60)$$

The ration  $R_x/R_z$  yields: [70]

$$\tan(\vartheta_R + \theta) = \frac{\cos^2(\vartheta_{CE} - \theta)}{\frac{\pi}{2} + \vartheta_{CE} - \theta + \frac{1}{2} \sin 2(\vartheta_{CE} - \theta)} \quad (61)$$

New variables  $\vartheta_{RCE}$  and  $\vartheta_H$  were introduced to express the equation (61) as written in equation (64). [70]

$$\vartheta_{RCE} = \frac{1}{2} (\vartheta_R + \vartheta_{CE}) \quad (62)$$

$$\vartheta_H = \theta - \frac{1}{2} (\vartheta_{CE} - \vartheta_R) \quad (63)$$

$$\tan(\vartheta_{RCE} + \vartheta_H) = \frac{\cos^2(\vartheta_{RCE} - \vartheta_H)}{\frac{\pi}{2} + \vartheta_{RCE} - \vartheta_H + \frac{1}{2} \sin 2(\vartheta_{RCE} - \vartheta_H)} \quad (64)$$

While  $\vartheta_{RCE}$  can be calculated from previous measurements and calculations,  $\vartheta_H$  must be calculated by solving the nonlinear equation (64). It can be solved numerically or by reading a nomogram constructed for this purpose [7]. In this work  $\vartheta_H$  was solved in MS Excel using Solver Add-in and its GRG Nonlinear solving method, which was the second improvement of the new model over the previous one. Due to knowledge of  $\vartheta_H$  the stress pole position can be obtained by expressing it from the equation (63) as: [70]

$$\theta = \vartheta_H + \frac{1}{2} (\vartheta_{CE} - \vartheta_R) \quad (65)$$

The value of stress in the stress pole can be obtained from the equation (58) by setting  $R_x = R \sin(\vartheta_R + \theta)$ . To get the dimensionless parameter independent of the radius of the femoral head and body weight, the resulting equation for the stress is further divided by the body weight and multiplied by the radius, resulting in: [70]

$$p_0 r^2 / W_B = \frac{3R \sin(\vartheta_R + \theta)}{2W_B \cos^2(\vartheta_{CE} - \theta)} \quad (66)$$

where the value of  $R/W_B$  is obtained from the equation (51).

To characterize the highest stress reached in the hip, the peak contact hip stress normalized by the body weight and the radius of the articular sphere  $p_{max} r^2 / W_B$  was introduced. It has the same value as the normalized stress in the stress pole in case that the stress pole angle is smaller than the centre-edge angle, i.e., if the vector from the centre of the femoral head is heading into the pelvis. Otherwise, if the vector is heading laterally outside of the pelvis, i.e., the stress pole angle is larger than the centre-edge angle, the normalized peak contact hip stress has the value of stress at the acetabular rim according to the equation (54). Both cases can be seen in the following equations: [70]

$$p_{max} r^2 / W_B = p_0 r^2 / W_B \text{ for } \theta \leq \vartheta_{CE} \quad (67)$$

$$p_{max} r^2 / W_B = p_0 r^2 / W_B \cos(\vartheta_{CE} - \theta) \text{ for } \theta > \vartheta_{CE} \quad (68)$$

The position of the stress pole is connected with the hip stress gradient index normalized by the body weight and the radius of the articular sphere  $G_p r^3 / W_B$ : [70]

$$G_p r^3 / W_B = -p_0 r^2 / W_B \sin(\vartheta_{CE} - \theta) \quad (69)$$

The value of the hip stress gradient index is negative if the stress pole lies within the hip joint and positive if the vector to the stress pole points laterally outside of the pelvis. If the value is positive, the hip is considered to be dysplastic. [70]

The size of the whole load-bearing area is characterized by the functional angle  $\vartheta_f$ : [70]

$$\vartheta_f = \frac{\pi}{2} + \vartheta_{CE} - \theta \quad (70)$$

Two criteria were suggested to define dysplastic hips. The hips are supposed to be dysplastic if dimensionless peak contact hip stress  $p_{max} r^2 / W_B > 2$  [7] or if the dimensionless hip stress gradient index  $G_p r^3 / W_B > 0$  [48].

Biomechanical parameters explained in this section are shown in Figure 18. The orange colour illustrates the rotated coordinate system in the direction of the stress pole.

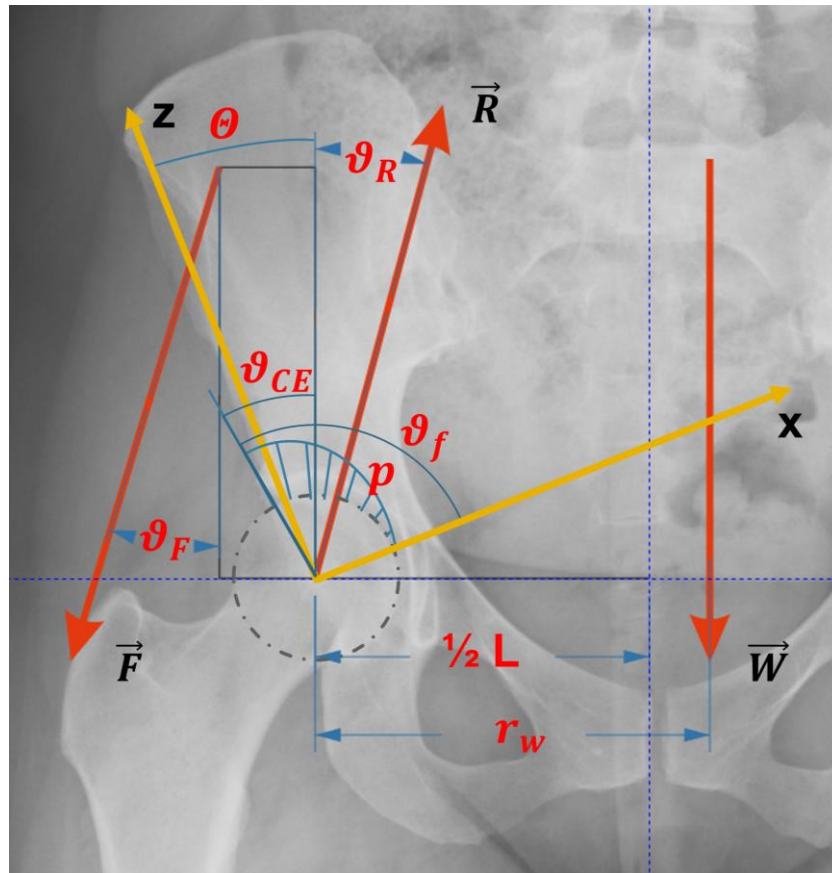


Figure 18: Visualisation of geometrical and biomechanical parameters used in HIPSTRESS model

#### 4.5. Resultant hip force according to in vivo measurements

The data of resultant hip forces used for the comparison with results from the models were obtained from the Orthoload database by selecting “Hip Joint III” implant and “One Legged Stance” activity [3], [16]. The measurements were performed using an instrumented implant, which monitored three contact forces and three friction moments. On the 24<sup>th</sup> of May 2022, fourteen measurements were available for ten patients, eight of whom were males and two females. Since the mathematical models are based on static posture, the values of resultant hip forces were taken approximately in the middle of the stance when the patient was standing still on one leg. Resultant hip forces were averaged and standard deviations were calculated.

## 5. Results

The resultant hip force was calculated for chosen models using optimization methods. The influence of the choice of the model on the resultant force can be seen in Figure 19. The forces in individual models vary between 1,25 and 1,7 times the body weight. The results were compared to resultant hip forces calculated using models based on reduction methods and to the in-vivo measurement obtained from the orthoLoad database. According to the in-vivo measurements, the mean value of the resultant hip force is 2,55 times the body weight. Similar results can be seen for models of Pauwels [28], Debrunner [29], Iglič [32] and Uršič [7]. In Figure 20 is shown the angle of the resultant hip force in the frontal plane. The results show that while the angle in the frontal plane in models using optimization methods varies between 0,6° and 3,1°, its value according to the in vivo measurement is about 17,45°. A similar value is obtained by Pauwels [28] model.

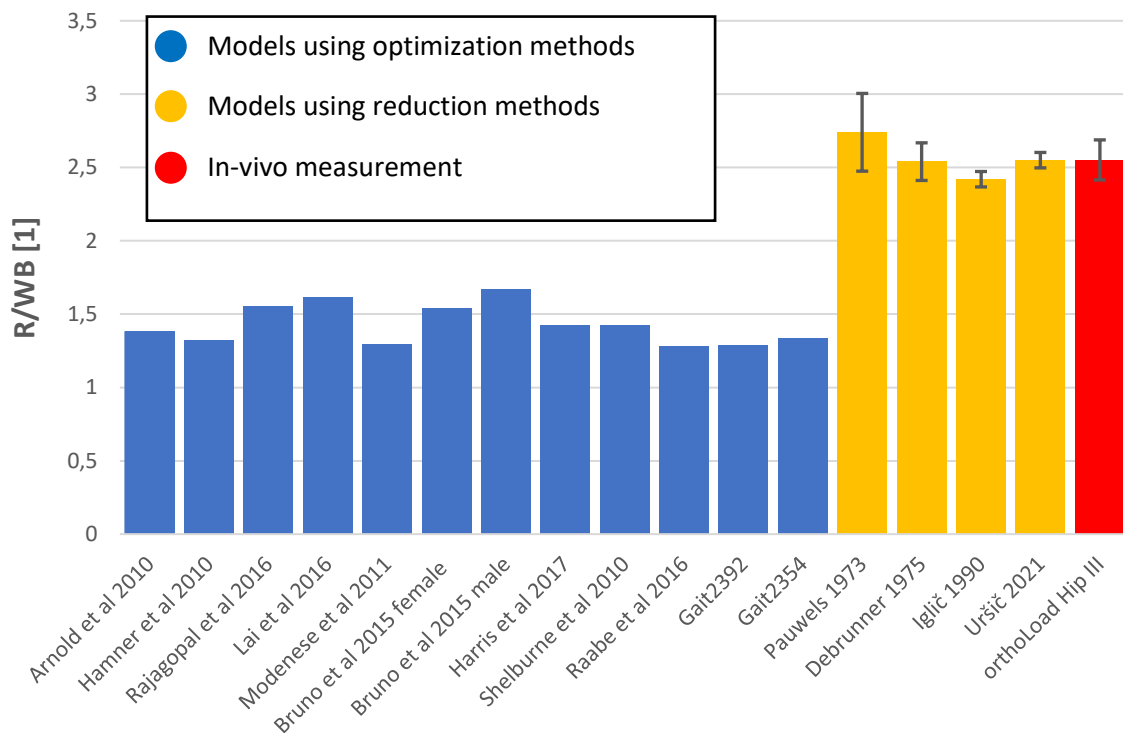


Figure 19: Comparison of the reaction force per body weight in different models. Minimum muscle activity for models using optimization methods was set to zero

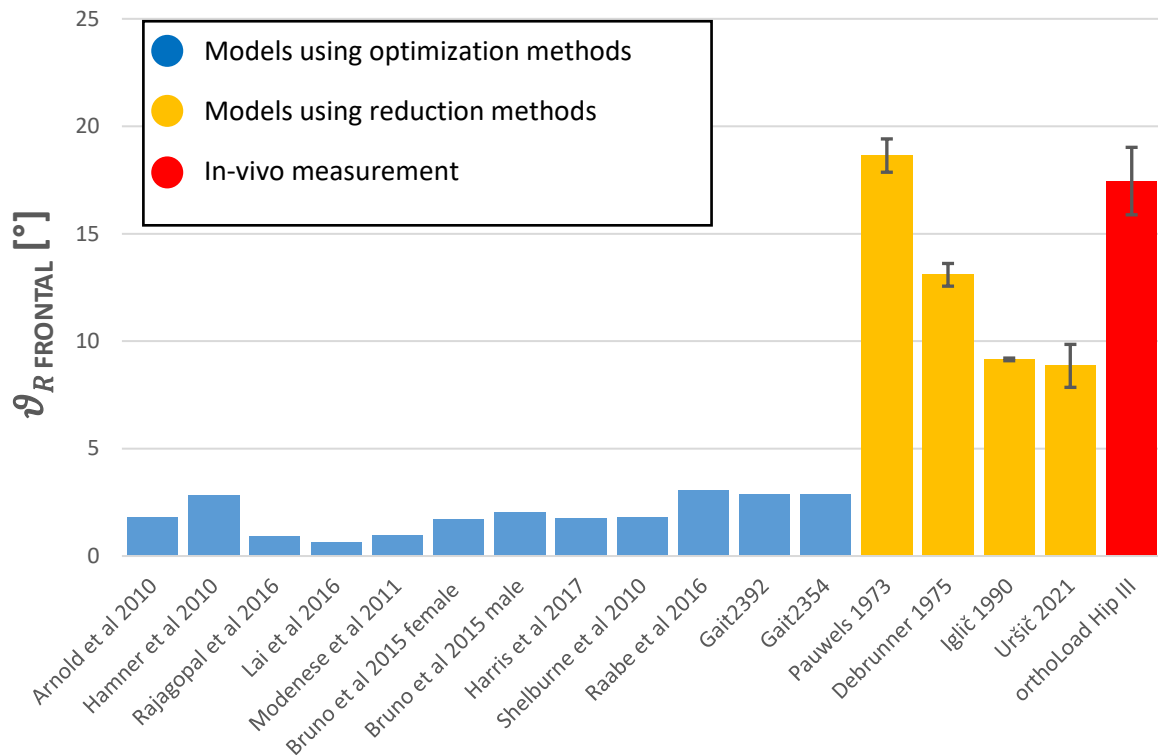


Figure 20: Comparison of the angle of the resultant hip force in the frontal plane in different models. Minimum muscle activity for models using optimization methods was set to zero

The resultant hip force values for individual models using optimization methods in Figure 19 were calculated with muscle fibre activity ranging between 0% and 100%. If minimum muscle fibre activity representing the passive tension is considered, the resultant force increases, as shown in Figure 21. The resultant hip force was calculated with minimum muscle fibre activity set from 0% to 10% with an increment of 1%. For Modenese et al., 2011 model, it was not possible to find a solution of the optimization calculations if the minimum muscle activity was set to 9% and 10%. The resultant hip force increased the most in Rajagopal et al., 2016 model by 58%. The resultant hip force increased by more than 50% also in Lai et al., 2017 model, by 52%. The lowest increase of the resultant hip force was 11% in Modenese et al., 2011 model. On average, the resultant hip force increased by 40%. At the highest minimum muscle fibre activity set, the resultant hip force in models Rajagopal et al., 2016, Lai et al., 2017 and Bruno et al., 2015 female increases to similar values as those measured, while for the other models, the resultant hip force remains below the measured values.



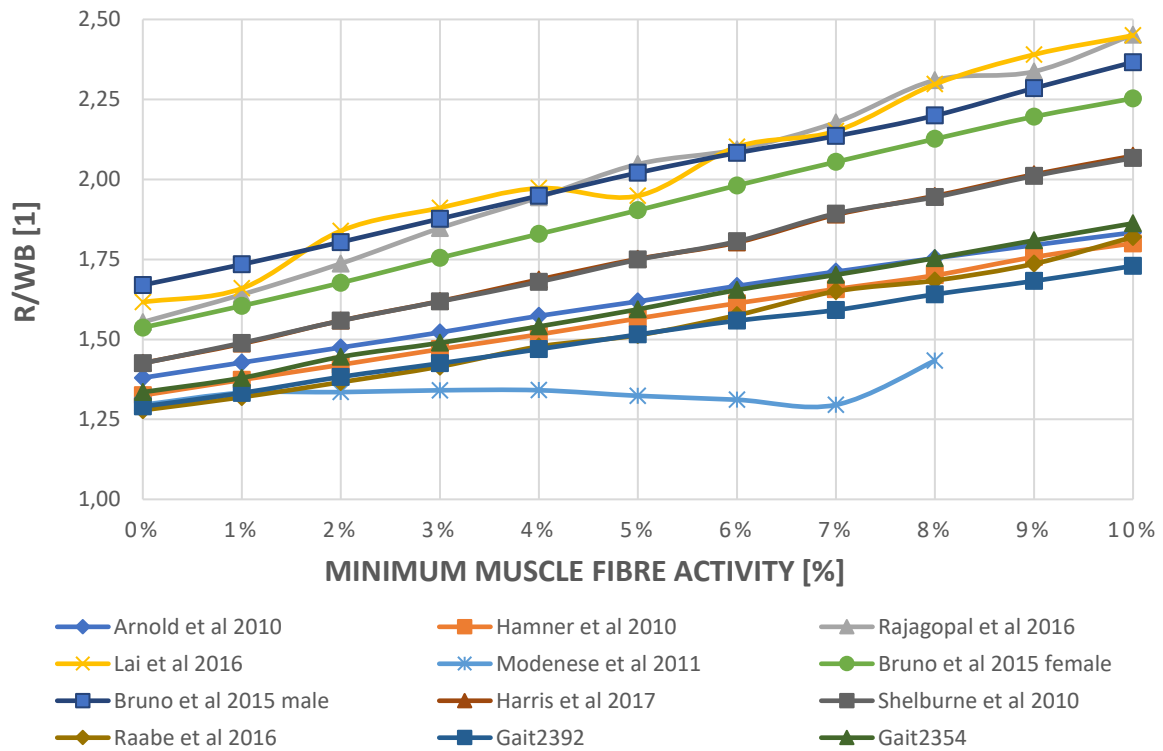


Figure 21: Resultant hip force per body weight as a function of minimum muscle fibre activity

A similar trend can be observed for the angle of the resultant hip force. As the minimum muscle fibre activity increases, the angle increases in most cases as well. In Figure 22 and Figure 23, it is shown how the angle changes when the minimum muscle fibre activity rises from 0% to 10%. It can be seen that the angle increases more in the frontal plane than in the sagittal plane. It can also be seen that the angle is smallest in models Rajagopal et al., 2016 and Lai et al., 2017, for which the resultant hip forces are the highest.

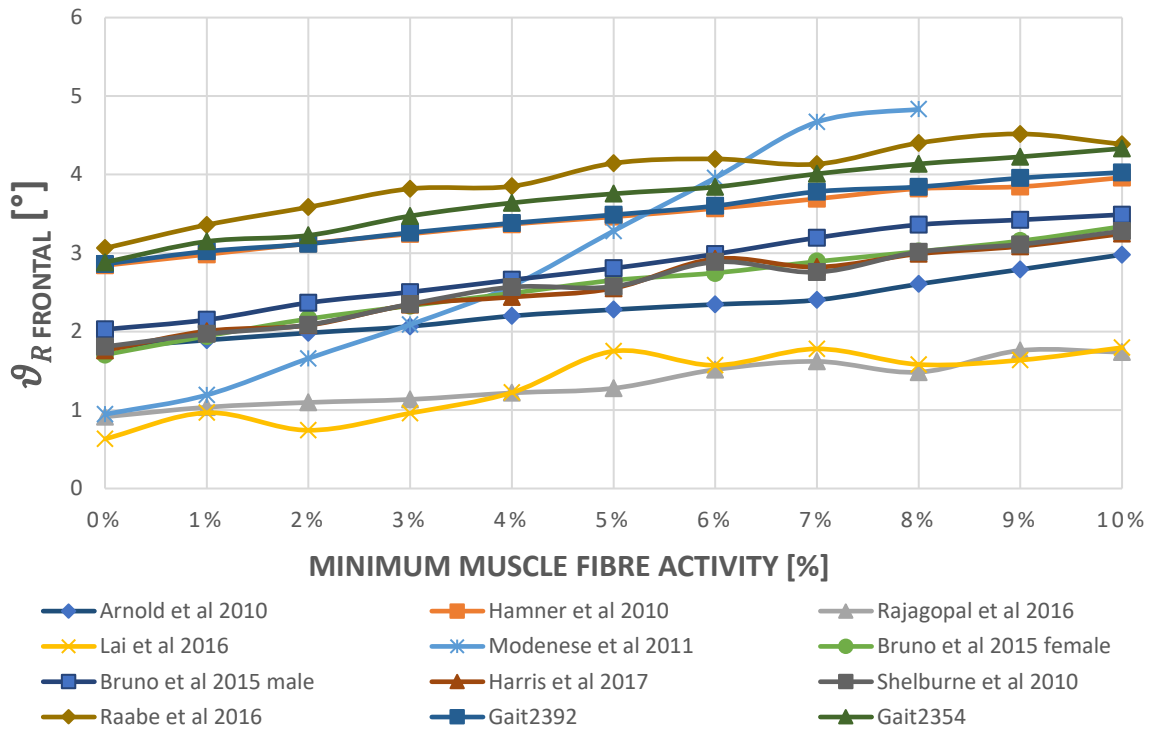


Figure 22: Resultant hip force angle  $\vartheta_R$  in the frontal plane in the medial direction as a function of minimum muscle fibre activity.

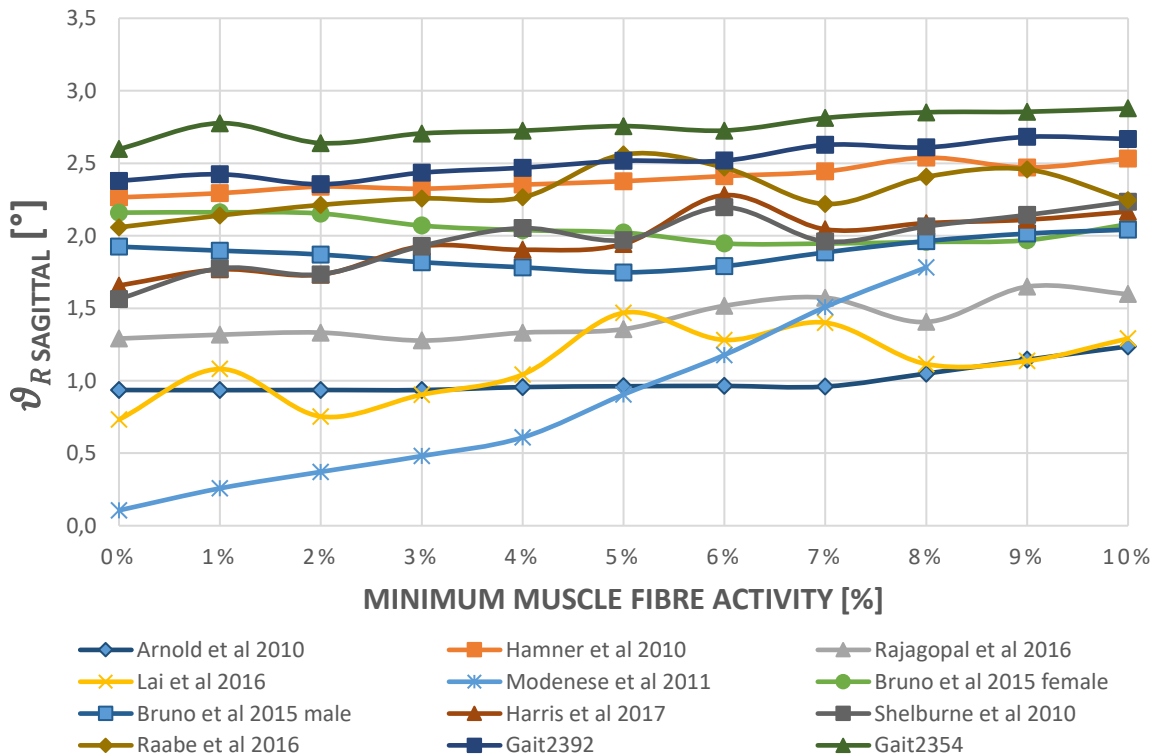


Figure 23: Resultant hip force angle  $\vartheta_R$  in the sagittal plane in the anterior direction as a function of minimum muscle fibre activity

Figure 24 shows the dependency of the resultant hip force  $R/W_B$  on the number of muscle fibres in individual models. There are two linear trendlines for the case where all models are considered ( $R^2 = 0,4326$ ) and for the case where only models using optimization methods are considered ( $R^2 = 0,1118$ ). Figure 25 shows the dependency of the resultant hip force  $R/W_B$  on the number of muscles in individual models. There are two linear trendlines for the case where all models are considered ( $R^2 = 0,8972$ ) and for the case where only models using optimization methods are considered ( $R^2 = 0,4118$ ). From the graphs can be seen that there was no dependency of the resultant muscle force on the number of muscle fibres or whole muscles in the models using optimization methods. A dependency on the number of muscles can be seen only if models using optimization methods are included.

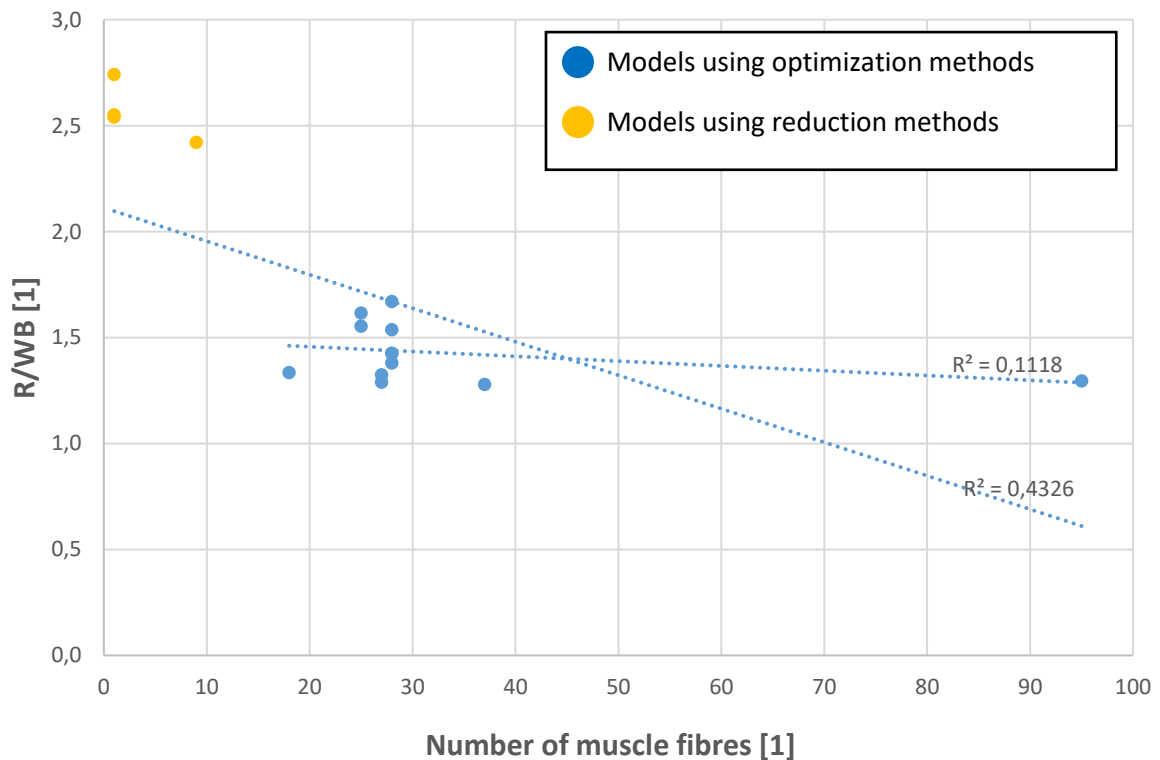


Figure 24: Resultant hip force  $R/W_B$  as a function of the number of muscle fibres in models

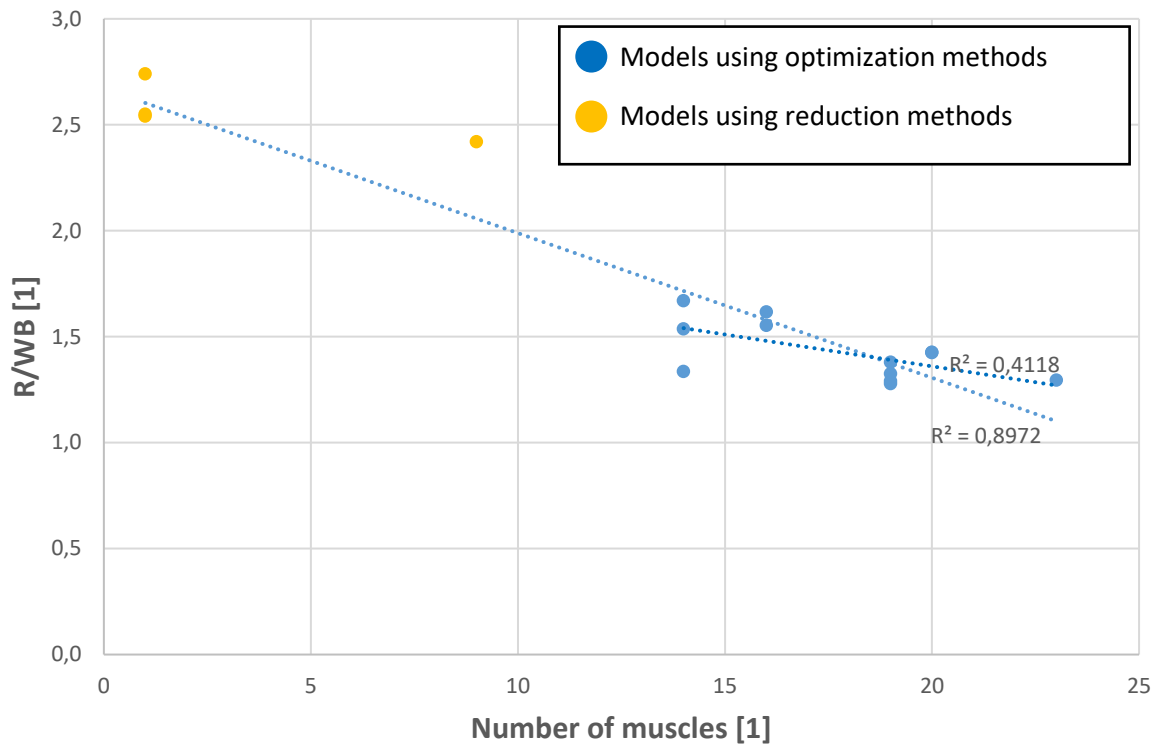


Figure 25: Resultant hip force  $R/W_B$  as a function of the number of muscles in models

The highest resultant muscle forces  $F_M$  in most models are transmitted by the gluteus medius and rectus femoris, averaging 1,1 and 0,87 per body weight, respectively, with standard deviation  $SD = 0,24$  and  $SD = 0,26$  for all models at 0% of minimum muscle activity. While increasing the minimum muscle fibre activity representing the passive tension, the resultant muscle force also increases in most muscles. At 10% of minimum muscle fibre activity, the forces transmitted by the gluteus medius and rectus femoris are 1,59 and 1,28 ( $SD = 0,29$  and  $0,51$ ) per body weight, respectively, on average for all models. An exception is Modenese et al., 2017 model, in which the force of the rectus femoris is lower and decreases significantly with higher minimum muscle activity. Other muscles that transmit considerable force (the average resultant muscle force of a muscle in all models is higher than the average resultant muscle force of all muscles in all models) are the iliacus, gluteus minimus and psoas major. In some models, gluteus maximus could also be included and in some models, psoas major would be excluded from the muscles transmitting considerable force.

A detailed comparison of resultant muscle forces between all models with minimum muscle fibre activity set to 0% and 10% can be seen in Figure 26. For Modenese et al., 2017 model, the minimum muscle activity is 0% and 8%, as it was not possible to find a solution

of optimization for higher percentages. It can also be seen which muscles are present in which models.

Figure 27 shows the resultant muscle activity  $a_M$  calculated for all models with minimum muscle fibre activity set to 0% and 10%. It can be seen that gluteus medius, as the muscle which transmits the highest forces, is activated on average for all models at 32% (SD = 7%) when minimum muscle activity is set to 0% and at 45% (SD = 9%) when set to 10%. Rectus femoris is activated at 48% (SD = 15%) and 67% (SD = 24%). It can be noticed that the activation of the rectus femoris in Modenese et al., 2017 model decreases to the minimum muscle fibre activity while psoas major gets fully activated. Other considerably activated muscles are the iliacus, gluteus minimus, psoas major, sartorius and tensor fasciae latae. There is no model in which the gluteus maximus would be considerably activated. In Modenese et al., 2017 model, a considerable activation of semimembranosus can be seen.

Model number	1		2		3		4		5		6a		6b		7		8		9		10		11	
	0%	10%	0%	10%	0%	10%	0%	10%	0%	10%	0%	10%	0%	10%	0%	10%	0%	10%	0%	10%	0%	10%	0%	10%
Adductor brevis	0,00	0,04	0,00	0,06	0,00	0,08	0,00	0,08	0,00	0,03	xxx	xxx	xxx	xxx	0,00	0,07	0,00	0,07	0,00	0,06	0,00	0,06	xxx	xxx
Adductor longus	0,01	0,19	0,00	0,09	0,00	0,12	0,00	0,12	0,00	0,04	xxx	xxx	xxx	xxx	0,00	0,10	0,00	0,10	0,00	0,08	0,00	0,09	xxx	xxx
Adductor magnus	0,00	0,16	0,00	0,15	0,00	0,29	0,00	0,29	0,00	0,15	0,00	0,39	0,00	0,32	0,00	0,18	0,00	0,18	0,00	0,15	0,00	0,15	0,00	0,32
Biceps femoris	0,00	0,10	0,00	0,12	0,00	0,18	0,00	0,18	0,00	0,08	0,00	0,45	0,00	0,36	0,00	0,13	0,00	0,13	0,00	0,12	0,00	0,12	0,00	0,37
Gemellus inferior	0,00	0,01	0,00	0,02	xxx	xxx	xxx	xxx	xxx	0,00	0,01	0,00	0,03	0,00	0,03	0,00	0,03	0,00	0,03	0,00	0,02	0,00	0,02	0,00
Gemellus superior	xxx	xxx	xxx	xxx	xxx	xxx	xxx	xxx	xxx	0,00	0,01	xxx	xxx	xxx	xxx	xxx	xxx	xxx	xxx	xxx	xxx	xxx	xxx	xxx
Gluteus maximus	0,00	0,25	0,17	0,35	0,00	0,45	0,00	0,45	0,04	0,20	0,00	0,31	0,00	0,26	0,22	0,40	0,20	0,45	0,08	0,26	0,16	0,34	0,07	0,26
Gluteus medius	1,05	1,40	1,13	1,57	0,82	1,23	0,73	1,18	0,85	1,51	1,50	2,16	1,32	1,67	0,99	1,55	1,00	1,54	1,16	1,59	1,08	1,48	1,53	2,16
Gluteus minimus	0,21	0,33	0,35	0,49	0,31	0,40	0,29	0,41	0,25	0,10	xxx	xxx	xxx	xxx	0,27	0,42	0,29	0,40	0,38	0,55	0,34	0,48	xxx	xxx
Gracilis	0,00	0,02	0,00	0,02	0,00	0,04	0,00	0,04	0,00	0,01	0,00	0,03	0,00	0,02	0,00	0,03	0,00	0,03	0,00	0,02	0,06	0,08	0,00	0,02
Iliacus	0,48	0,81	0,29	0,55	0,18	0,63	0,14	0,71	0,20	0,79	0,93	1,60	0,93	1,44	0,30	0,63	0,31	0,68	0,39	0,94	0,31	0,58	0,35	0,72
Obturator Externus	xxx	xxx	xxx	xxx	xxx	xxx	xxx	xxx	0,00	0,09	xxx	xxx	xxx	xxx	0,00	0,03	0,00	0,03	xxx	xxx	xxx	xxx	xxx	xxx
Obturator Internus	xxx	xxx	xxx	xxx	xxx	xxx	xxx	xxx	0,00	0,07	xxx	xxx	xxx	xxx	xxx	xxx	xxx	xxx	xxx	xxx	xxx	xxx	xxx	xxx
Pectineus	0,03	0,06	0,00	0,04	xxx	xxx	xxx	xxx	0,00	0,02	0,00	0,04	0,00	0,12	0,00	0,04	0,00	0,04	0,00	0,04	0,00	0,04	0,00	0,04
Piriformis	0,07	0,11	0,05	0,06	0,12	0,14	0,14	0,14	0,00	0,02	0,08	0,13	0,11	0,28	0,00	0,07	0,00	0,07	0,07	0,09	0,06	0,06	0,05	0,06
Quadratus Femoris	0,00	0,03	0,00	0,05	xxx	xxx	xxx	xxx	0,00	0,04	0,00	0,06	0,00	0,05	0,00	0,06	0,00	0,06	0,00	0,05	0,05	0,05	0,00	0,05
Sartorius	0,04	0,07	0,04	0,06	0,05	0,07	0,04	0,07	0,14	0,03	0,07	0,12	0,07	0,18	0,04	0,08	0,03	0,07	0,03	0,05	0,04	0,06	0,04	0,06
Semimembranosus	0,00	0,16	0,00	0,17	0,00	0,30	0,00	0,30	0,00	0,31	xxx	xxx	xxx	xxx	0,00	0,20	0,00	0,20	0,00	0,17	0,00	0,17	xxx	xxx
Semitendinosus	0,00	0,04	0,00	0,06	0,00	0,08	0,00	0,08	0,00	0,04	xxx	xxx	xxx	xxx	0,00	0,09	0,00	0,09	0,00	0,08	0,00	0,06	xxx	xxx
Tensor fasciae latae	0,07	0,12	0,09	0,13	0,08	0,17	0,14	0,21	0,11	0,22	0,12	0,22	0,12	0,30	0,09	0,15	0,07	0,13	0,11	0,17	0,09	0,13	0,08	0,12
Psoas minor	xxx	xxx	xxx	xxx	xxx	xxx	xxx	xxx	0,00	0,01	xxx	xxx	xxx	xxx	xxx	xxx	xxx	xxx	xxx	xxx	xxx	xxx	xxx	xxx
Psoas major	0,23	0,40	0,33	0,60	0,31	0,78	0,07	0,61	0,19	0,70	0,00	0,22	0,03	0,30	0,02	0,19	0,00	0,18	0,00	0,15	0,35	0,62	0,40	0,77
Rectus femoris	0,84	1,15	0,63	0,98	1,06	1,85	1,17	1,81	0,50	0,08	1,25	1,96	1,23	1,57	0,93	1,51	0,96	1,52	0,53	0,89	0,64	0,96	0,64	1,03

Figure 26: Comparison of resultant muscle forces  $F_M$  between models for minimum muscle fibre activity set to 0% and 10%

Model number	1		2		3		4		5		6a		6b		7		8		9		10		11	
	0%	10%	0%	10%	0%	10%	0%	10%	0%	10%	0%	10%	0%	10%	0%	10%	0%	10%	0%	10%	0%	10%	0%	10%
Min muscle activity	0%	10%	0%	10%	0%	10%	0%	10%	0%	10%	0%	10%	0%	10%	0%	10%	0%	10%	0%	10%	0%	10%	0%	10%
Adductor brevis	0%	10%	0%	10%	0%	10%	0%	10%	0%	10%	0%	10%	0%	10%	0%	10%	0%	10%	0%	10%	0%	10%	0%	10%
Adductor longus	2%	35%	0%	10%	0%	10%	0%	10%	0%	10%	0%	10%	0%	10%	0%	10%	0%	10%	0%	10%	0%	10%	0%	10%
Adductor magnus	0%	10%	0%	10%	0%	10%	0%	10%	0%	10%	0%	10%	0%	10%	0%	10%	0%	10%	0%	10%	0%	10%	0%	10%
Biceps femoris	0%	10%	0%	10%	0%	10%	0%	10%	0%	10%	0%	10%	0%	10%	0%	10%	0%	10%	0%	10%	0%	10%	0%	10%
Gemellus inferior	0%	10%	0%	10%	0%	10%	0%	10%	0%	10%	0%	10%	0%	10%	0%	10%	0%	10%	0%	10%	0%	10%	0%	10%
Gemellus superior	0%	10%	0%	10%	0%	10%	0%	10%	0%	10%	0%	10%	0%	10%	0%	10%	0%	10%	0%	10%	0%	10%	0%	10%
Gluteus maximus	0%	10%	7%	14%	0%	10%	0%	10%	0%	10%	0%	10%	0%	10%	0%	10%	0%	10%	0%	10%	0%	10%	0%	10%
Gluteus medius	35%	46%	42%	57%	21%	31%	19%	29%	29%	29%	54%	32%	44%	34%	42%	30%	45%	30%	45%	29%	39%	40%	54%	39%
Gluteus minimus	27%	42%	30%	42%	19%	26%	18%	26%	25%	11%	11%	11%	11%	11%	11%	11%	11%	11%	11%	11%	11%	11%	11%	11%
Gracilis	0%	10%	0%	10%	0%	10%	0%	10%	0%	10%	0%	10%	0%	10%	0%	10%	0%	10%	0%	10%	0%	10%	0%	10%
Iliacus	57%	96%	20%	38%	13%	46%	10%	52%	19%	77%	52%	89%	65%	100%	17%	36%	18%	39%	18%	43%	21%	40%	24%	49%
Obturator Externus	0%	10%	0%	10%	0%	10%	0%	10%	0%	10%	0%	10%	0%	10%	0%	10%	0%	10%	0%	10%	0%	10%	0%	10%
Obturator internus	0%	10%	0%	10%	0%	10%	0%	10%	0%	10%	0%	10%	0%	10%	0%	10%	0%	10%	0%	10%	0%	10%	0%	10%
Pectineus	14%	25%	0%	10%	0%	10%	0%	10%	0%	10%	0%	10%	0%	10%	0%	10%	0%	10%	0%	10%	0%	10%	0%	10%
Piriformis	17%	27%	9%	10%	8%	10%	10%	10%	0%	8%	10%	18%	18%	48%	0%	10%	0%	10%	0%	10%	12%	15%	9%	10%
Quadratus Femoris	0%	10%	0%	10%	0%	10%	0%	10%	0%	10%	0%	10%	0%	10%	0%	10%	0%	10%	0%	10%	0%	10%	0%	10%
Sartorius	27%	45%	20%	30%	14%	21%	13%	22%	34%	8%	27%	47%	33%	85%	18%	30%	14%	26%	15%	24%	19%	30%	18%	30%
Semimembranosus	0%	10%	0%	10%	0%	10%	0%	10%	0%	10%	0%	10%	0%	10%	0%	10%	0%	10%	0%	10%	0%	10%	0%	10%
Semitendinosus	0%	10%	0%	10%	0%	10%	0%	10%	0%	10%	0%	10%	0%	10%	0%	10%	0%	10%	0%	10%	0%	10%	0%	10%
Tensor fasciae latae	36%	58%	28%	41%	15%	31%	24%	37%	35%	70%	32%	56%	40%	96%	23%	40%	18%	35%	23%	37%	28%	40%	24%	39%
Psoas minor	0%	10%	0%	10%	0%	10%	0%	10%	0%	10%	0%	10%	0%	10%	0%	10%	0%	10%	0%	10%	0%	10%	0%	10%
Psoas major	35%	61%	22%	40%	16%	40%	4%	31%	26%	100%	0%	10%	1%	10%	1%	10%	0%	10%	0%	10%	23%	41%	27%	51%
Rectus femoris	73%	100%	39%	62%	36%	62%	39%	61%	48%	8%	64%	100%	78%	100%	41%	66%	42%	66%	34%	56%	40%	60%	40%	65%

Figure 27: Comparison of resultant muscle activity  $a_M$  between models for minimum muscle fibre activity set to 0% and 10%

The aim of the clinical study was to evaluate hips of patients who underwent a periacetabular osteotomy according to a suitable model. It was decided to use HIPSTRESS model according to the reasons described in 4.4.1.

X-Ray scans of patients were obtained from three different medical centres (C1, C2, C3). The numbers of patients whose X-Ray scans were evaluated in the three centres were 93, 42 and 46, respectively. X-Ray images of patients were evaluated according to HIPSTRESS model before and after the operation. Some patients also underwent a second operation on the contralateral side, and the hips were also evaluated before and after the second operation. There were 37 patients from C1, 3 from C3 and 0 from C2 who were operated on the contralateral side for the second time. The evaluations of the first and the second operation were put together and considered independent. In total, the results of 221 operations were evaluated. Geometrical and biomechanical parameters of hips on the operated side and the contralateral side before the first operation are shown in Table 5 and Table 6, respectively. Below each centre name in the first column is mentioned the number of hips evaluated.

		$\vartheta_F$	$\frac{F}{W_B}$	$\vartheta_R$	$\frac{R}{W_B}$	$\vartheta_{CE}$	$\theta$	$\frac{p_{max}r^2}{W_B}$	$\frac{G_p r^3}{W_B}$	$\vartheta_f$
C1	M	16,35	1,76	10,99	2,57	19,59	25,16	3,23	1,19	84,43
93	SD	2,95	0,23	1,79	0,23	8,84	12,51	3,53	3,44	21,00
C2	M	12,01	2,00	8,39	2,83	19,85	31,21	3,33	1,10	78,64
42	SD	3,46	0,29	2,35	0,30	8,81	11,93	1,73	1,69	20,18
C3	M	15,44	1,82	10,41	2,64	19,50	26,84	3,36	1,27	82,66
46	SD	3,59	0,39	2,31	0,39	8,50	13,57	4,00	3,85	21,61

*Table 5: Evaluation of hips before the first operation (initial parameters of the patients) on the operated side*

		$\vartheta_F$	$\frac{F}{W_B}$	$\vartheta_R$	$\frac{R}{W_B}$	$\vartheta_{CE}$	$\theta$	$\frac{p_{max}r^2}{W_B}$	$\frac{G_p r^3}{W_B}$	$\vartheta_f$
C1	M	15,90	1,74	10,61	2,56	23,70	20,10	2,15	0,10	93,61
93	SD	2,57	0,21	1,56	0,21	6,66	9,35	1,07	1,00	15,66
C2	M	12,19	1,92	8,44	2,74	24,14	24,84	2,51	0,34	89,30
42	SD	3,39	0,27	2,39	0,27	8,78	10,29	1,18	1,12	18,41
C3	M	14,93	1,73	9,92	2,55	25,23	20,46	2,10	0,08	94,77
46	SD	2,64	0,37	1,63	0,37	9,67	11,05	1,01	0,84	20,27

*Table 6: Evaluation of hips before the first operation (initial parameters of the patients) on the contralateral side*

Results of operations were evaluated for each medical centre separately. Values of all biomechanical parameters were averaged before and after the operation and the standard



deviation (SD) of each parameter was calculated using STDEV.S function in MS Excel. To determine statistical significance of the results, two-tailed paired t-test was performed using MS Excel and its T.TEST function. Followingly, a percentage difference  $P_{difference}$  of each parameter was calculated:

$$P_{difference} = \frac{P_{after} - P_{before}}{\left| \frac{P_{after} + P_{before}}{2} \right|} \quad (71)$$

where  $P_{after}$  is a value of a parameter after the operation and  $P_{before}$  is a value of the parameter before the operation.

			$p_{max}r^2/W_B$	$G_p r^3/W_B$	
C1 130	Before	Mean	3,01	0,97	
		SD	3,07	2,98	
	After	Mean	1,53	-0,47	
		SD	0,64	0,52	
	Diff	Mean	-0,49	-2,91	
		SD	0,32	5,45	
		t-test	5E-9	1E-8	
		improved	98%	98%	
	C2 42	Before	Mean	3,51	1,28
			SD	2,10	2,03
After		Mean	1,82	-0,54	
		SD	1,22	0,92	
Diff		Mean	-0,62	-3,71	
		SD	0,49	5,28	
		t-test	4E-6	4E-7	
		improved	90%	93%	
C3 49		Before	Mean	3,34	1,25
			SD	3,88	3,73
	After	Mean	1,83	-0,27	
		SD	0,88	0,79	
	Diff	Mean	-0,42	-4,03	
		SD	0,37	10,03	
		t-test	0,002	0,001	
		improved	88%	94%	

Table 7: Evaluation of hips on the operated side

It was found that both the dimensionless peak contact hip stress and the dimensionless hip stress gradient index statistically significantly improved on average on the operated side, as can be seen in Table 7. Rows called “improved” show what percentage of hips improved due to the operation according to the given parameter. It can be seen that the

most successful operations were made in medical centre C1, while the lowest success rate was in medical centre C3.

On average, there were no changes in all considered parameters on the contralateral side, and the number of hips that improved is very similar to the ones that got worse. However, since the fluctuation of parameters is considerable, it might indicate that there were significant changes in individual patients that averaged out. In Table 8 are shown the average values of all geometrical and biomechanical parameters included in the analysis.

			$\vartheta_F$	$\frac{F}{W_B}$	$\vartheta_R$	$\frac{R}{W_B}$	$\vartheta_{CE}$	$\theta$	$\frac{p_{max}r^2}{W_B}$	$\frac{G_p r^3}{W_B}$	$\vartheta_f$
C1 130	Bef	M	15,82	1,73	10,55	2,55	26,41	17,10	1,94	-0,09	99,31
		SD	2,71	0,21	1,67	0,21	7,88	9,95	0,99	0,91	17,46
	Aft	M	15,53	1,71	10,35	2,52	27,00	16,76	1,87	-0,14	100,24
		SD	2,84	0,21	1,74	0,22	7,63	9,65	0,84	0,76	16,88
	Dif	M	-0,02	-0,01	-0,02	-0,01	0,03	-0,04	-0,03	0,01	0,01
		SD	0,15	0,08	0,14	0,05	0,12	0,60	0,14	1,51	0,07
t-test		0,14	0,04	0,10	0,048	0,02	0,35	0,03	0,07	0,10	
improved								54%	52%		
C2 42	Bef	M	12,19	1,92	8,44	2,74	24,14	24,84	2,51	0,34	89,30
		SD	3,39	0,27	2,39	0,27	8,78	10,29	1,18	1,12	18,41
	Aft	M	11,79	1,99	8,21	2,82	24,15	25,40	2,66	0,42	88,75
		SD	3,46	0,39	2,35	0,39	8,53	10,93	1,35	1,19	18,84
	Dif	M	-0,03	0,03	-0,02	0,02	0,05	0,00	0,02	-0,59	0,00
		SD	0,28	0,12	0,25	0,09	0,35	0,24	0,25	4,22	0,12
t-test		0,50	0,11	0,53	0,12	0,91	0,72	0,84	0,65	0,83	
improved								45%	50%		
C3 49	Bef	M	14,90	1,75	9,92	2,57	25,42	20,24	2,10	0,07	95,19
		SD	2,71	0,37	1,65	0,38	9,76	11,13	1,01	0,83	20,45
	Aft	M	14,01	1,83	9,51	2,65	26,01	20,33	2,13	0,03	95,68
		SD	2,92	0,31	1,83	0,31	9,61	10,65	0,89	0,74	19,78
	Dif	M	-0,07	0,06	-0,05	0,04	0,03	0,06	0,03	0,09	0,01
		SD	0,20	0,19	0,19	0,12	0,21	0,64	0,24	2,93	0,12
t-test		0,02	0,06	0,11	0,06	0,32	0,91	0,78	0,66	0,72	
improved								41%	53%		

*Table 8: Evaluation of hips on the contralateral side*

In order to exclude the error in estimation of the geometrical parameters as the cause of the differences found, only the records for which the changes in dimensionless peak contact hip stress were larger than 20% were included for further analysis. Followingly, records of operations which were considered unsuccessful, i.e., one of the two criteria for hip dysplasia worsened during the operation on the operated hip, were removed. The

remaining group of records was divided into two groups based on the sign of the difference in the dimensionless peak contact hip stress on the contralateral side. Results of the group of hips, which improved by more than 20% are shown in Table 9, and results of the group of hips, which worsened by more than 20% can be seen in Table 10. It can be seen that the number of hips which improved and which worsened is similar in C2 and C3, but in C1, there is a higher number of hips that got better.

			$\vartheta_F$	$\frac{F}{W_B}$	$\vartheta_R$	$\frac{R}{W_B}$	$\vartheta_{CE}$	$\theta$	$\frac{p_{max}r^2}{W_B}$	$\frac{G_p r^3}{W_B}$	$\vartheta_f$
C1 12	Bef	M	13,62	1,89	8,77	2,71	21,47	27,94	2,93	0,79	83,52
		SD	4,49	0,26	2,48	0,26	9,41	12,27	1,74	1,67	21,17
	Aft	M	15,17	1,70	10,01	2,52	26,67	18,65	2,05	0,07	98,03
		SD	4,59	0,29	2,82	0,30	11,19	13,36	1,18	1,10	23,87
	Dif	M	0,12	-0,10	0,13	-0,07	0,21	-0,65	-0,33	-1,6	0,15
		SD	0,26	0,13	0,26	0,09	0,20	0,80	0,09	1,85	0,06
t-test			0,20	0,01	0,11	0,01	0,002	3E-7	7E-4	0,002	4E-6
C2 6	Bef	M	10,90	1,85	7,47	2,68	20,34	32,26	3,05	0,93	78,08
		SD	2,51	0,15	1,66	0,15	6,92	10,97	1,54	1,58	17,56
	Aft	M	10,33	1,81	7,02	2,64	25,90	25,42	2,28	0,17	90,48
		SD	3,08	0,24	2,06	0,24	5,85	10,35	0,96	0,82	15,67
	Dif	M	-0,07	-0,03	-0,07	-0,02	0,28	-0,25	-0,27	-6,76	0,16
		SD	0,34	0,13	0,31	0,09	0,21	0,07	0,06	10,95	0,07
t-test			0,70	0,75	0,63	0,76	0,01	1E-4	0,04	0,09	5E-4
C3 6	Bef	M	13,34	1,98	9,28	2,80	18,19	31,14	3,30	1,09	77,05
		SD	2,66	0,39	1,67	0,39	7,33	11,75	1,65	1,47	18,84
	Aft	M	13,82	1,82	9,41	2,64	25,75	20,27	2,03	-0,08	95,48
		SD	3,38	0,22	2,18	0,22	6,73	10,29	0,56	0,54	16,61
	Dif	M	0,02	-0,08	0,00	-0,05	0,39	-0,48	-0,41	-1,48	0,22
		SD	0,16	0,09	0,14	0,07	0,21	0,27	0,25	0,95	0,13
t-test			0,59	0,12	0,81	0,13	8E-04	0,009	0,06	0,07	0,004
ALL 24	Bef	M	13,02	1,90	8,67	2,72	19,52	31,00	3,57	1,43	78,52
		SD	3,68	0,27	2,12	0,27	9,03	12,89	2,99	2,98	21,53
	Aft	M	13,95	1,75	9,31	2,57	25,24	21,83	2,32	0,29	93,41
		SD	4,32	0,26	2,69	0,26	10,04	13,20	1,47	1,46	22,63
	Dif	M	0,05	-0,08	0,05	-0,06	0,35	-0,53	-0,36	-2,70	0,18
		SD	0,27	0,11	0,26	0,08	0,41	0,63	0,16	5,24	0,09
t-test			0,18	0,002	0,16	0,002	2E-7	5E-11	0,001	0,002	6E-11

Table 9: Evaluation of hips on the contralateral side, which improved by more than 20% in stress

			$\vartheta_F$	$\frac{F}{W_B}$	$\vartheta_R$	$\frac{R}{W_B}$	$\vartheta_{CE}$	$\theta$	$\frac{p_{max}r^2}{W_B}$	$\frac{G_p r^3}{W_B}$	$\vartheta_f$
C1 2	Bef	M	15,18	1,88	10,40	2,70	23,21	21,77	2,41	0,28	91,43
		SD	2,49	0,41	1,01	0,41	11,26	17,27	1,47	1,17	28,53
	Aft	M	11,77	1,99	8,24	2,82	22,08	28,32	2,95	0,73	83,76
		SD	1,53	0,31	0,69	0,32	10,92	17,27	1,80	1,61	28,18
	Dif	M	-0,25	0,06	-0,23	0,05	-0,05	0,34	0,20	0,39	-0,11
		SD	0,03	0,06	0,01	0,04	0,01	0,24	0,00	0,16	-0,07
t-test			0,12	0,35	0,07	0,33	0,14	5E-5	0,26	0,4	0,02
C2 4	Bef	M	15,75	2,05	11,26	2,87	20,28	23,11	2,59	0,31	87,17
		SD	4,79	0,23	3,75	0,22	9,79	8,14	0,89	0,84	16,85
	Aft	M	11,10	2,57	8,34	3,40	16,83	35,23	4,20	1,54	71,59
		SD	3,54	0,70	2,84	0,69	7,05	6,39	1,70	1,24	12,63
	Dif	M	-0,34	0,20	-0,29	0,16	-0,14	0,44	0,44	1,37	-0,19
		SD	0,18	0,16	0,16	0,13	0,26	0,34	0,34	0,94	0,16
t-test			0,04	0,13	0,051	0,13	0,22	0,08	0,14	0,15	0,10
C3 7	Bef	M	14,82	1,63	9,41	2,45	23,85	22,58	2,02	0,07	91,27
		SD	3,51	0,50	1,78	0,51	5,31	9,93	0,75	0,53	14,99
	Aft	M	12,68	2,10	8,96	2,92	20,73	27,96	2,90	0,58	82,77
		SD	4,27	0,31	2,86	0,31	6,68	9,94	1,05	1,04	15,57
	Dif	M	-0,17	0,28	-0,08	0,19	-0,17	0,25	0,35	2,62	-0,10
		SD	0,41	0,30	0,42	0,19	0,21	0,36	0,14	5,91	0,12
t-test			0,26	0,04	0,75	0,04	0,07	0,12	0,003	0,08	0,06
ALL 13	Bef	M	15,16	1,80	10,14	2,62	22,65	22,62	2,26	0,18	90,03
		SD	3,55	0,44	2,44	0,44	7,17	9,53	0,85	0,67	15,97
	Aft	M	12,05	4,05	8,66	3,05	19,74	30,25	3,31	0,90	79,48
		SD	3,61	4,52	2,51	0,49	7,00	9,82	1,39	1,16	16,04
	Dif	M	-0,24	0,22	-0,17	0,16	-0,14	0,32	0,36	1,89	-0,13
		SD	0,31	0,24	0,32	0,16	0,20	0,32	0,21	4,30	0,19
t-test			0,01	0,10	0,09	0,005	0,01	0,004	0,002	0,012	0,003

Table 10: Evaluation of hips on the contralateral side which got worse by more than 20% in stress

## 6. Discussion

There are two approaches how to estimate the resultant hip force. The first option is to perform a direct in vivo measurement using an instrumented hip implant. The other possibility is to use mathematical models. For calculating the resultant hip force in a static position, they can be divided into two groups according to the way the equations of equilibrium are solved. Simplified models with a reduced number of muscles can be solved with simple reduction methods, and in more complicated models, optimization methods are necessary.

According to the first hypothesis, it was expected that if a model is scaled to the same patient, the resultant hip force should not differ considerably. Even though the patients evaluated according to the models using reduction methods were not the same ones as the ones evaluated by the models using optimization methods, the resultant hip forces were normalized by the weight force, and therefore, the results are comparable. The results showed that while the force calculated from models using optimization methods ranged between 1,25 and 1,7 times the body weight, the force calculated from models using reduction methods was about 2,5 times the body weight. It can be stated that the resultant hip force highly depends on the choice of the type of model. On the other hand, it can be seen that all models using optimization methods showed similar results of the resultant hip force (1,25 - 1,7 times the body weight force). Similarly, the resultant hip force calculated from the models using reduction methods shows only slight differences. The models using optimization methods also showed similar results in the angle of the resultant hip force in the frontal plane ( $1^\circ - 3^\circ$ ) and the sagittal plane ( $0^\circ - 2,5^\circ$ ). On the other hand, the angle in the frontal plane differs in the models using reduction methods ( $8^\circ - 18^\circ$ ), which is caused by the different determination of the muscle force.

Secondly, it was hypothesised that anatomically more accurate models would provide a more realistic estimation of the hip joint loading than models with fewer muscles. The results show that it was not hypothesised correctly. While the force calculated from models using optimization methods ranged between 1,25 and 1,7 times the body weight, the force measured in vivo was about 2,55 on average. Similarly, the angle of the resultant hip force was significantly lower in models using optimization methods compared to the values from the in vivo measurement. On the other hand, the simplified models using reduction

methods (models of Pauwels [28], Debrunner [29], Iglič [32], Uršič [7] and the one used in the clinical study) showed very similar values of the resultant hip force as the measurements and values of the resultant hip force angle in the frontal plane were much closer to the in vivo measurements. The model of Pauwels even showed almost the exact value of the angle.

One of the reasons why the resultant hip force calculated from models using optimization methods was much lower might be that the models are ideal. While the model is in a given fixed position for the calculation, a human cannot stand completely still, activating a greater number of muscles. It is supported by the EMG measurement in Figure 8, where it is shown that the activity of every muscle fluctuates. Such fluctuations do not occur in the models, allowing them to transmit the smallest possible forces. Similarly, the models have no history of pathology, whereas the resulting hip force is measured postoperatively using an instrumented implant, suggesting that the patients had some hip problems, which may have led to higher values of the resultant hip force.

Even if the previous arguments are considered, the difference between measured and calculated values still seems quite large. Another reason might be the passive tension of muscles, which was neglected. As hypothesised, incorporating the passive tension as a minimum muscle activity leads to the increase of the resultant hip force. On average, the resultant hip force increased by 40% when the minimum muscle activity was set to 10%. It increased the most in Rajagopal et al., 2016 and Lai et al., 2017 models, where the force increased by more than 50% and reached values similar to the ones measured in vivo. The lowest increase of the resultant hip force was in Modenese et al., 2011 model, where it increased only by 15%. On the other hand, the angle of the resultant hip force in the sagittal and frontal plane increased rapidly and by a much higher percentage in Modenese et al., 2011 model than in the others (by 410% in the frontal plane and by 1580% in the sagittal plane).

The fourth hypothesis concerned the number of muscles. It was hypothesized that the more muscles included in the model, the better the distribution of forces across the muscles and, therefore, the lower the resulting force. This hypothesis shows to be correct between the models using reduction and optimization methods. The resultant hip force estimated by the latter shows to be significantly lower. However, this hypothesis does not

apply to the models using optimization techniques alone. It cannot be clearly stated that a relationship would be found between the number of muscles (and especially of muscle fibres) and the resultant hip force.

Lastly, it was hypothesised that the muscle forces would differ considerably between models, and some expectations were stated. The distribution of forces into muscles is shown in Figure 26 and the muscle activity can be seen in Figure 27. The results support the hypothesis that the gluteus medius and rectus femoris would transmit the highest forces. Results showed considerable forces also in the iliacus, gluteus medius and in some models also in the gluteus maximus and psoas major. It was expected that the lowest forces would be found in adductor muscles and gluteus maximus. That is supported by the results, as the forces in the adductor muscles were found to be mostly minimum possible. The forces in the gluteus maximus were found to be considerable in some models, however, its activity equalled or got very close to the minimum muscle activity. The considerable force was obtained due to higher maximal isometric force. Based on the EMG measurements, it was also expected that tensor fasciae latae would be active. From the results, it can be concluded that tensor fasciae latae is considerably active, but unlike gluteus maximus, it has a small value of maximal isometric force, and therefore the resultant muscle force is relatively small.

The pattern of muscle forces and muscle activity is very similar for the models, however, some differences can be found. The first difference is in the number of muscles and muscle fibres. The highest number of muscle fibres can be found in Modenese et al., 2011 model. Furthermore, this model is the only one that includes all muscles located in the hip joint area. The most significant difference in the pattern can be seen in Modenese et al., 2011 model, where, as opposed to other models, the value of the resultant muscle force and resultant muscle activity of rectus femoris decreased when minimum muscle activity was set. The activity of psoas major and semimembranosus increased more significantly than in other models.

The clinical study focused on evaluating the hips of patients who underwent a periacetabular osteotomy, a surgical treatment performed to improve hip dysplasia. Hips were evaluated according to HIPSTRESS model from X-Ray scans. This model was selected because of its simplicity and suitability for this type of application (as described in section

4.4.1). The hips of 181 patients from three different medical centres were evaluated in total.

HIPSTRESS method defines several geometrical and biomechanical parameters, measured on the X-Ray scans and followingly calculated. The most important parameters for evaluating hip dysplasia are dimensionless peak contact hip stress  $p_{max}r^2/W_B$  (further called only stress) and dimensionless hip stress gradient index  $G_p r^3/W_B$  (further called only gradient). A hip is considered dysplastic if the stress value increases above two or if the gradient sign is positive. Overall, it was found that the gradient is more favourable when evaluating the improvement on both the operated and contralateral sides. Similarly, more hips were evaluated as dysplastic according to the stress than the gradient in all centres and all cases, preoperatively and postoperatively, and on both the operated and contralateral sides. A reason for that might be a shift of the body weight force laterally over the unloaded leg, which was made as an improvement over the previous model [7], where the criterion for evaluating hip dysplasia by the stress was suggested according to the gradient criterion. However, that would require further investigation and comparison of the two models.

The focus of this work was not on evaluating hip dysplasia. It had already been shown by Uršič et al., 2021 [7] that the HIPSTRESS model can be used for that cause. The aim of this work was instead focused on the unoperated hip on the contralateral side and monitoring the changes in geometrical and biomechanical parameters that happen on the contralateral side during the operation.

It was found that on the contralateral side, there was a similar number of hips that improved as those which got worse. That may indicate two possibilities. Either firstly, it may indicate only a mistake in evaluations of the geometrical parameters from X-Ray scans and that there were actually no changes on the contralateral side. Similarly, the positioning of patients for the X-Ray scans may play a role, resulting in an incorrect evaluation of the actual geometrical parameters. Or secondly, it may indicate that in about half of the operations, the geometry of the contralateral hip was changed in such a way that there became higher loads on the hip. Such change could further lead to hip arthritis or another operation on the contralateral side.



To eliminate an error in the evaluation of the geometrical parameters and to highlight the best and worst cases, only those hips for which the stress (as the less favourable parameter) changed by more than 20% were considered for further analysis. Records of hips, for which the operation was evaluated as unsuccessful, were also removed from the further analysis. It showed that a similar number of hips improved and got worse in centres C2 (6 improved, 4 got worse) and C3 (6 improved, 7 got worse). On the contrary, 12 hips improved while only 2 got worse in centre C3.

For better visualization, two cases from centre C1 are shown in Figure 28. In the first case, the situation on the contralateral side improved most from all cases in centre C1, i.e., the stress decreased most. Picture A shows hips preoperatively and picture B postoperatively. It can be seen that the values of the centre-edge angle  $\vartheta_{CE}$  and the muscle force angle  $\vartheta_F$  increased from  $7,67^\circ$  to  $10,09^\circ$  and from  $12,78^\circ$  to  $18,75^\circ$ , respectively. The value of the stress decreased from 6,51 to 3,23 and the value of the gradient decreased from 4,23 to 1,41. It means that the contralateral hip was also dysplastic, and the patient had to undergo a second operation on that side. It can also be seen that due to the operation, the radius of the femoral head on the operated side noticeably decreased. That is because the radius is drawn to fit the region of the femoral head where the highest load is expected. Due to the operation, this region enlarged.

On the other hand, in the second case, the stress on the contralateral side increased most from all the cases in centre C1 and therefore, the situation worsened. Picture C shows hips preoperatively and picture D postoperatively. It can be seen that it was already the second operation of that person and that the currently contralateral hip had already been operated before. Value of  $\vartheta_{CE}$  decreased from  $31,17^\circ$  to  $29,08^\circ$  and  $\vartheta_F$  angle decreased from  $16,94^\circ$  to  $12,85^\circ$ . The stress increased from 1,37 to 1,68 and the gradient increased from -0,54 to -0,41.

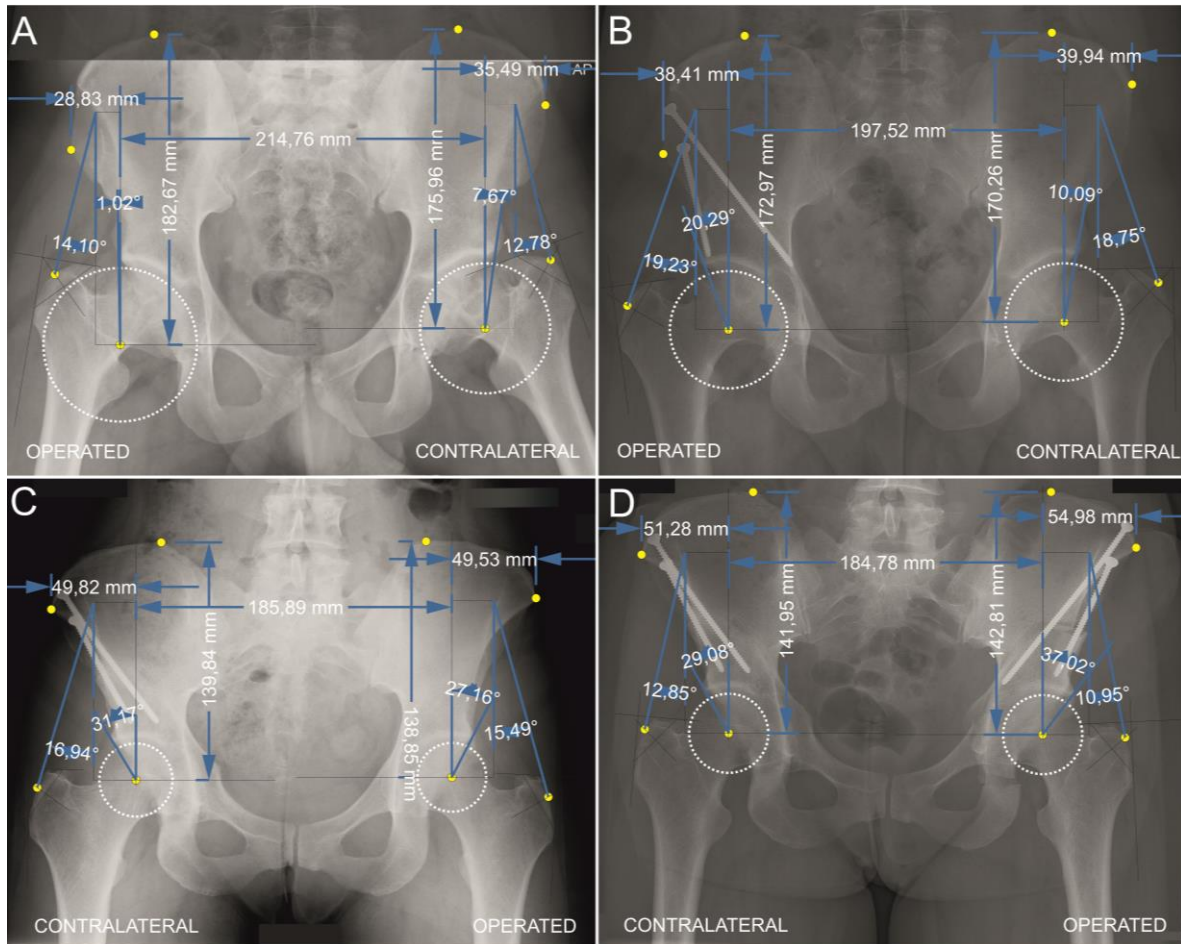


Figure 28: X-Ray scans of two cases of the operation from centre C1 in which the stress on the contralateral side improved most (before and after the operation (A, B)) and in which worsened most (before and after the operation (C, D))

An advantage of this model is that the parameters are dimensionless and therefore do not depend on the magnification of pictures of X-Ray scans, which is often unknown. At the same time, however, it is a drawback of this model because the influence of initial geometrical parameters can be studied only for the angles. The angles can be compared preoperatively and postoperatively as well as between patients. Other parameters differ according to the magnification of the image. It would be possible to compare the ratios of some parameters, for example,  $H/L$  or  $C/L$ , however, there is a problem that both of these parameters may change during the operation. For that reason, it would be advantageous if some circular items were added to the X-Ray scans of known diameter, for example, a coin, which would allow calculating the magnification of the scan. Another possibility could be to measure a pelvic structure which does not change during the operation and introduce new dimensionless variables of geometrical parameters relative to this structure. It would

still be impossible to compare the variables between patients, however, it would allow calculating a percentage difference, which would already be comparable.

This work focused mainly on the evaluation of X-Ray scans, calculation of biomechanical parameters and obtaining statistical results. It was shown that the angles  $\vartheta_{CE}$  and  $\vartheta_F$  are connected with the resulting stress and gradient. The aim of further research should be to look at the results more deeply and try to find a cause of why some contralateral hips improved and some worsened during the operation. If a reason were found, it would allow new proposals to be put forward to improve the operation process.

## 7. Conclusion

This work is composed of two main parts. The first part focused on different approaches on how to estimate the resultant hip force during the one-legged stance, which is considered a representative body position for the long-term effect of the hip contact stress [5]. Three approaches were described: in-vivo measurement using an instrumented implant, simplified models using reduction methods and more complex models using optimization methods. Available models using optimization methods were found in the OpenSim database [6], from which were extracted positions of attachments of muscles located in the hip area. The resultant hip force was calculated using the optimization method SLSQP solver in Python, during which the distribution of forces was calculated into individual muscle fibres. Results were followingly compared to the results of models using reduction methods and in vivo measurements obtained from different studies.

It was shown that the resultant hip force depends on the choice of the model. As expected, under the presumption of the number of muscles contained in models, the resultant hip force calculated from the models using optimization methods was lower than from the models using reduction methods. On the other hand, the resultant hip force in models using optimization methods was lower compared to the measurements, while if calculated by the simplified models, the resultant hip force corresponded to the measurements, which is contrary to expectations. Similarly, the angle of the resultant hip force was lower in models using optimization methods than in the simplified models, in which the angle was still lower than the measured angle. Only in the model of Pauwels [28], the angle was similar to the measured one. It was expected that a relationship between the number of muscles/muscle fibres and the value of the resultant hip force would be observed in the models using optimization methods, but no clear relationship was found.

If a minimum muscle activity representing the passive tension was added, the resultant hip force increased as expected. Its value in some models reached the measured values. On the other hand, the value of the angle in the frontal plane remained much lower than the measured one.

The distribution of forces into muscles according to the minimum muscle fatigue optimization criterion mostly showed consistency with the predictions. The highest forces were calculated in the gluteus medius and rectus femoris. Considerable forces were also

found in the iliacus and gluteus minimus and in some models in the psoas major and gluteus medius. In the case of the gluteus maximus, it was caused rather because it has a higher maximal isometric force than some other muscles and therefore, when the minimum muscle activation was set, it reached higher forces. On the contrary, the results showed that some muscles were considerably activated, but since they have small maximal isometric force, the force in them did not reach considerable values.

Most models showed similar behaviour when the minimum muscle activation was increased and similar distribution of the muscle forces into the muscles. Modenese et al., 2011 model showed the most significant difference. While other models contain around 25 muscle fibres in the hip area, Modenese et al., 2011 contains 95. The model showed differences when the minimum muscle activity was set in both the resultant hip force and the distribution of forces into muscles. The resultant hip force did not increase as in the other models but remained at mostly the same level. On the other hand, the angle of the resultant hip force increased much more than in the other models. With the increase in minimum muscle activity, the resultant muscle activity (and therefore the resultant muscle force) of the rectus femoris and gluteus minimus decreased. In the case of the rectus femoris, it decreased to its minimum, while the activity of psoas major increased to its maximum and the activity of semimembranosus increased to 50%. In the other models, the activity of semimembranosus was minimal.

The second part of this work was a clinical study which was a part of ongoing research on hip dysplasia at the University of Ljubljana. Altogether, 442 X-Ray scans of 181 patients who underwent a periacetabular osteotomy in three different medical centres were evaluated. The hips were evaluated according to two-dimensional HIPSTRESS model, which was chosen for its simplicity, suitability and the possibility of comparing the results with previous studies. Two criteria were suggested to define dysplastic hips. Firstly, if the dimensionless peak contact hip stress increases above two  $p_{max}r^2/W_B > 2$  [7] and secondly, if the dimensionless hip stress gradient index is positive  $G_p r^3/W_B > 0$  [48].

The study was primarily focused on evaluating hips on the contralateral side. It was found that about half of the hips improved during the operation and half of them worsened. The ratio indicates that in about half of the surgeries, the geometry of the hips on the contralateral side was changed in such a way that there became higher loads on the

hip. On the other hand, the ratio might have been caused only by a wrong positioning of the patients for the X-Ray imaging and by slight inaccuracies in the evaluation of the geometrical parameters, which would mean that no changes actually occurred on the contralateral side.

In order to exclude the inaccuracies of measurement and to highlight the cases when the stress on the contralateral side improved most and least, only the records for which the changes in dimensionless peak contact hip stress were larger than 20% remained included for further analysis. Afterwards, the ratio persisted in centres C2 and C3. As opposed to them, in centre C1, twelve contralateral hips improved while only two worsened.

So far, it cannot be clearly stated what happens on the contralateral side. However, this work implies that further investigations are required to find a cause for why about half of the contralateral hips gets worse after the biomechanical evaluation. If it were proved that the operation on the operated side influences the hip on the contralateral side and the reasons were found, it would allow to improve the operation process in such a way that the stress distribution becomes more convenient and its peak value decreases not only in the operated hip but also in the hip on the contralateral side.

The results also show differences between the medical centres. The highest success rate of the operations was in centre C1, where the condition of the operated hips improved in 98% of cases. The success rate in the other two centres was about 90%. Hips on the contralateral side also improved more in centre C1, especially according to the dimensionless peak contact hip stress criterion.

This work showed two approaches how to estimate the resultant hip force by mathematical models. The clinical study showed that a simple two-dimensional model could be well used for predicting hip dysplasia. The advantage of the model is that it can adapt well to a patient-specific geometry of the hip and that the evaluation can be done easily and quickly based on X-Ray scans. That would not be so easily possible in more complex models using optimization methods since the scaling procedures described by Song et al., 2019 [38] are more time-consuming and require CT scans. On the other hand, these models can reflect patient-specific anatomy more precisely and allow calculation of muscle forces.

## BIBLIOGRAPHY

- [1] R. A. Brand, D. R. Pedersen, D. T. Davy, G. M. Kotzar, K. G. Heiple, and V. M. Goldberg, 'Comparison of hip force calculations and measurements in the same patient', *The Journal of Arthroplasty*, vol. 9, no. 1, pp. 45–51, Feb. 1994, doi: 10.1016/0883-5403(94)90136-8.
- [2] G. Bergmann *et al.*, 'Hip contact forces and gait patterns from routine activities', *J Biomech*, vol. 34, no. 7, pp. 859–871, Jul. 2001, doi: 10.1016/s0021-9290(01)00040-9.
- [3] G. Bergmann, A. Bender, J. Dymke, G. Duda, and P. Damm, 'Standardized Loads Acting in Hip Implants', *PLoS ONE*, vol. 11, no. 5, p. e0155612, May 2016, doi: 10.1371/journal.pone.0155612.
- [4] J. Hornová, A. Iglič, V. Kralj-Iglič, D. R. Pedersen, and M. Daniel, 'Effect of patient-specific model scaling on hip joint reaction force in one-legged stance – study of 356 hips', p. 6.
- [5] H. Debevec, D. R. Pedersen, A. Iglíc, and M. Daniel, 'One-legged stance as a representative static body position for calculation of hip contact stress distribution in clinical studies', *J Appl Biomech*, vol. 26, no. 4, pp. 522–525, Nov. 2010, doi: 10.1123/jab.26.4.522.
- [6] 'Musculoskeletal Models - OpenSim Documentation - Global Site'. <https://simtk-confluence.stanford.edu:8443/display/OpenSim/Musculoskeletal+Models> (accessed Jun. 02, 2022).
- [7] B. Uršič, B. Kocjančič, A. Romolo, A. Iglič, V. Kralj-Iglič, and O. Zupanc, 'Assessment of coxarthrosis risk with dimensionless biomechanical parameters', *Acta Bioeng Biomech*, vol. 23, no. 1, 2021, doi: 10.37190/ABB-01738-2020-03.
- [8] R. Galmiche, H. Migaud, and P.-E. Beaulé, 'Hip Anatomy and Biomechanics Relevant to Hip Replacement', in *Personalized Hip and Knee Joint Replacement*, C. Rivière and P.-A. Vendittoli, Eds. Cham (CH): Springer, 2020. Accessed: Jun. 27, 2022. [Online]. Available: <http://www.ncbi.nlm.nih.gov/books/NBK565771/>
- [9] 'Hip Anatomy', *Physiopedia*. [https://www.physio-pedia.com/Hip\\_Anatomy](https://www.physio-pedia.com/Hip_Anatomy) (accessed Jun. 27, 2022).
- [10] 'Hip disorders - Better Health Channel'. <https://www.betterhealth.vic.gov.au/health/conditionsandtreatments/hip-disorders> (accessed Jun. 27, 2022).
- [11] 'Hip Problems', Aug. 08, 2021. <https://www.hopkinsmedicine.org/health/conditions-and-diseases/hip-problems> (accessed Jun. 27, 2022).
- [12] 'Hip Fractures - OrthoInfo - AAOs'. <https://www.orthoinfo.org/en/diseases--conditions/hip-fractures/> (accessed Jun. 27, 2022).
- [13] 'Gait - Physiopedia'. <https://www.physio-pedia.com/Gait> (accessed Jun. 28, 2022).
- [14] R. Baker, A. Esquenazi, M. G. Benedetti, and K. Desloovere, 'Gait analysis: clinical facts', *European Journal of Physical and Rehabilitation Medicine*, vol. 52, no. 4, p. 15, 2016.
- [15] L. Yu *et al.*, 'Principal Component Analysis of the Running Ground Reaction Forces With Different Speeds', *Frontiers in Bioengineering and Biotechnology*, vol. 9, 2021, Accessed: Jun. 28, 2022. [Online]. Available: <https://www.frontiersin.org/article/10.3389/fbioe.2021.629809>
- [16] 'Database « OrthoLoad'. <https://orthoload.com/database/> (accessed Jun. 02, 2022).
- [17] E. Jonsson, Å. Seiger, and H. Hirschfeld, 'One-leg stance in healthy young and elderly adults: a measure of postural steadiness?', *Clinical Biomechanics*, vol. 19, no. 7, pp. 688–694, Aug. 2004, doi: 10.1016/j.clinbiomech.2004.04.002.
- [18] 'Single leg stance or "One-legged stance test"', *Shirley Ryan AbilityLab*. <https://www.sralab.org/rehabilitation-measures/single-leg-stance-or-one-legged-stance-test> (accessed Jul. 01, 2022).
- [19] S. Prior *et al.*, 'The influence of changes in trunk and pelvic posture during single leg standing on hip and thigh muscle activation in a pain free population', *BMC Sports Sci Med Rehabil*, vol. 6, p. 13, Mar. 2014, doi: 10.1186/2052-1847-6-13.

- [20] S. L. Delp *et al.*, 'OpenSim: Open-Source Software to Create and Analyze Dynamic Simulations of Movement', *IEEE Trans. Biomed. Eng.*, vol. 54, no. 11, pp. 1940–1950, Nov. 2007, doi: 10.1109/TBME.2007.901024.
- [21] A. Seth *et al.*, 'OpenSim: Simulating musculoskeletal dynamics and neuromuscular control to study human and animal movement', *PLoS Comput Biol*, vol. 14, no. 7, p. e1006223, Jul. 2018, doi: 10.1371/journal.pcbi.1006223.
- [22] 'AnyBody Technology - musculoskeletal modeling & simulations'. <https://www.anybodytech.com/> (accessed Jun. 02, 2022).
- [23] 'SimTK: OpenSim: Project Home'. <https://simtk.org/projects/opensim> (accessed Jun. 27, 2022).
- [24] D. Tsirakos, V. Baltzopoulos, and R. Bartlett, 'Inverse optimization: functional and physiological considerations related to the force-sharing problem', *Crit Rev Biomed Eng*, vol. 25, no. 4–5, pp. 371–407, 1997, doi: 10.1615/critrevbiomedeng.v25.i4-5.20.
- [25] R. D. Crowninshield and R. A. Brand, 'A physiologically based criterion of muscle force prediction in locomotion', *Journal of Biomechanics*, vol. 14, no. 11, pp. 793–801, Jan. 1981, doi: 10.1016/0021-9290(81)90035-X.
- [26] R. D. Crowninshield and R. A. Brand, 'The prediction of forces in joint structures; distribution of intersegmental resultants', *Exerc Sport Sci Rev*, vol. 9, pp. 159–181, 1981.
- [27] A. Nasr, K. A. Inkol, S. Bell, and J. McPhee, 'InverseMuscleNET: Alternative Machine Learning Solution to Static Optimization and Inverse Muscle Modeling', *Frontiers in Computational Neuroscience*, vol. 15, 2021, Accessed: Jun. 27, 2022. [Online]. Available: <https://www.frontiersin.org/article/10.3389/fncom.2021.759489>
- [28] F. Pauwels, *Atlas zur Biomechanik der gesunden und kranken H?fte: Prinzipien, Technik und Resultate einer kausalen Therapie*. Berlin: Springer Berlin Heidelberg, 2013.
- [29] H. U. Debrunner, '[Biomechanics of the hip joint. I. A new model for the calculation of the forces in the hip joint]', *Z Orthop Ihre Grenzgeb*, vol. 113, no. 3, pp. 377–388, Jun. 1975.
- [30] J. Eschweiler *et al.*, 'Application and evaluation of biomechanical models and scores for the planning of total hip arthroplasty', *Proc Inst Mech Eng H*, vol. 226, no. 12, pp. 955–967, Dec. 2012, doi: 10.1177/0954411912445261.
- [31] S. Blumentritt, '[The relationship between the gait of humans and the hip joint structure in the frontal plane]', *Gegenbaurs Morphol Jahrb*, vol. 136, no. 6, pp. 677–693, 1990.
- [32] A. Igljič, F. Srakar, V. Antolič, V. Kralj-Igljič, and V. Batagelj, 'MATHEMATICAL ANALYSIS OF CHIARI OSTEOTOMY\* MATEMATICKA ANALIZA OSTEOTOMIJE PO CHIARIJU', p. 5.
- [33] J. Eschweiler, J. Hawlitzky, V. Quack, M. Tingart, and B. Rath, 'Biomechanical model based evaluation of Total Hip Arthroplasty therapy outcome', *Journal of Orthopaedics*, vol. 14, no. 4, pp. 582–588, Dec. 2017, doi: 10.1016/j.jor.2017.09.002.
- [34] M. Asseln *et al.*, 'Evaluation of Biomechanical Models for the Planning of Total Hip Arthroplasty', *Biomedical Engineering / Biomedizinische Technik*, Jan. 2013, doi: 10.1515/bmt-2013-4116.
- [35] L. Scheys, A. Spaepen, P. Suetens, and I. Jonkers, 'Calculated moment-arm and muscle-tendon lengths during gait differ substantially using MR based versus rescaled generic lower-limb musculoskeletal models', *Gait & Posture*, vol. 28, no. 4, pp. 640–648, Nov. 2008, doi: 10.1016/j.gaitpost.2008.04.010.
- [36] L. Scheys, A. Van Campenhout, A. Spaepen, P. Suetens, and I. Jonkers, 'Personalized MR-based musculoskeletal models compared to rescaled generic models in the presence of increased femoral anteversion: Effect on hip moment arm lengths', *Gait & Posture*, vol. 28, no. 3, pp. 358–365, Oct. 2008, doi: 10.1016/j.gaitpost.2008.05.002.
- [37] T. A. Correa, R. Baker, H. Kerr Graham, and M. G. Pandy, 'Accuracy of generic musculoskeletal models in predicting the functional roles of muscles in human gait', *Journal of Biomechanics*, vol. 44, no. 11, pp. 2096–2105, Jul. 2011, doi: 10.1016/j.jbiomech.2011.05.023.



- [38] K. Song, A. E. Anderson, J. A. Weiss, and M. D. Harris, 'Musculoskeletal Models with Generic and Subject-Specific Geometry Estimate Different Joint Biomechanics in Dysplastic Hips', *Comput Methods Biomech Biomed Engin*, vol. 22, no. 3, pp. 259–270, Feb. 2019, doi: 10.1080/10255842.2018.1550577.
- [39] M. D. Harris, B. A. MacWilliams, K. Bo Foreman, C. L. Peters, J. A. Weiss, and A. E. Anderson, 'Higher medially-directed joint reaction forces are a characteristic of dysplastic hips: A comparative study using subject-specific musculoskeletal models', *Journal of Biomechanics*, vol. 54, pp. 80–87, Mar. 2017, doi: 10.1016/j.jbiomech.2017.01.040.
- [40] M. F. Norcross, J. Troy Blackburn, and B. M. Goerger, 'Reliability and interpretation of single leg stance and maximum voluntary isometric contraction methods of electromyography normalization', *Journal of Electromyography and Kinesiology*, vol. 20, no. 3, pp. 420–425, Jun. 2010, doi: 10.1016/j.jelekin.2009.08.003.
- [41] L. A. Bolgla, T. R. Malone, B. R. Umberger, and T. L. Uhl, 'COMPARISON OF HIP AND KNEE STRENGTH AND NEUROMUSCULAR ACTIVITY IN SUBJECTS WITH AND WITHOUT PATELLOFEMORAL PAIN SYNDROME', *The International Journal of Sports Physical Therapy*, vol. 6, no. 4, p. 12, 2011.
- [42] N. Kaur, K. Bhanot, and G. Ferreira, 'Lower Extremity and Trunk Electromyographic Muscle Activity During Performance of the Y-Balance Test on Stable and Unstable Surfaces', *Int J Sports Phys Ther*, vol. 17, no. 3, pp. 483–492, 2022, doi: 10.26603/001c.32593.
- [43] 'Periacetabular Osteotomy: An Overview - HSS', *Hospital for Special Surgery*. [https://www.hss.edu/conditions\\_periacetabular-osteotomy-pao.asp](https://www.hss.edu/conditions_periacetabular-osteotomy-pao.asp) (accessed Jul. 06, 2022).
- [44] J. G. Hussell, J. W. Mast, K. A. Mayo, D. W. Howie, and R. Ganz, 'A comparison of different surgical approaches for the periacetabular osteotomy', *Clin Orthop Relat Res*, no. 363, pp. 64–72, Jun. 1999.
- [45] 'Periacetabular Osteotomy Park City, UT | Hip Dysplasia Salt Lake City, UT'. <https://www.jameswyliemd.com/periacetabular-osteotomy-orthopedic-surgeon-murray-provo-ut.html> (accessed Aug. 11, 2022).
- [46] S. Chen, L. Zhang, Y. Mei, H. Zhang, Y. Hu, and D. Chen, 'Role of the Anterior Center-Edge Angle on Acetabular Stress Distribution in Borderline Development Dysplastic of Hip Determined by Finite Element Analysis', *Frontiers in Bioengineering and Biotechnology*, vol. 10, 2022, Accessed: Aug. 11, 2022. [Online]. Available: <https://www.frontiersin.org/articles/10.3389/fbioe.2022.823557>
- [47] B. Mavčič, B. Pompe, V. Antolič, M. Daniel, A. Iglič, and V. Kralj-Iglič, 'Mathematical estimation of stress distribution in normal and dysplastic human hips', *J. Orthop. Res.*, vol. 20, no. 5, pp. 1025–1030, Sep. 2002, doi: 10.1016/S0736-0266(02)00014-1.
- [48] B. Pompe, M. Daniel, M. Sochor, R. Vengust, V. Kralj-Iglič, and A. Iglič, 'Gradient of contact stress in normal and dysplastic human hips', *Medical Engineering & Physics*, vol. 25, no. 5, pp. 379–385, Jun. 2003, doi: 10.1016/S1350-4533(03)00014-6.
- [49] A. T. Masi and J. C. Hannon, 'Human resting muscle tone (HRMT): narrative introduction and modern concepts', *J Bodyw Mov Ther*, vol. 12, no. 4, pp. 320–332, Oct. 2008, doi: 10.1016/j.jbmt.2008.05.007.
- [50] E. M. Arnold, S. R. Ward, R. L. Lieber, and S. L. Delp, 'A Model of the Lower Limb for Analysis of Human Movement', *Ann Biomed Eng*, vol. 38, no. 2, pp. 269–279, Feb. 2010, doi: 10.1007/s10439-009-9852-5.
- [51] S. R. Hamner, A. Seth, and S. L. Delp, 'Muscle contributions to propulsion and support during running', *Journal of Biomechanics*, vol. 43, no. 14, pp. 2709–2716, Oct. 2010, doi: 10.1016/j.jbiomech.2010.06.025.
- [52] A. Rajagopal, C. L. Dembia, M. S. DeMers, D. D. Delp, J. L. Hicks, and S. L. Delp, 'Full-Body Musculoskeletal Model for Muscle-Driven Simulation of Human Gait', *IEEE Trans. Biomed. Eng.*, vol. 63, no. 10, pp. 2068–2079, Oct. 2016, doi: 10.1109/TBME.2016.2586891.

- [53] A. K. M. Lai, A. S. Arnold, and J. M. Wakeling, 'Why are Antagonist Muscles Co-activated in My Simulation? A Musculoskeletal Model for Analysing Human Locomotor Tasks', *Ann Biomed Eng*, vol. 45, no. 12, pp. 2762–2774, Dec. 2017, doi: 10.1007/s10439-017-1920-7.
- [54] L. Modenese, A. T. M. Phillips, and A. M. J. Bull, 'An open source lower limb model: Hip joint validation', *Journal of Biomechanics*, vol. 44, no. 12, pp. 2185–2193, Aug. 2011, doi: 10.1016/j.jbiomech.2011.06.019.
- [55] A. G. Bruno, M. L. Boussein, and D. E. Anderson, 'Development and Validation of a Musculoskeletal Model of the Fully Articulated Thoracolumbar Spine and Rib Cage', *Journal of Biomechanical Engineering*, vol. 137, no. 8, Jun. 2015, doi: 10.1115/1.4030408.
- [56] A. G. Bruno, K. Burkhart, B. Allaire, D. E. Anderson, and M. L. Boussein, 'Spinal Loading Patterns From Biomechanical Modeling Explain the High Incidence of Vertebral Fractures in the Thoracolumbar Region', *Journal of Bone and Mineral Research*, vol. 32, no. 6, pp. 1282–1290, 2017, doi: 10.1002/jbmr.3113.
- [57] K. Burkhart, D. Grindle, M. L. Boussein, and D. E. Anderson, 'Between-session reliability of subject-specific musculoskeletal models of the spine derived from optoelectronic motion capture data', *J Biomech*, vol. 112, p. 110044, Nov. 2020, doi: 10.1016/j.jbiomech.2020.110044.
- [58] M. E. Raabe and A. M. W. Chaudhari, 'An investigation of jogging biomechanics using the full-body lumbar spine model: Model development and validation', *J Biomech*, vol. 49, no. 7, pp. 1238–1243, May 2016, doi: 10.1016/j.jbiomech.2016.02.046.
- [59] 'minimize(method='SLSQP') — SciPy v1.9.0 Manual'. <https://docs.scipy.org/doc/scipy/reference/optimize.minimize-slsqp.html> (accessed Aug. 11, 2022).
- [60] 'lxml - Processing XML and HTML with Python'. <https://lxml.de/> (accessed Aug. 11, 2022).
- [61] 'Muscle Editor - OpenSim Documentation - Global Site'. <https://simtk-confluence.stanford.edu:8443/display/OpenSim/Muscle+Editor> (accessed Jun. 21, 2022).
- [62] A. T. M. Phillips, C. C. Villette, and L. Modenese, 'Femoral bone mesoscale structural architecture prediction using musculoskeletal and finite element modelling', *International Biomechanics*, vol. 2, no. 1, pp. 43–61, Jan. 2015, doi: 10.1080/23335432.2015.1017609.
- [63] R. J. van Arkel, L. Modenese, A. T. M. Phillips, and J. R. T. Jeffers, 'Hip abduction can prevent posterior edge loading of hip replacements', *Journal of Orthopaedic Research*, vol. 31, no. 8, pp. 1172–1179, 2013, doi: 10.1002/jor.22364.
- [64] L. Modenese and A. T. M. Philips, 'OpenSim plugin to extract the muscle lines of action'. SimTK, 2020. doi: 10.18735/XSXP-QS03.
- [65] C. E. Clauser, J. T. McConville, and J. W. Young, 'WEIGHT, VOLUME, AND CENTER OF MASS OF SEGMENTS OF THE HUMAN BODY', Defense Technical Information Center, Fort Belvoir, VA, Aug. 1969. doi: 10.21236/AD0710622.
- [66] R. D. McLeish and J. Charnley, 'Abduction forces in the one-legged stance', *J Biomech*, vol. 3, no. 2, pp. 191–209, Mar. 1970, doi: 10.1016/0021-9290(70)90006-0.
- [67] A. W. Eberhardt, J. L. Lewis, and L. M. Keer, 'Contact of layered elastic spheres as a model of joint contact: effect of tangential load and friction', *J Biomech Eng*, vol. 113, no. 1, pp. 107–108, Feb. 1991, doi: 10.1115/1.2894076.
- [68] H. Lipshitz and M. J. Glimcher, 'In vitro studies of the wear of articular cartilage II. Characteristics of the wear of articular cartilage when worn against stainless steel plates having characterized surfaces', *Wear*, vol. 52, no. 2, pp. 297–339, Feb. 1979, doi: 10.1016/0043-1648(79)90070-X.
- [69] C. W. McCutchen, 'The frictional properties of animal joints', *Wear*, vol. 5, no. 1, pp. 1–17, Jan. 1962, doi: 10.1016/0043-1648(62)90176-X.
- [70] V. K. - Igli, D. Dolinar, M. Ivanovski, I. List, and M. Daniel, 'Role of Biomechanical Parameters in Hip Osteoarthritis and Avascular Necrosis of Femoral Head', in *Applied Biological Engineering - Principles and Practice*, G. R. Naik, Ed. InTech, 2012. doi: 10.5772/30159.